Regulation of protein import by a thioredoxin reductive pathway in the intermembrane space of mitochondria

By

Mauricio Cárdenas Rodríguez

MSc.

Submitted in fulfilment of the requirements for the degree of

Doctor of Philosophy

Institute of Molecular, Cell and System Biology

College of Medical, Veterinary and Life Sciences

University of Glasgow

April 2019

Abstract

Mitochondria are organelles that fulfil main roles in cellular metabolism. From the total mitochondrial proteome, 99% of proteins are encoded in the nucleus and have to be imported into mitochondria. Hence, mitochondria have developed at least five import pathways to drive those proteins into the four mitochondrial compartments (the outer and inner membranes, the matrix and the mitochondrial intermembrane space (IMS)). The main pathways are the presequence pathway, the carrier pathway, the β-barrel pathway, the insertion of α-helical proteins and the oxidative folding (MIA) pathway. MIA pathway imports most proteins residing in the IMS by inserting disulfide bridges onto characteristic cysteine motifs in the incoming reduced protein precursors. The import through the MIA pathway depends on the redox homeostasis of the compartments where it takes place, the cytosol and the IMS. This redox homeostasis is the balance between the oxidative and reductive pathways. In particular, the main reductive pathways are the glutaredoxin (Grx) and thioredoxin (Trx) systems, both of which share NADPH as their final electron donor. Despite extensive knowledge on the oxidative pathway, a reducing mechanism in the IMS is yet to be discovered. In this work, we studied the molecular and mechanistic aspects of redox perturbations on the MIA pathway. We found that reductive impairment in the yeast cell specifically decreased the import through the MIA pathway because the key effector, Mia40 is in an unbalanced redox state towards its oxidising form. Furthermore, based on the recent discovery of cytosolic Trx system residing also in the mitochondrial IMS, we investigate its role as this unknown reductive system in this compartment. We found that Trx interacts with Mia 40 and restores its redox state to a functional balanced oxidising and reducing state and that this partially recovers the import capacity of this yeast strain. We conclude by proposing a model in which redox state of Mia40 acts as a sensor of the import of MIA substrates in a Trx-dependent manner.

Table of Contents

List of Tables

List of Figures

List of Accompanying Material

Appendix: List of publications

Acknowledgement

To my mom.

I would like to thank my dad Carlos, my sister and brother, Dianela and Carlos, and my brother in law, Arturo, for all their love, support and encouragement throughout my life and my studies and for always making me feel good and close regardless of the distance.

I would like to thank Sylvia, for all the love, the many good moments and for making me a better person and being my partner in crime in this adventure.

I would like to thank my supervisor, Prof. Kostas Tokatlidis first of all for the opportunity to come to Glasgow and join his lab, for all the advice, the patience, laughs and good moments as well as for his kindness and for being an excellent role model both as a scientist and as a person.

I would also like to thank my friends, the four Daniels and Osvaldo for becoming part of my family and an important part of my life.

I would also like to thank my Mexican and Glaswegian friends that have always made me feel at home either in Mexico or in Glasgow.

I would like to thank the past and present members of the lab, in particular Afroditi, Emmanuella, Georgia, Phanee and Ruairidh for made me feel welcome when I arrived to Glasgow and for all the fun and good conversations.

Author's Declaration

I declare that, except where explicit reference is made to the contribution of others, this thesis is the result of my own work and has not been submitted for any other degree at the University of Glasgow or any other institutions.

Definitions/Abbreviations

Ab Antibody

ADP Adenosine diphosphate

ATP Adenosine triphosphate

Bam ß-barrel assembly

CCCP Carbonyl cyanide m-chlorophenyl hydrazine

DDP1 Deafness dystonia peptide

DDS Deafness dystonia syndrome

DHFR Dihydrofolate reductase

DTT Dithiothreitol

EDTA Ethylenediaminetetraacetic acid

ER Endoplasmic reticulum

Erv1 Essential for respiration and viability

FAD Flavin adenine dinucleotide

G6pd Glucose-6-phosphate dehydrogenase

GA Glutaraldehyde

Grx Glutaredoxin

GSH Glutathione

GSSG Glutathione oxidised

HEPES 4-(2-Hydroxyethyl) piperazine-1-ethanesulfonic acid

Hsp Heat shock protein

IM Inner membrane

IMP Inner membrane protease

IMS Intermembrane space

IPTG Isopropyl ß-D-1-thiogalactopyranoside

ITS/MISS Intermembrane space targeting signal/mitochondrial intermembrane space sorting signal

KO Knockout

Mal-PEG Maleimide polyethylene glycol

MIA Mitochondrial import and assembly

MOPS 3-(N-morpholino)-propane sulfonic acid

MPP Mitochondrial processing peptidase

MTS Mitochondrial targeting signal

NAD Nicotinamide adenine dinucleotide

NADH Reduced nicotinamide adenine dinucleotide

NADP Nicotinamide adenine dinucleotide phosphate

NADPH Reduced nicotinamide adenine dinucleotide phosphate

Ni-NTA Nickel-charged nitrilotriacetic acid resin beads

OM Outer membrane

PAGE Polyacrylamide gel electrophoresis

PAM Presenquence translocase-associated motor

PDH Pyruvate dehydrogenase

PDI Protein disulphide isomerase

PMSF Phenylmethylsulfonyl fluoride

ROS Reactive oxygen species

S. cerevisiae Saccharomyces cerevisiae

SAM Sorting and assembly machinery

SDS Sodium dodecyl sulfate

Su9 Subunit 9 of ATPase

TCA Trichloroacetic acid

TIM Translocase of the inner membrane

TNT Coupled transcription and translation

TOM Translocase of the outer membrane

Tris 2-Amino-2-(hydroxymethyl)-1,3-propanediol

TrR Thioredoxin reductase

Trx Thioredoxin

WT Wild type

$\Delta\Psi$ Inner mitochondrial membrane potential

Chapter 1 Introduction

1.1 Mitochondria

The name mitochondrion comes from the Greek words ‘mitos’, which means thread, and ‘chondros’, which means granule, and was coined by the German microbiologist Carl Benda in 1898 due to the organelle’s characteristic to form long chains (Ernster and Schatz, 1981). Mitochondria are subcellular double-membrane and semi-autonomous organelles that originated form an α-proteobacterium engulfed by an eukaryotic ancestor (Lane and Martin, 2010). They are present in almost every eukaryotic cell. These organelles were discovered by Rudolf Albrect von Kolliker around the 1860s (Schatz, 2013) and were first identified as ubiquitous cytoplasmic structures that resembled bacteria and were called ‘bioblasts’ by the German pathologist Richard Altmann (Ernster and Schatz, 1981).

Mitochondria are normally considered the energy producing factory of the cell. However, extensive studies have widened their importance in cell metabolism and fate. It was shown that mitochondria are a hub for important catabolic pathways like the Krebs cycle, as well as fatty acid oxidation and are involved in the urea cycle, heme, cardiolipin and steroid synthesis (see (Scheffler, 2002)). Furthermore, mitochondria have been linked to different diseases such as cancer (Weinberg et al., 2010) and neurodegenerative disorders (Park et al., 2018), as well as with aging (Sun et al., 2016) and cell death (Tait and Green, 2012).

Structurally, mitochondria, like their bacterial ancestors, comprise of two aqueous compartments separated by two phospholipid bilayers (Figure 1.1). Mitochondria are separated from and communicate with the cellular environment by the mitochondrial outer membrane (OM). This membrane represents the entry and exit point of mitochondria as it contains proteins that serve as gates to incoming protein precursors, cofactors and small molecules important for the mitochondrial and cell fate and function (Chacinska et al., 2009, Vander Heiden et al., 2000). The second mitochondrial membrane, the inner membrane (IM), separates the two aqueous mitochondrial compartments and bends inwards to form characteristic structures named cristae, which are important in the mitochondrial IM organisation and function (Aaltonen et al.,

2016, Friedman et al., 2015). The IM is the most protein-rich membrane in cells (75% protein and 25% lipid in mass ratio) and contains the proteins responsible for the mitochondrial oxidative phosphorylation chain, protein translocation and assembly and is involved in metabolite interchange between the matrix and the mitochondrial intermembrane space (IMS) (Claypool et al., 2008, Kramer and Klingenberg, 1977, Wohlrab, 2009). The two membranes differ principally in their lipid content and in particular in the content of cardiolipin (about 20% in the IM) (Claypool et al., 2008, de Kroon et al., 1997), which is a unique type of phospholipid located mainly in the mitochondrial IM and has been involved in the organisation of the respiratory chain complexes among other metabolic processes (Paradies et al., 2014, Houtkooper and Vaz, 2008). On the other hand, the inner membrane envelops the mitochondrial matrix, which contains the majority of mitochondrial proteins (roughly 2/3 of the total mitochondrial protein content) and hosts important pathways such as the tricarboxylic acid cycle (Robinson and Srere, 1985), protein transamination (Kispal et al., 1996) and Fe/S cluster biogenesis (Cardenas-Rodriguez et al., 2018) among others. Finally, the mitochondrial IMS is the compartment between the outer and inner membranes. The IMS is involved in sorting mitochondrial proteins into the other three compartments and with important metabolic processes such as oxidative phosphorylation (Glick et al., 1993) and mitochondrial oxidative folding (Banci et al., 2009, Chacinska et al., 2004, Mesecke et al., 2005). Proteins residing in the IMS include Cytochrome b2, Mia40, Erv1 and the small Tims, Tim9, Tim10, Tim12 (Herrmann and Hell, 2005)

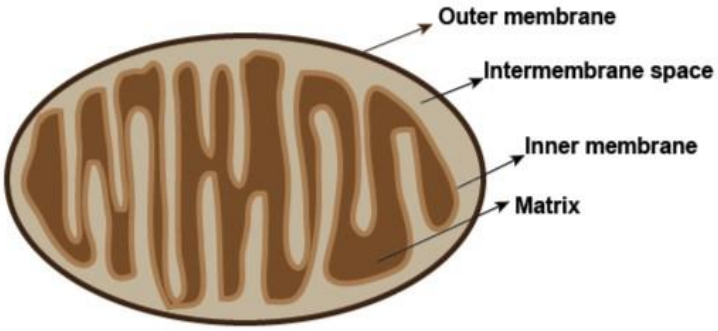

Figure 1.1 Mitochondrial structure. Schematic representation of the four mitochondrial compartments: the Outer (dark brown) and Inner (light brown) membranes, the mitochondrial intermembrane space (beige) and the mitochondrial matrix (brown).

Mitochondria have retained part of their genome, although this mitochondrial DNA only encodes less than 1% of the total mitochondrial proteome, encoding only 13 polypeptides (all of them involved in the respiratory chain). Thus, specialised import pathways have evolved to ensure the proper targeting and sub-mitochondrial sorting of essentially all the mitochondrial proteins (Becker et al., 2012, Chacinska et al., 2009, Chatzi et al., 2016, Wiedemann and Pfanner, 2017).

1.2 Mitochondrial import pathways

Mitochondria are formed by approximately 1000 proteins for the yeast *Saccharomyces cerevisiae* (*S. cerevisiae*) (Vögtle et al., 2017), and over 1500 proteins for mammalian mitochondria (Pagliarini et al., 2008, Taylor et al., 2003). However, these genomes encode only 13 proteins and 7 proteins for humans and yeast, respectively (Wiedemann and Pfanner, 2017). Hence, the remaining 99% of mitochondrial proteins are encoded in the nucleus and translated in cytosolic ribosomes and need to be imported. Therefore, mitochondria possess elegant and complex mechanisms that control the mitochondrial protein biogenesis. Most of the mitochondrial protein precursors are synthesised with targeting signals that not only lead the proteins to mitochondria but also directs them to their correct mitochondrial compartment. There are five main import pathways described so far, i.e. the presequence pathway, the carrier pathway, the ß-barrel pathway, the mitochondrial import and assembly pathway (MIA) and the import pathway followed by OM proteins with α-helical transmembrane segments (Figure 1.2).

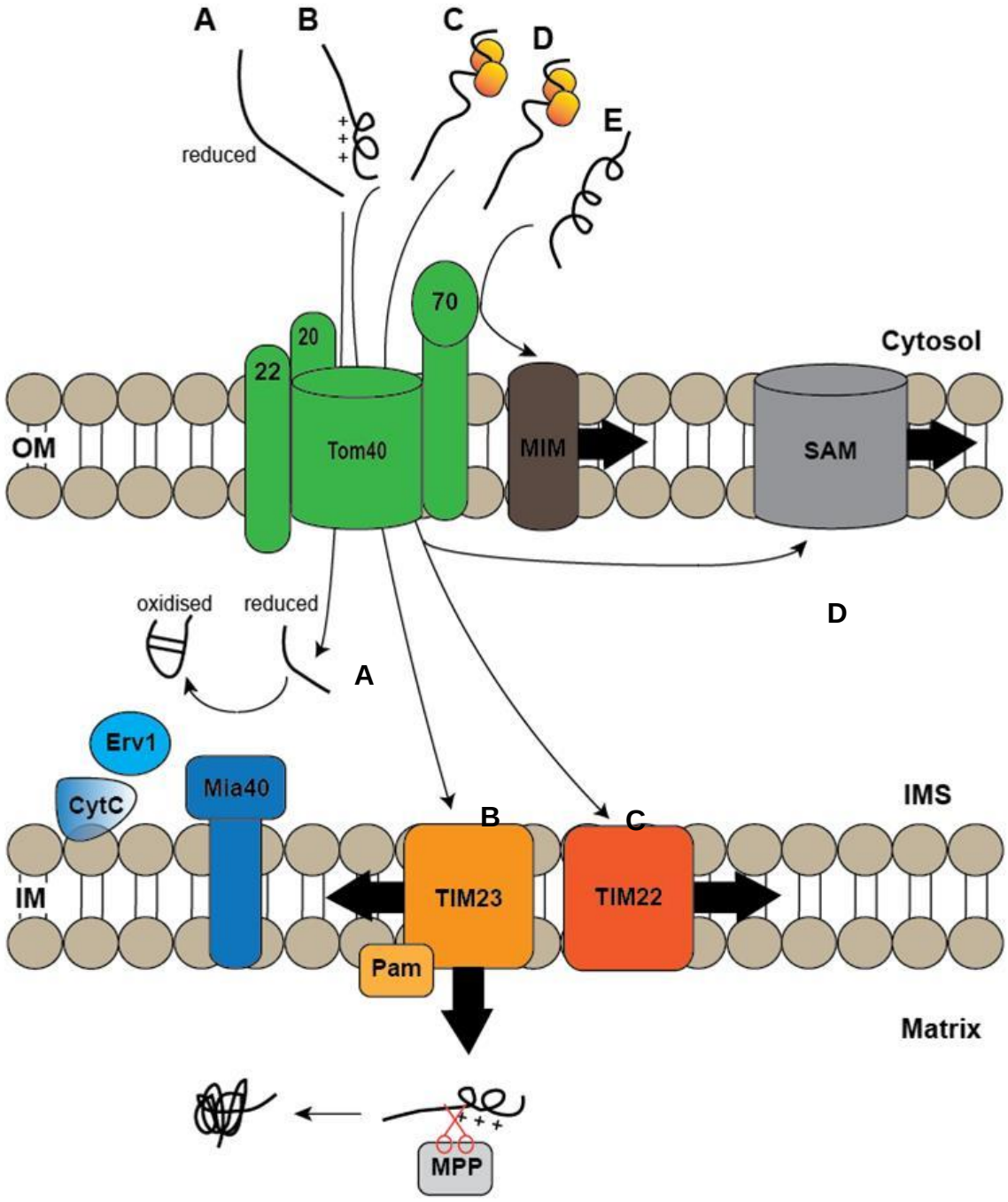

Figure 1.2 Overview of the import pathways into mitochondria. Protein precursors translated in the cytosol cross the mitochondrial OM through the Tom40 channel. Once inside mitochondria, these precursors are sorted into **(A)** the mitochondrial IMS, **(B)** the mitochondrial matrix, **(C)** the mitochondrial IM or **(D)** the mitochondrial OM. **(A)** Reduced protein precursor is oxidised by the MIA pathway which folds and traps the protein. **(B)** Precursors containing a positively charged mitochondrial targeting-sequence (MTS) cross the IM on a membrane potential dependent fashion. Once in the matrix, mitochondrial protein peptidases cleave the MTS and the protein is folded. **(C)** Protein precursors are chaperoned to the mitochondrial OM vicinity by cytosolic chaperones. Once in the IMS, the small Tims complexes take them to the TIM22 complex before their insertion into the mitochondrial IM. **(D)** β-barrel protein precursors interact with the small Tims complexes in the IMS lumen and a β-signal in their last β-sheet is recognised by the inner face of the Sam50 channel prior their lateral release into the mitochondrial OM. **(E)** α-helical precursors presumably are inserted into the mitochondrial OM membrane by interaction with the MIM complex with or without the help of other proteins like Tom70.

1.2.1 Translocase of the outer membrane (TOM)

The main gate for protein translocation into mitochondria is the translocase of the outer membrane (TOM) complex, which is formed by the channel-forming ß-barrel protein Tom40, three protein receptors (Tom22, Tom20 and Tom70) and three non-essential small Tom proteins (Tom5, Tom6 and Tom7) (Mokranjac and Neupert, 2015, Hill et al., 1998, Yamano et al., 2008). Tom20 and Tom70 recognise incoming protein precursors and transfer them onto the central receptor, Tom22, and from there to the Tom40 channel. Tom22 is important in the formation of a mature TOM complex (van Wilpe et al., 1999, Mokranjac and Neupert, 2015). Together with Tom22, the three small Tom proteins play a structural role in the assembly and stability of the complex (Wiedemann and Pfanner, 2017).

1.2.2 Presequence pathway

The majority of protein precursors are synthesised with N-terminal extensions of 10-60 amino acids length that form positively charged amphiphilic α-helical structures which are specifically recognized by the Tom20 receptor (Abe et al., 2000). The precursors are then transferred to Tom22 and then to the channel formed by Tom40. After crossing through the Tom40 channel, the protein precursors are transferred to Tom7 and the IMS domain of Tom22. Then, these presequence-precursors engage with the translocase of the inner membrane (TIM), the TIM23 complex, formed by Tim50, Tim23, Tim 17 and Tim21. Here, Tim50 binds to the precursors emerging from Tom40 (Tamura et al., 2009b). Tim50 interacts with the channel forming protein Tim23 so that the TIM23 channel opens to allow further translocation into the matrix (Meinecke et al., 2006). Finally, the presequence translocase-associated motor (PAM), whose central component is the adenosine triphosphate (ATP) dependent heat shock protein (Hsp) 70, completes the translocation across the IM in an inner membrane potential ($\Delta\Psi$) and ATP dependent manner (Nelson and Schatz, 1979). This latter is facilitated by Tim44, which tethers the Tim23 channel with the PAM complex. The matrix side of mitochondria is negatively charged and thus attracts the positively charged presequence (Martin et al., 1991). Additionally, some mitochondrial IM proteins (like the cytochrome b2 and cytochrome c1) follow the same import pathway but they contain a hydrophobic segment behind

the presequence which arrests the transfer across the IM and are laterally released from the Tim23 channel (this is a specific sorting pathway that follows the stop-transfer mechanism). Once in the mitochondrial matrix, the presequence is cleaved by the matrix processing peptidase (MPP, a zinc-binding heterodimeric protein) (Hawlitschek et al., 1988). Some proteins of the IM are cleaved a second time to remove the hydrophobic sorting sequence by the IM peptidase (IMP) (Mossmann et al., 2012). Alternatively, some precursors are imported into the matrix and then incorporated into the IM from the matrix side by the oxidase assembly (OXA) export machinery (Stiller et al., 2016). This OXA pathway is responsible also for facilitating the association to the IM of the hydrophobic proteins that are encoded by the mtDNA and are then assembled into the OPXHOS complexes in the IM. The schematic representation of the presequence pathway is shown in Figure 1.3.

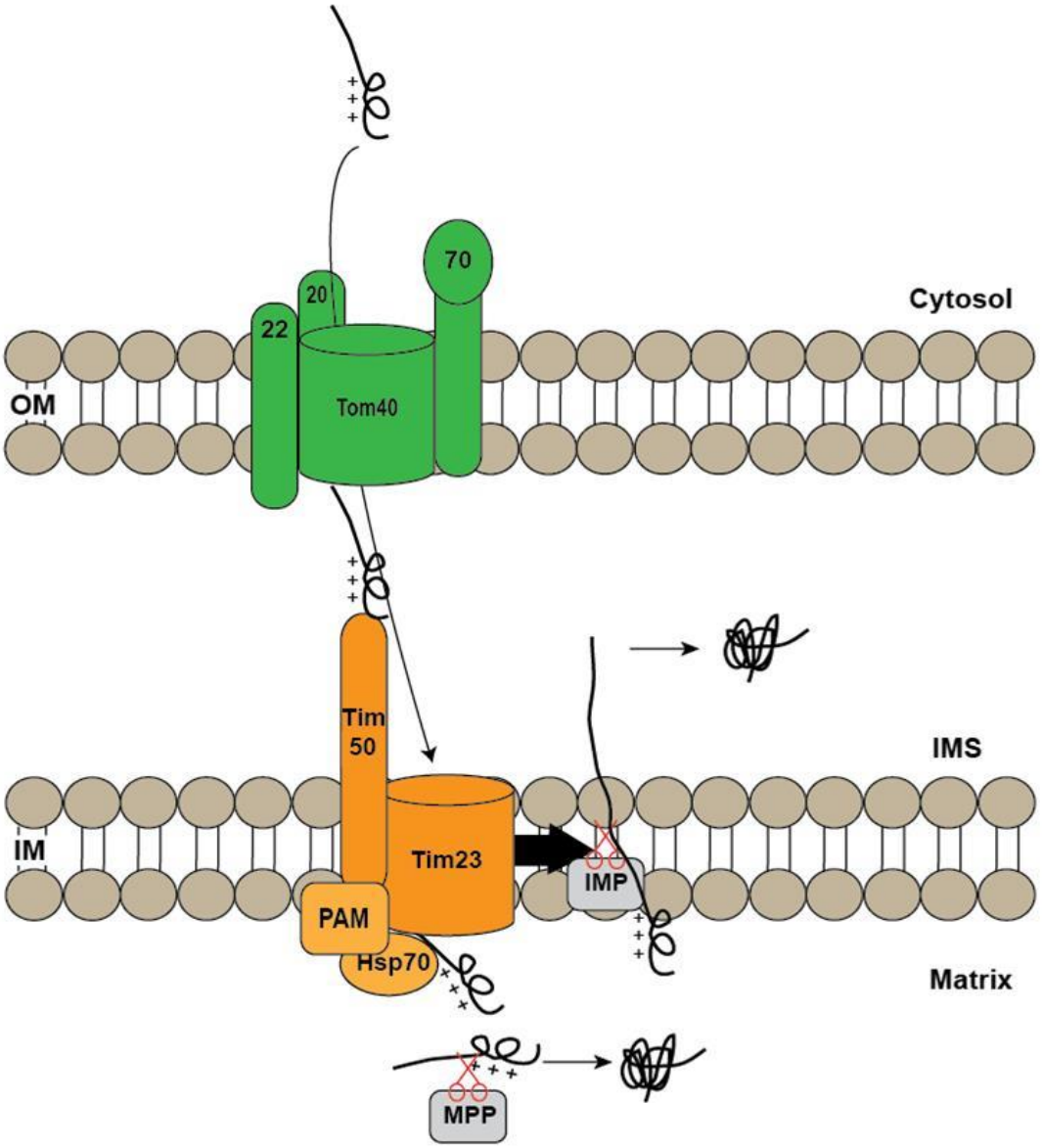

Figure 1.3 Presequence import pathway. Schematic representation of the presequence import pathway. Mitochondrial protein precursors containing a positively charged MTS are recognised by the receptor Tom20 and translocate the OM through the Tom40 channel. As the precursors emerge to the IMS, the receptor of the TIM23 complex, Tim50, interacts with them and hands them over the Tim23 channel. The presequence precursors can then be released to the matrix or be trapped into the IM by a hydrophobic extra segment before the positively charged signal and then laterally released to the IM. Finally, peptidases on the matrix side or the IM cleave off the presequence.

1.2.3 Carrier pathway

Hydrophobic inner membrane proteins that do not possess a presequence follow a different pathway. Many of these proteins belong to the family of metabolite carrier proteins that are embedded in the IM and are responsible for the transport of specific metabolites between the cytosol and the matrix. The specific pathway that transports these proteins into mitochondria and underpins their integration into the IM is called the carrier pathway. Members of this family contain usually six α-helical transmembrane segments. Members of the metabolite carriers are responsible for the translocation of critical metabolites like ATP, ADP (the ADP/ATP carrier) and phosphate (the phosphate carrier). To reach mitochondria, carrier precursors bind to cytosolic chaperones of the Hsp70 and Hsp90 family (Figure 1.4). Once in proximity to the OM, the carrier precursor-Hsp70/Hsp90 complex binds to the Tom70, which has binding regions for both the carrier precursor and the chaperone (Young et al., 2003). The chaperones are then released upon ATP hydrolysis and the carrier precursors are transferred through the Tom40 channel (Wu and Sha, 2006, Young et al., 2003). Upon entering the IMS, the protein precursors interact with the Tim9-Tim10 or Tim8-Tim13 chaperone complexes (small Tims complexes) of the IMS. These are heterohexameric complexes (Beverly et al., 2008, Vial et al., 2002) that transport the precursor to the TIM22 complex in the IM (Lu et al., 2004b, Gebert et al., 2008). The TIM22 complex consists in the receptor Tim54, the channel-forming protein Tim22 and the small Tims complex (Figure 1.4). The small Tims complex is recruited by Tim54 (Gebert et al., 2008) Then, using $\Delta\Psi$ as energy source, the precursor is inserted in the Tim22-channel and finally is laterally released into the IM.

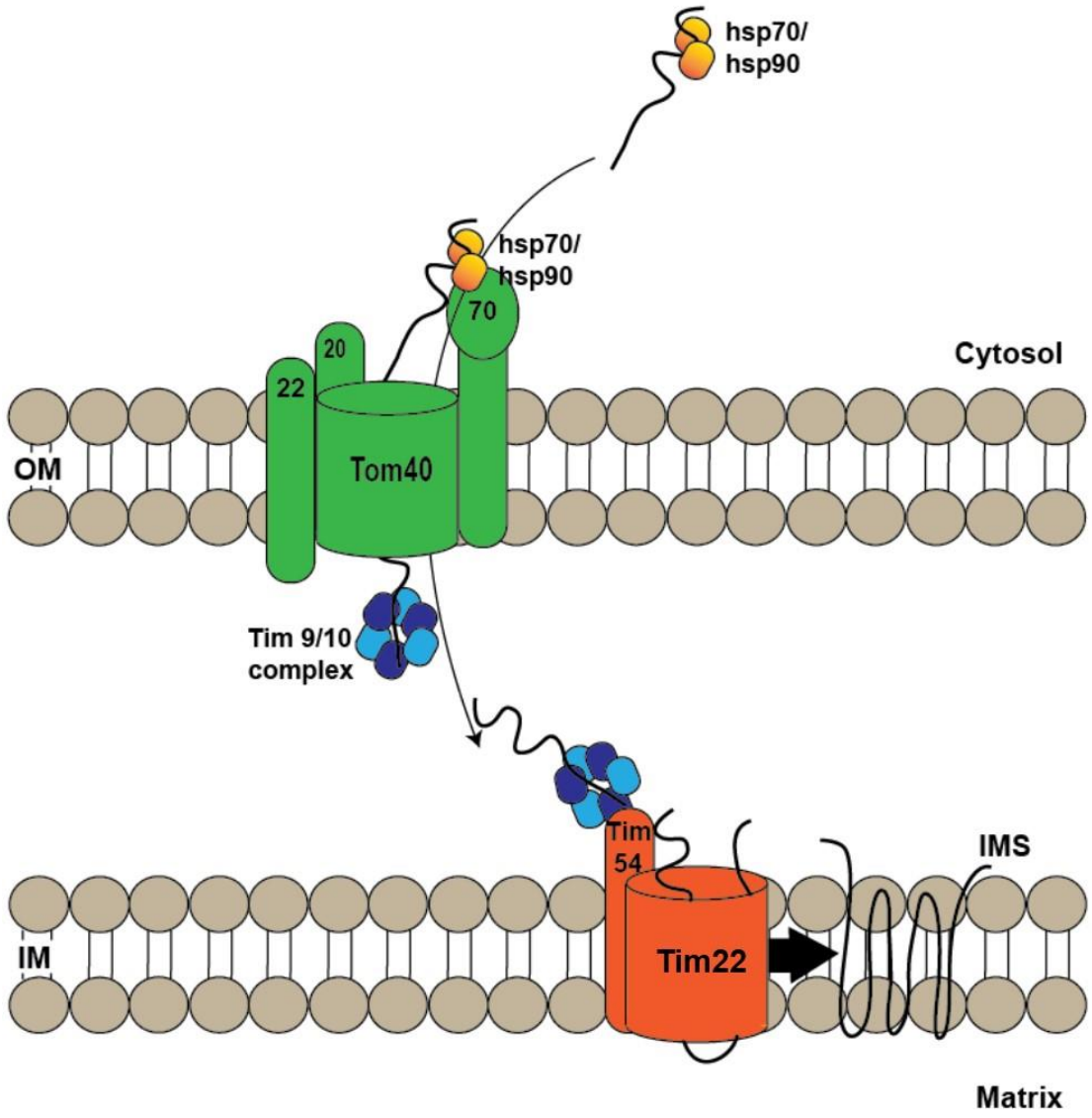

Figure 1.4 Carrier import pathway. Schematic representation of the carrier import pathway. Protein precursors are chaperoned in the cytosol by hsp70 and hsp90 to the Tom70 receptor. After the chaperones are released, the precursor crosses through the Tom40 channel and once in the IMS, the chaperone complex of small Tims takes the incoming precursor and delivers it to the Tim54 receptor and then to the Tim23 channel. Finally, the protein precursor is laterally released into the IM.

1.2.4 β-barrel pathway

There are two different types of integral proteins in the outer membrane of mitochondria, the α-helical and the ß-barrel proteins (Walther and Rapaport, 2009). The presence of ß-barrel proteins witnesses the endosymbiotic origin of mitochondria from Gram negative bacteria. Among the mitochondrial OM ß-barrel proteins are the channel-forming proteins Tom40 and Sam50 and the metabolite channel, porin. The cytosolic translated ß-barrel precursors contain a ß-hairpin element that is recognised by the TOM complex (Jores et al., 2016). In the IMS lumen, the small Tims complex pulls the incoming precursor out of the channel. Then, the insertion into the OM is driven by the SAM complex, which comprises the channel-forming protein Sam50 (also known as Tom55) and two peripheral proteins, Sam35 and Sam 37. The incoming precursor interacts with the inner mitochondrial face of Sam50 by a signal (the ß-signal) that is present in the last ß-strand of these ß-barrel proteins (Kutik et al., 2008). This ß-signal replaces the internal ß-signal of Sam50 between the Sam50's ß-strands 1 and 16 in a hairpin orientation (Höhr et al., 2018). After this gate-opening, the subsequent hairpins insert and the folded ß-barrel protein is finally laterally released into the OM (Höhr et al., 2018). A schematic representation of this model is shown in section 7.1.2 of Chapter 7 and in panel A of Figure 1.5.

1.2.5 Insertion of α-helical proteins into the mitochondrial OM

The import mechanisms of the second group of OM integral proteins, the α-helical proteins are not well defined yet. However, the mitochondrial import complex (MIM) has been shown to aid the insertion of these types of proteins. Additionally, it has been shown that other proteins like Tom70 and proteins from the SAM complex, together with the MIM complex are involved in the insertion of these α-helical tail or signal-anchored and polytopic proteins (panel B Figure 1.5) (Berthold et al., 1995, Popov-Celeketic et al., 2008, Papić et al., 2011).

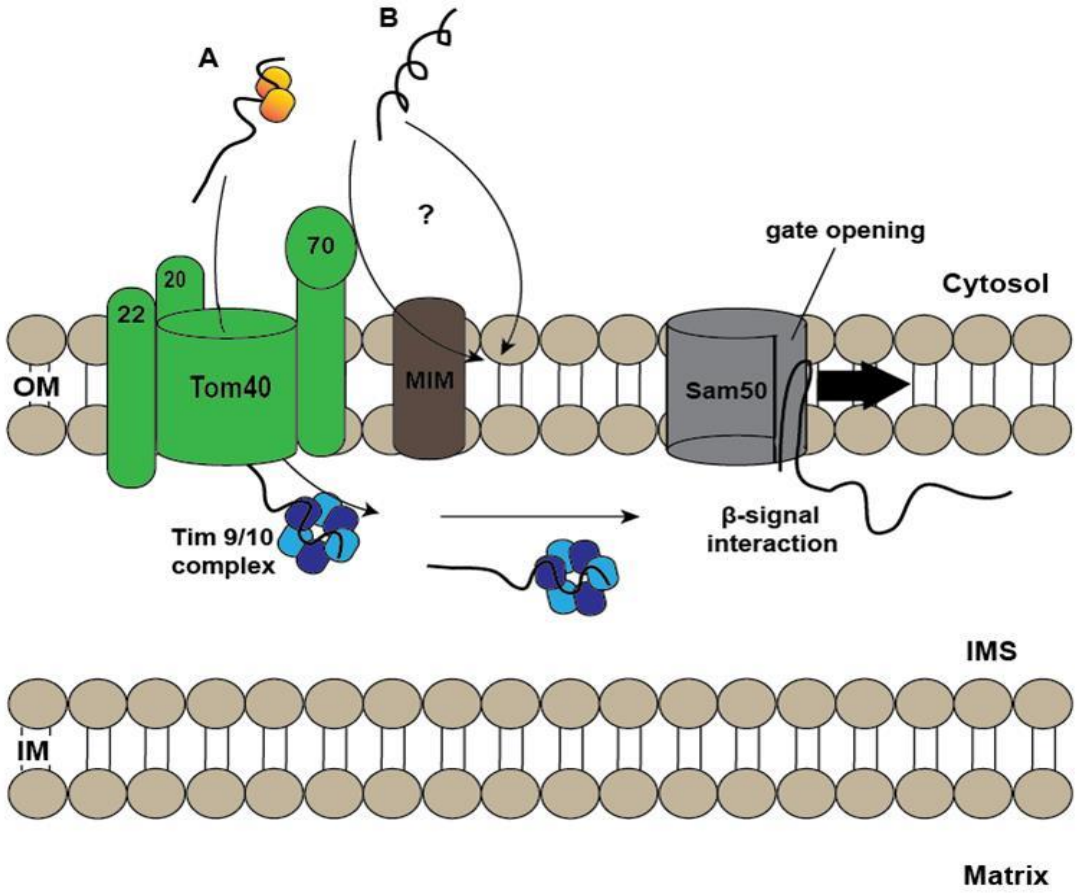

Figure 1.5 Insertion of β-barrel and α-helical proteins into the mitochondrial OM. (A) The β-barrel protein precursor crosses the mitochondrial OM via the TOM complex and then in the IMS, the small Tims complex drives it to the SAM complex. There, the β signal of the precursor interacts with β strand 1 of Sam50, this event opens a gate in Sam50 between β1 and β16. The protein precursor is inserted in hairpins until its laterally released into the OM. **(B)** α-helical precursors presumably are inserted into the mitochondrial OM membrane by interaction with the MIM complex with or without the help of other proteins like Tom70.

1.2.6 Mitochondria Import and Assembly pathway for IMS proteins

The mitochondrial intermembrane space assembly machinery (MIA) is the mechanism that accounts for the import of most of the IMS proteins ((Sideris and Tokatlidis, 2010) and Figure 1.6) . Typical substrates of this pathway are proteins that contain characteristic cysteine motifs within their sequence, such as CX_3C and CX_9C motifs that can form intramolecular disulfide bonds (Lu et al., 2004a, Lutz et al., 2003, Gabriel et al., 2007). Those protein precursors are targeted to the IMS of mitochondria by an internal mitochondrial IMS signal (ITS) which consists on a docking Cys residue and two critical residues, one hydrophobic residue and one aromatic residue located in positions +/- 4 and +/- 7, respectively, from the docking Cys residue (Milenkovic et al., 2009, Sideris et

al., 2009). Then, the IMS precursors translocate into the mitochondrion through the TOM complex in an unfolded, thus reduced conformation (Stojanovski et al., 2012, Durigon et al., 2012).

The main effector of this pathway is the oxidoreductase Mia40 (Banci et al., 2009, Chacinska et al., 2004, Kloppel et al., 2011), which is called CHCHD4 in humans (Erdogan et al., 2018). Mia40 possess two stable intramolecular disulfide bonds buried in the folded core of the protein and one disulfide between a pair of cysteines exposed to the surface of the protein, the active (oxidised) motif, the CPC motif (Banci et al., 2009). Once in the IMS, hydrophobic interactions between a hydrophobic-binding cleft in Mia40 and the precursors place the Cys residue of the substrate in a position that favours its electrophilic attack by one of the Cys on Mia40 (Milenkovic et al., 2009, Sideris et al., 2009, Sideris and Tokatlidis, 2010). The latter results in a mixed disulfide between Mia40 and the protein precursor. This mixed disulfide is then resolved by a nucleophilic attack from a second cysteine in the substrate, resulting in an intramolecular disulfide in the protein. This process causes the CPC motif of Mia40 to be reduced. In turn, Mia40 is re-oxidized by the other main component of the MIA pathway, the protein essential for respiration and viability 1 (Erv1). Erv1 is a flavin adenine dinucleotide (FAD) sulfhydryl oxidase with three conserved Cys pairs (Lionaki et al., 2010). Erv1 oxidises the CPC motif in Mia40 and shuttles the electrons to its FAD domain and from there onto molecular oxygen either directly or via cytochrome c (Banci et al., 2011, Bien et al., 2010). Furthermore, the re-oxidation of Mia40 is aided by the helper of Tim of 13kDa (Hot13) keeping Mia40 in a Zn-free state (Curran et al., 2004, Mesecke et al., 2008). Finally, if the oxidative folding of MIA substrates is impaired, the substrates can be translocated outside Tom40 where they are degraded by the proteasome (Bragoszewski et al., 2013, Bragoszewski et al., 2015). In addition, a recent study proposed that the thiol peroxidase Gpx3 has a role in the redox quality control of the MIA pathway (Kritsiligkou et al., 2017).

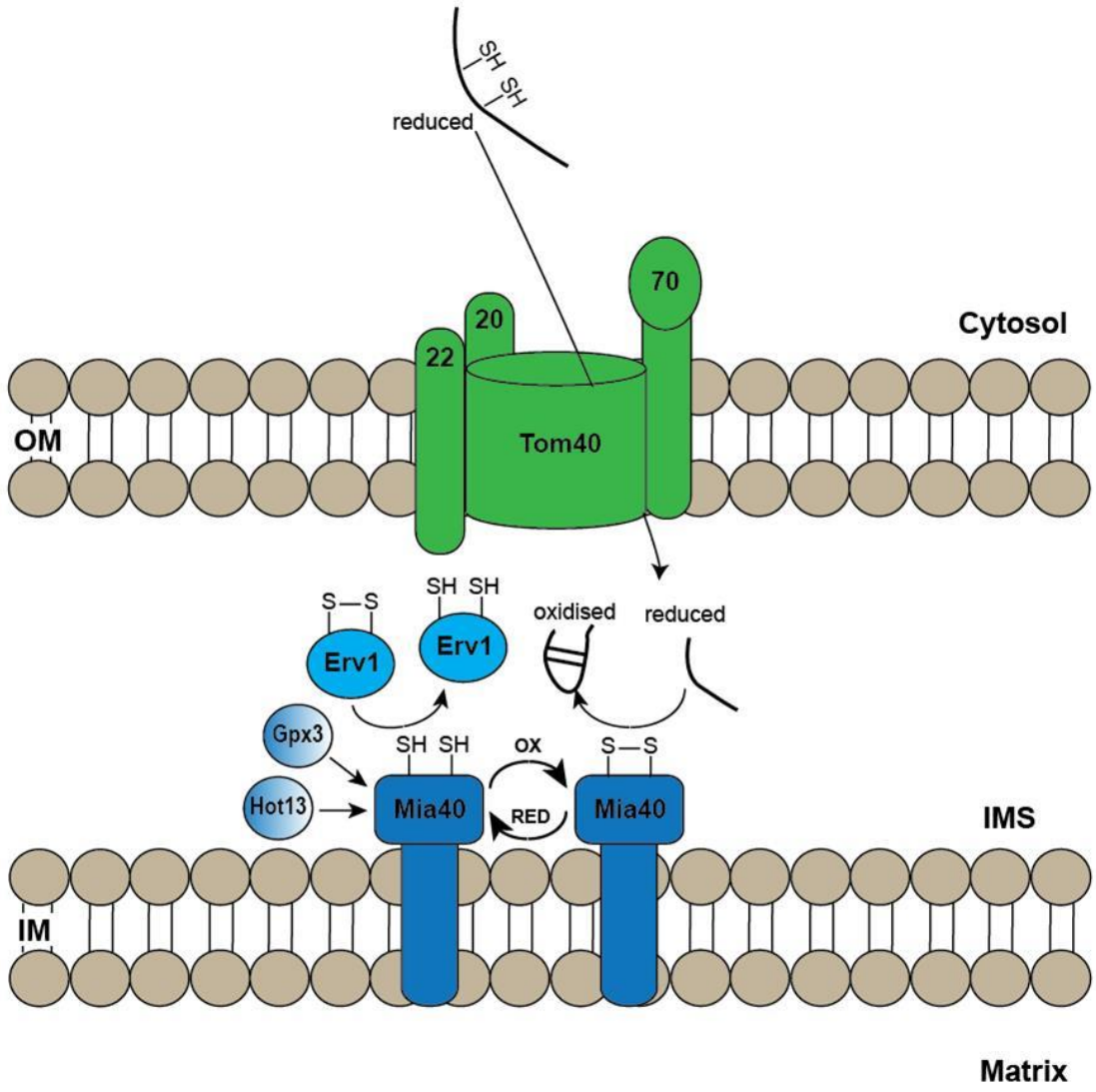

Figure 1.6 Mitochondrial Import and Assembly pathway. Most of the proteins residing in the IMS are imported through the mitochondrial Import and Assembly machinery (MIA pathway). The protein precursor enters mitochondria through the Tom40 channel in an unfolded (reduced) state. In the IMS, the oxidoreductase Mia40 oxidises intramolecular Cys of the precursors into disulfide bond. The resulting protein is folded and trapped in the IMS. On the other hand, reduced Mia40 is re-oxidised by the sulfhydryl Erv1, which transfers the electrons to molecular oxygen via a FAD domain. The re-oxidation of Mia40 is also facilitated by Gpx3 and Hot13.

The aforementioned import pathways take place in different cellular compartments that represent a variety of conditions (e.g. pH levels and redox state) that influence their function. Among these conditions, the reducing and oxidising (redox) environment is of particular importance as it is involved in essential processes like cellular proliferation and death (Trachootham et al., 2008, Schafer and Buettner, 2001). This redox environment is determined by the balance between the generation and removal of both reactive oxygen species (ROS) and reactive nitrogen species (RNS). ROS and RNS are products of normal cell metabolism which in low concentrations are involved in beneficial cell

signalling and regulation, whilst at elevated levels they lead to the formation of damaging species (Zhang et al., 2016, Phull et al., 2018).

1.3 Redox homeostasis in the cell

1.3.1 ROS and RNS

Reactive nitrogen species are a group of strong oxidants that includes peroxynitrite, which is formed by the non-enzymatic reaction between nitric oxide (NO^-) and O_2^- (Martínez and Andriantsitohaina, 2009). Other RNS like nitrogen dioxide and nitrosoperoxycarbonate derive from peroxynitrite. RNS has been shown to exhibit cytotoxic effects damaging lipids, DNA and proteins (Pacher et al., 2007, Wink et al., 1991, Hibbs et al., 1987, Radi et al., 1994).

On the other hand, reactive oxygen species (ROS) are free radical products of respiratory metabolism. ROS species include the superoxide anion (O_2^-), hydrogen peroxide (H_2O_2) and hydroxyl radicals (OH-). The main source of ROS is leakage of electrons during reduction of oxygen to H_2O (Boveris, 1984). Additionally, the oxidative folding process of the mitochondrial IMS can also lead to the production of hydrogen peroxide. Accordingly, it has been shown that up to 85% of the cellular ROS is produced by mitochondria (Aon et al., 2012). In particular, O_2^- is produced from the reduction of molecular oxygen, this species is moderately reactive but it also serves as precursor of most of the other species. Dismutation of O_2^- generates H_2O_2 and is catalysed by the enzyme superoxide dismutase (Sod) (Sturtz et al., 2001). Furthermore, hydrogen peroxide can be reduced and form the high reactive species hydroxyl radical which reacts almost indiscriminately with the cellular components (Beckman et al., 1994). Hydroxyl radical damages proteins primarily by oxidation of amino acyl residues (e.g. cysteine residues), these oxidised proteins are reactive and lead to unfolded proteins and the generation of more free radicals and the production of phenoxy-radicals (Gebicki et al., 2002, Fu et al., 1995). Another major target of hydroxyl radical is the unsaturated fatty acyl groups which induce lipid peroxidation forming lipid hydroperoxides which can affect the composition and structure of the cellular membranes (Poljak et al., 2003, Ademowo et al., 2017). This oxidation not only affects the cellular structure and

dynamics but is also associated with DNA damage, cell death (Fleury et al., 2002) and different diseases like cancer and neurodegenerative disorders.

However, as mentioned before ROS and RNS are produced naturally as side products of metabolic reactions and in physiologic concentrations are involved in signalling of many important cellular pathways such as growth regulation and apoptosis (Shadel and Horvath, 2015). The fine equilibrium that maintains the redox homeostasis in the cell is achieved by the balance between ROS and RNS producing pathways and the reductive machinery of the cell. This reductive machinery includes both enzymatic and non-enzymatic reactions.

1.3.2 Reductive machinery of the cell

Among the several mechanisms that the cell possesses to scavenge the excess of oxidative species are the cofactors glutathione (GSH), reduced nicotinamide adenine dinucleotide (NADH) and reduced nicotinamide adenine dinucleotide phosphate (NADPH). In addition, the enzymatic reductive response includes catalases, superoxide dismutases and the two main thiol-reductive systems of the cell, the thioredoxin (Trx) and the glutaredoxin (Grx) systems.

1.3.2.1 Glutathione

Glutathione (GSH) was first discovered in the late 1800s and named *philotion* (from the Greek words for love and sulfur) (Meister, 1988). It is an L-γ-glutamyl-L-cysteinyl-glycine tripeptide involved in many essential roles for the cell such as signalling regulation (mainly through glutathionylation of proteins) and acting as the main redox buffer in the cell (Schafer and Buettner, 2001). Furthermore, GSH has also been proposed as critical in iron metabolism and that its antioxidant properties are only used as backup of other mechanisms like the Trx system (Kumar et al., 2011).

GSH is synthesised in the cell in two consecutive reactions that depend on adenosine triphosphate (ATP). In the first step, γ-glutamylcysteine synthetase (GSH1) catalyses the formation of γ-glutamylcysteine from glutamic acid and cysteine, and in the next step glutathione synthetase (GSH2) catalyses the addition of glycine to the dipeptide (Meister, 1988). GSH is present in high concentrations of up to 10mM in most living cells, its structure determines

important features as the γ-glutamyl bond confers it resistance to proteolytic challenges and the thiol moiety has strong nucleophilic properties (Meister and Anderson, 1983). Glutathione is essential for yeast viability and its defence against oxidative stress, mainly in the form of ROS derived reactions (Grant et al., 1996). However, it has been shown that the presence of GSH2 is dispensable for yeast growth as the accumulation of the γ-glutamylcysteine dipeptide helps to maintain the mitochondrial function, although the dipeptide did not fully cover the functions of GSH (Grant et al., 1997).

In the cell, glutathione can be found in its reduced (GSH) and oxidised (GSSG) forms. In fact, due to the presence of glutathione in virtually all the cellular compartments, the measurement of the GSH/GSSG ratio is taken as an indication of the total cellular redox state (Schafer and Buettner, 2001). The overall ratio of glutathione is the result of the particular GSH/GSSG ratios in each cellular compartment. An interesting example is that of yeast mitochondria, which contains two different subcompartments, the mitochondria matrix and the IMS, each one with distinct GSH/GSSG ratios. The latter also exemplifies the difficulty to measure this ratio and the impact that other factors have on it since the matrix has been shown to be more reducing (GSH/GSSG ratio 900/1) than the IMS (Hu et al., 2008). However, the IMS ratio has been a matter of debate as two different studies report opposite results. On the one hand, one claims the GSH/GSSG ratio of the IMS to be independent of the cytosolic one and more oxidising than that of the matrix (GSH/GSSG ratio 250/1) (Hu et al., 2008). On the other hand, it was reported that the IMS GSH pool is connected and in equilibrium to that of the cytosol and that even the cytosolic but not the mitochondrial isoform of the GSH reductase influences this pool (Kojer et al., 2012). The difference between both results can be attributed to the way they measure the GSH levels. In the first study they used a probe that was prone to oxidation only when the full Grx system was present, thus it did not merely depend on the presence of GSH in the subcompartment but also in the presence of the effector proteins (Hu et al., 2008). In the second study they used a probe fused to Grx and thus bypassed the problem as this probe only depended on GSH for its reduction (Kojer et al., 2012).

1.3.2.2 NADPH

The phosphorylated form of nicotinamide adenine dinucleotide (NADP) is a pyridine nucleotide that is present in almost every organism identified so far. Together with the non-phosphorylated form (NAD), they serve as cofactors in electron transfer reactions in the cell but also have important signalling and regulatory roles as they have been associated with the expression of several genes (Rutter et al., 2001, Liou et al., 2005, Guse and Lee, 2008). Despite of their structural similarity (Figure 1.7) and the fact that their redox pairs $NADH/NAD^+$ and $NADPH/NADP^+$ have similar redox potentials, their roles in the cell are very different and in cases opposite.

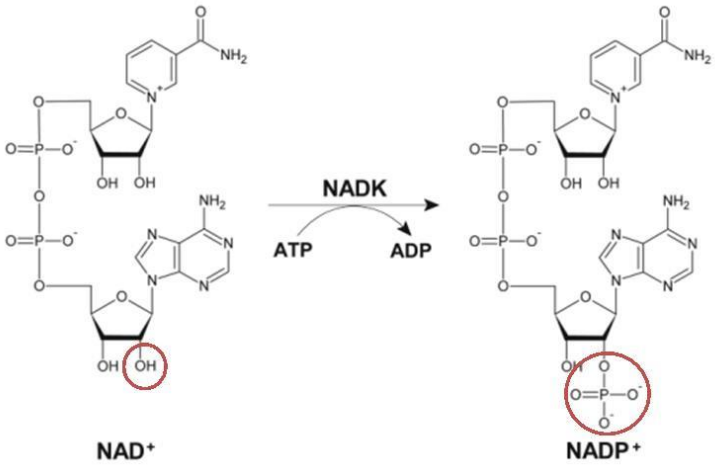

Figure 1.7 Structure of NAD and NADP. NADP can be generated through the phosphorylation of NAD by an NAD kinase where ATP serves as Pi donor. The phosphate group is added onto the adenosine ribose. The redox active site is localised on pyridine ring of the nicotinamide (top part of both structures). Modified from Agledal *et al.* 2010

In particular, the reduced form of nicotinamide adenine dinucleotide phosphate (NADPH) is generated by the transfer of a phosphate group onto the adenosine ribose of NAD at its 2'-hydroxyl group in a reaction catalysed by NAD kinase (Outten and Culotta, 2003, Agledal et al., 2010). Thereby NADP is composed by a ribosylnicotinamide 5'-phosphate coupled with the 5'-phosphate of the adenosine 2'-5'-bisphosphate by a pyrophosphate linkage with the redox active site localised in the pyridine ring from the nicotinamide. NADP is found mainly in its reduced form within the cell. NADPH is formed from the reduction of its oxidized form ($NADP^+$) by the pentose phosphate pathway (PPP) enzymes glucose 6-phosphate dehydrogenase (g6pd) and 6-phosphogluconate dehydrogenase (6PGD) (Kruger and von Schaewen, 2003, Riganti et al., 2012), the

mitochondrial, cytosolic and peroxisomal isoforms of NADP-specific isocitrate dehydrogenase (Idp1, Idp2 and Idp3 respectively) (Minard et al., 1998), the cytosolic acetaldehyde dehydrogenase (Grabowska and Chelstowska, 2003), the malic enzyme and the transhydrogenase (Ying, 2008). NADPH serves as an electron donor for many biosynthetic and antioxidant defence reactions (Agledal et al., 2010, Minard and McAlister-Henn, 2001) and it is the electron donor of both main thiol-reductive pathways in the cell, the glutaredoxin and the thioredoxin systems. Besides that, NADPH also integrates a huge metabolic network that couples all the processes involving these enzymes (see Figure 4.1), which are directly related with the conditions of the environment where the different stages of protein biogenesis take place.

1.3.2.3 Superoxide dismutase and Catalases

In the yeast *S. cerevisiae*, two different superoxide dismutase (Sod) exists. Sod1, which localises mainly in the cytosol and requires binding of Cu^{2+} and Zn^{2+} ions for its optimal function (Slekar et al., 1996). On the other hand, Sod2 depends on Mn^{2+} cations for its function and localises to the mitochondrial matrix (Lyons et al., 2000). The dismutation is a reaction in which one compound converts into two products of different oxidation states. Thus, both Sod enzymes catalyse the dismutation of O_2^- into molecular oxygen or hydrogen peroxide, which can be converted into water by catalases.

Catalases are involved in the breakdown of hydrogen peroxide to water and oxygen but also in the oxidation of H^+ donors such as ethanol and methanol. *S. cerevisiae* possess a cytosolic catalase, Ctt1, and a dually localised catalase, Cta1 which can be found in peroxisomes and mitochondrial matrix (Petrova et al., 2004, Hartig and Ruis, 1986). Catalase has been proposed as part of the adaptive stress response to hydrogen peroxide especially during stationary growth phase in yeast (Izawa et al., 1996).

1.3.2.4 The glutaredoxin (Grx) system

The glutaredoxin system comprises the effector protein glutaredoxin, the reductase glutathione reductase (Glr) and GSH (Figure 1.8). In yeast *S. cerevisiae*, two Grx (Grx1-2) and three Grx-related (Grx3-5) proteins can be

found. The Grx and Grx-related proteins differ in their putative active sites where Grx have a dithiol mechanism and Grx-related proteins a monothiol mechanism for the transfer of electrons onto their targets (Bushweller et al., 1992).

Grx are oxidoreductases involved in protein regulation and sulfur metabolism (Grant, 2001). The reductive role of Grx proteins in the cell is important in particular due to its involvement in the removal of S-glutathionylation of proteins (Ghezzi, 2013), as protein glutathionylation is involved in regulation of protein activity, in particular that involving redox reactions (Gilbert, 1984, Ghezzi, 2005). For their function, Grx depend on GSH for their reducing activity and it has been demonstrated that both isoforms have different specificity for oxidising species. Grx1 has been related to oxidative stress by O_2^- whereas Grx2 shows affinity to hydrogen peroxide as shown by specific sensitivity to this oxidising species in KO mutants for each Grx protein (Luikenhuis et al., 1998). Interesting is the case of Grx2, which is responsible for the majority of Grx activity in yeast (Grant et al., 2000), because it can be found both in the cytosol and the mitochondria. In fact, it was proposed as the reductive effector that bridges the high amounts of GSH in mitochondria to the redox balance of the organelle (Kojer et al., 2015).

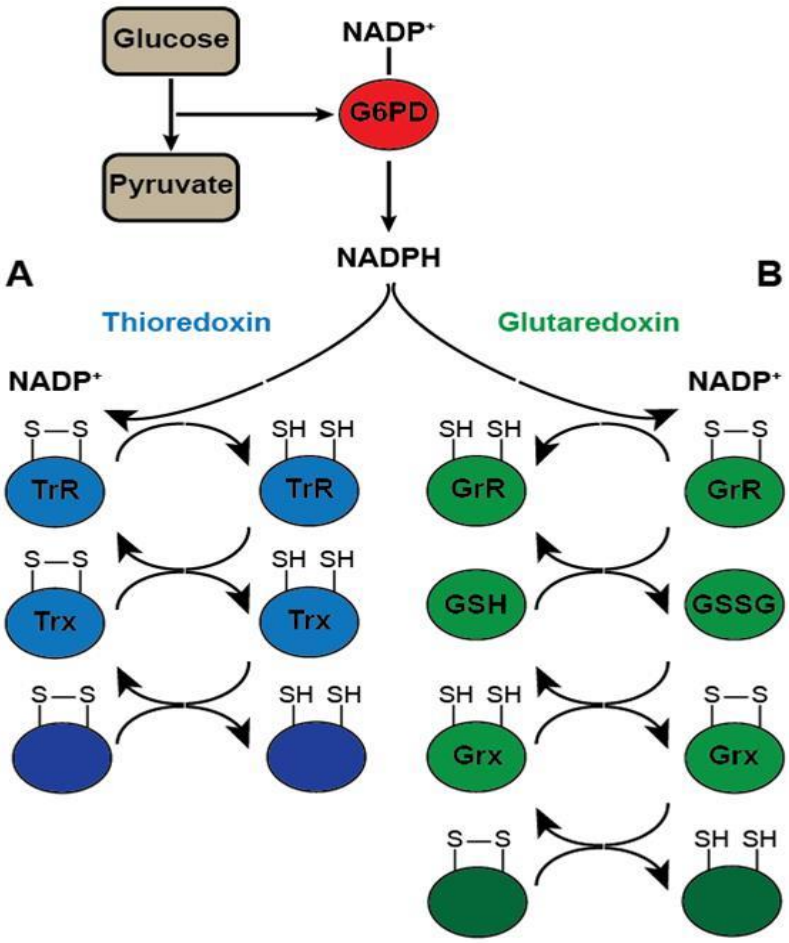

Figure 1.8 Glutaredoxin and Thioredoxin systems. The electron flux for both the Grx and Trx systems starts from NADPH, which is mainly produced by glucose-6-phosphate dehydrogenase in the cytosol. **(A)** The thioredoxin reductase is reduced by electrons derived from NADPH and the reductase in turn then reduces the thioredoxin protein. Finally, the thioredoxin protein transfers these electrons onto its substrates. **(B)** The glutaredoxin system follows a similar electron flux with an extra step involving transfer of electrons from glutathione reductase onto glutathione, and subsequently, from glutathione onto glutaredoxin and then to glutaredoxin substrates. Image taken from Cardenas-Rodriguez, M. and Tokatlidis, K. 2017.

1.3.2.5 The thioredoxin (Trx) system

The main thiol-reductive system in the cell is the thioredoxin system. It consists in the protein effector thioredoxin and its reductase, the thioredoxin reductase (TrR) (Figure 1.8). In *S. cerevisiae* three Trx (Trx1-3) isoforms and two TrR (TrR1-2) isoforms have been found (Pedrajas et al., 1999, Kojer et al., 2012). They differ in their cellular localisation; Trx1 has a dual mitochondrial and cytosolic localisation whereas Trx2 is exclusively cytosolic and Trx3 localises to the mitochondrial matrix. Likewise, TrR1 localises to both the cytosol and the mitochondria and TrR2 to the mitochondrial matrix.

Together with Grx, thioredoxin is involved in the antioxidant cellular response (Draculic et al., 2000) and their reductive capacity is also determined by their active CXXC motif. They are part of the thioredoxin superfamily whose members share a characteristic thioredoxin fold domain (See section 6.1.1).

Unlike the Grx system, the Trx system is present in all known organisms and plays important antioxidant roles (Pedrajas et al., 1999, Draculic et al., 2000, Garrido and Grant, 2002). The last is supported by the fact that Yap-1, a transcriptional activator protein that regulates several oxidative stress responsive genes, is constitutively activated in a Trx1 and Trx2 KO yeast strain (Izawa et al., 1999). Furthermore, deletions of Trx1 and Trx2 have been shown to impact cell cycle and sulfate assimilation (Muller, 1991). Despite these redox and protective functions, it has been shown that overexpression of Trx can have deleterious effects on aging and lifespan in mice studies (Cunningham et al., 2018). However, another study showed that these effects are particular of certain stage of life and that in early stages of mice life, overexpression of Trx might actually be beneficial (Cunningham et al., 2015). In this sense, the fine regulation and possibly the expression of the Trx system might changes as the organism develops throughout its life.

Besides these functions, members of the Trx are implicated in the regulation of protein import inside the cell like is the case of the endoplasmic reticulum, the mitochondrial IMS and bacterial periplasm.

1.4 Reductive and oxidative pathways in protein import

The disulfide insertion into proteins is a prone to error process that can harm the cell through protein misfolding. Thus, reductive systems together with the oxidative folding pathways regulate the import and proper folding of a considerable amount of proteins in the endoplasmic reticulum and the mitochondrial IMS. This process is also present in the bacterial periplasm which shows that it is conserved through evolution.

1.4.1 The bacterial periplasm

In the periplasm of Gram-negative bacteria, oxidative folding is driven by the periplasmic thiol-disulphide oxidoreductase disulphide bond (Dsb) A and B. DsbA is member of the thioredoxin family and is one of the most oxidising proteins known so far (Martin et al., 1993, Grauschopf et al., 1995). Just as its eukaryotic counterpart (see section 1.2.6 of this chapter), it oxidises Cys residues in the substrate protein (Collet and Bardwell, 2002) which results in the reduced form of DsbA (left panel A Figure 1.9). To recycle DsbA back to its functional oxidised form, DsbB accepts electrons from DsbA (Bardwell et al., 1993) to further transfer them onto quinone and then to molecular oxygen under aerobic conditions (Takahashi et al., 2004), or onto menaquinone and fumarate under anaerobic conditions (Takahashi et al., 2004).

On the other hand, to correct the formation of non-functional disufides bacteria possess the oxidoreductases DsbC and DsbD. DsbC has both isomerase and chaperone activity as shown by the accumulation of misfolded proteins in DsbC bacterial mutants (Rietsch et al., 1996). In turn, DsbC is kept reduced by the action of dsbD, which is embedded in the inner membrane with two periplasmic-exposed domains that transfer electrons from NADPH via Trx ((Missiakas et al., 1995) (right panel A Figure 1.9)). Although both mechanisms occur on the same compartment, they are kept kinetically separated in order to prevent non-functional disulfide reactions to happen (Rozhkova et al., 2004).

1.4.2 The endoplasmic reticulum (ER)

The ER is responsible for the formation of disulfides from a wide set of proteins that includes antibodies, among others. The oxidation of cysteines in this compartment is driven by members of the protein disulfide isomerase (PDI) family and the ER oxidase (Ero) 1. PDIs are also members of the thioredoxin family and thus, contain at least one thioredoxin fold that accepts electrons from the target protein (Gruber et al., 2006). Finally, the cysteines on PDI are re-oxidised by Ero1, which as Erv1 in the IMS, shuttles the electrons to molecular oxygen via a FAD domain ((Mezghrani et al., 2001) (left panel B Figure 1.9)).

In contrast, reshuffling of disulfide bonds in the ER is driven by members of the PDI family itself. This reaction is mediated by direct interaction of PDI with the wrongly formed disulfide or by interaction of the latter with GSH ((Sevier et al., 2007) (right panel B Figure 1.9)). GSH is believed to be transported from the cytosol in which is kept in its reduced state by the NADPH-dependant reductase Glr1 (Jessop and Bulleid, 2004). Unlike the bacterial periplasm, these two ER redox machineries depend on PDIs proteins. PDIs exist in an oxidised/reduced balanced state, which dictates the flux towards oxidising or reducing purposes (Sevier et al., 2007).

1.4.3 The mitochondrial intermembrane space (IMS)

Unlike cellular compartments that share important characteristics such as the presence of oxidative folding machineries, no reductive pathway has been described so far for the mitochondrial IMS. Although the influence of GSH pools and enzymes like Glr1 and Grx2 with Mia40 has been reported (Kojer et al., 2012, Kojer et al., 2015), direct interactions with this oxidoreductase or a full pathway are yet to be discovered. However, the report of mixed reductive and oxidising forms of proteins from the MIA pathway suggests that the presence of such a pathway is crucial. Furthermore, the recent description of an updated version of the IMS proteome found members of the Trx system to be present in this mitochondrial compartment, namely Trx1 and TrR1 (Vögtle et al., 2012).

Taken all this information together, in this work I studied the influence of reductive perturbations in the import of proteins into mitochondria. Additionally, the discovery of a specific effect on the import of proteins that are substrates for the MIA pathway and the recently found Trx system in the IMS, lead us to identify that the Trx pathway is the main reductive regulator of the MIA pathway in the IMS.

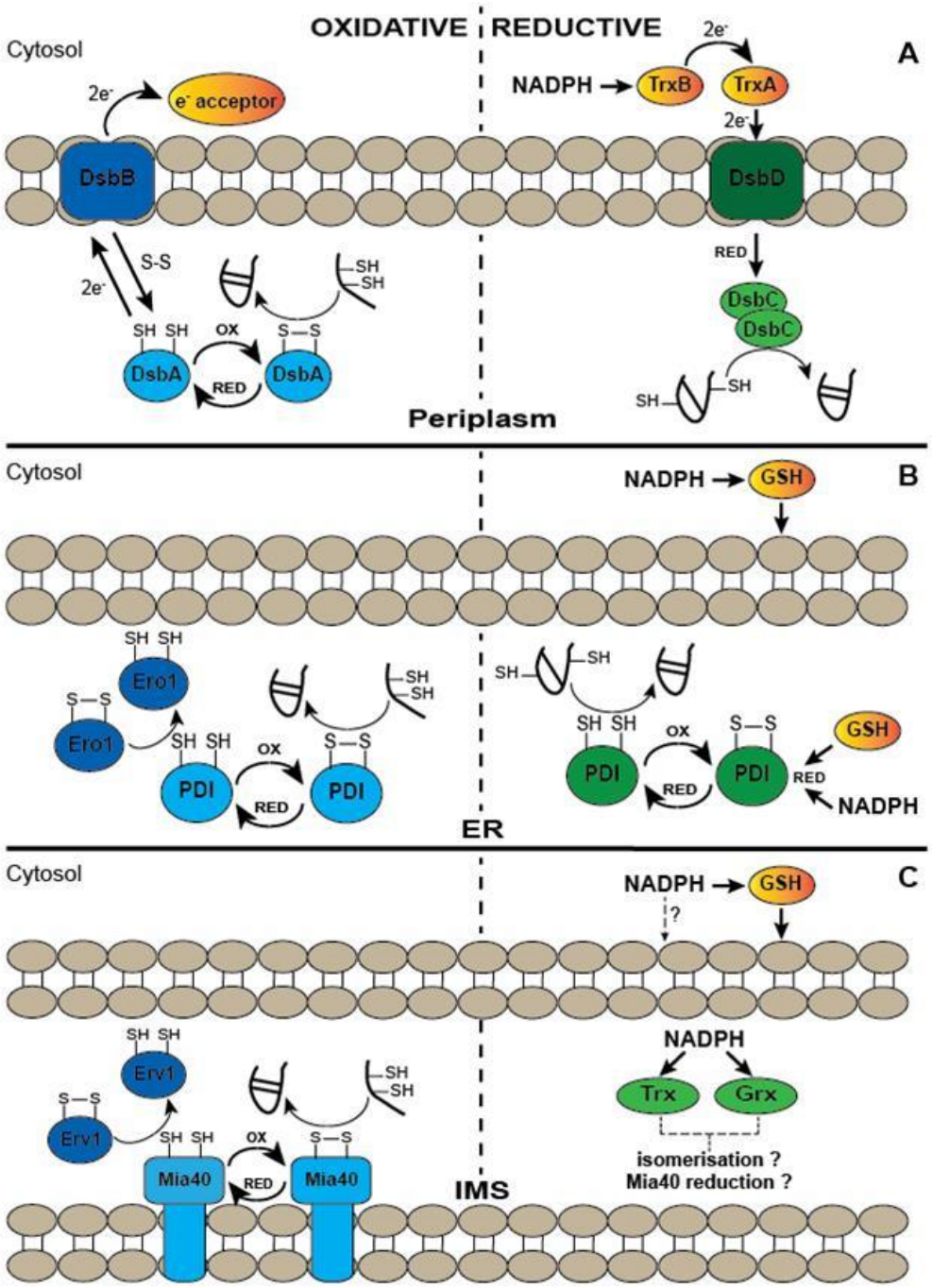

Figure 1.9 Oxidative and reductive pathways in the bacterial periplasm, the ER and the mitochondrial IMS. (A) The bacterial periplasm: oxidation of proteins by DsbA, which is in turn oxidised by the membrane protein DsbB (left). Electron flux from the cytosolic Trx system onto DsbD, then to DsbC and finally to the protein (right). **(B)** The ER: Protein oxidation by PDI and reduced PDI recycling by e^- transfer onto Ero1 (left). Protein reduction/isomerisation pathway by PDI reduced by either GSH or NADPH (right). **(C)** The mitochondrial IMS: Protein import mediated by the Mia40 oxidation of protein precursors. Mia40 is kept in an oxidised state by Erv1, or alternatively by Gpx3. This process may be facilitated by Hot13 which is proposed to keep Mia40 in its reduced state (left). The Trx and Grx systems were recently localised in the IMS. It is likely that these reductive systems play a role in Mia40 reduction to keep the oxidised/reduced overall state of Mia40 necessary for its import function and that they play a role in protein isomerisation (right). Image from Cardenas-Rodriguez, M. and Tokatlidis, K. 2017.

Chapter 2 Aims

The general aim of this thesis was to determine the molecular and mechanistic links between redox perturbations and protein biogenesis in the mitochondrial intermembrane space. More specifically, to investigate the localisation and function of the thioredoxin system as the critically missing reductive pathway controlling the redox balance in the intermembrane space. The working hypothesis was that the reductive thioredoxin system controls the redox balance in the intermembrane space of yeast and that this redox balance impacts on the import of proteins into mitochondria.

2.1 Specific aims

2.1.1 Phenotype determination of Δ*g6pd*, Δ*trx*1/2, *Δtrr1* and Δgsh1 yeast strains

- To determine the influence of mutations in the two main thiol-reductive pathways on the growth of yeast cells

- To measure the levels of the cofactors $NADP^+$ and NADPH in Δ*g6pd*, Δ*trx*1/2, Δ*trr*1 and Δ*gsh*1 yeast strains

- To measure the mitochondrial inner membrane potential in Δ*g6pd*, Δ*trx*1/2, Δ*trr*1 and Δ*gsh*1 yeast strains

2.1.2 Protein levels and protein import into isolated mitochondria from Δ*g6pd*, Δ*trx*1/2, Δ*trr*1 and Δ*gsh*1 yeast strains

- To test the steady state levels of mitochondrial proteins in isolated mitochondria from Δ*g6pd*, Δ*trx*1/2, Δ*trr*1 and Δ*gsh*1 yeast

- To determine the import capacity of mitochondria isolated from Δ*g6pd* yeast

- To determine the redox state of Mia40 in Δ*g6pd* yeast

2.1.3 The thioredoxin system in the IMS of yeast mitochondria

- To probe that the thioredoxin system can get imported into mitochondria from Δ*g6pd* yeast

- To test the *in vitro* and *in organello* interaction between Trx1 and Mia40

- To determine if the Trx system can restore the import capacity and the Δψ defect in mitochondria isolated from Δ*g6pd* yeast

2.1.4 Import pathway of Trx1 into mitochondria

- To discover and characterise putative import signal(s) in the Trx1 sequence

- To set the tools to test the influence of the targeting signal in the import of Trx1 into mitochondria

- To set the tools to determine the protein import channel through which Trx1 translocates across the mitochondrial outer membrane

- To determine if a protein with this import signal in its sequence can translocate across the mitochondrial outer membrane with a folded cargo

Chapter 3 Materials and Methods

3.1 Materials

3.1.1 Enzymes

All the restrictions enzymes used in this work as well as the T4 DNA ligase and Taq DNA polymerase were purchased from New England Biolabs (NEB). Pfu DNA polymerase and DpnI were obtained from Promega.

3.1.2 Membranes

Semi-dry transfer for western blot was performed using Amersham™ Protran 0.45µm nitrocellulose (Fisher).

3.1.3 Antibodies

The antibodies (Ab) used in this work are listed in Table 1 . Anti-His Ab was purchased from Bio-Rad. The rest of primary Abs were produced by Davids Biotechnologie (Germany). Briefly, rabbits were immunised with the desired recombinant protein. Sera from the rabbit's blood containing polyclonal Abs against the protein was sent to us by the company. No further purification was done to the sera.

Table 1 List of antibodies. Antibodies and their concentration used in this study. The company and the species in which the Ab was generated are also listed

Antibody	Company	Origin	Concentration	Source
α-Hsp70	Davids Biotechnologie	Rabbit polyclonal	1:15000	Prof. Nikolaus Pfanner lab
α-Tom70	Davids Biotechnologie	Rabbit polyclonal	1:1000	Prof. Nikolaus Pfanner lab
α-Mia40	Davids Biotechnologie	Rabbit polyclonal	1:1000	Sideris *et al.* 2009
α-Tom40	Davids Biotechnologie	Rabbit polyclonal	1:1000	Prof. Nikolaus Pfanner lab
α-Porin	Davids Biotechnologie	Rabbit polyclonal	1:10000	Prof. Nikolaus Pfanner lab

α-Tim23	Davids Biotechnologie	Rabbit polyclonal	1:1000	Prof. Nikolaus Pfanner lab
α-Tim22	Davids Biotechnologie	Rabbit polyclonal	1:750	Prof. Kostas Tokatlidis lab
α-Erv1	Davids Biotechnologie	Rabbit polyclonal	1:1000	Lionaki *et al.* 2010
α-Cytochrome c	Davids Biotechnologie	Rabbit polyclonal	1:750	Prof. Nikolaus Pfanner lab
α-Tim10	Davids Biotechnologie	Rabbit polyclonal	1:1000	Prof. Kostas Tokatlidis lab
α-Tim9	Davids Biotechnologie	Rabbit polyclonal	1:1000	Prof. Kostas Tokatlidis lab
α-Trx1	Davids Biotechnologie	Rabbit polyclonal	1:1000	Manganas, P. 2017
α-His	BioRad	Mouse monoclonal	1:10000	BioRad

3.1.4 Plasmids

Table 2 List of plasmids. The gene of interest was cloned into pSP plasmid, for TNT ^{35}S-Methionine radiolabelling, and pET plasmid for expression and purification.

Insert	Plasmid
Mia40	pET22-ΔN290Mia40His
Erv1	pSP64-Erv1His
Su9-DHFR	pSP65-SuDHFR
Tom5	pSP65-Tom5
Tim12	pSP64-Tim12
Tim10	pSP64-Tim10
Tim9	pSP64-Tim9
Tim11	pSP64-Tim11
hCox17	pSP64-hCox17
Trx1	pET24-Trx1His pET24-Trx1C30/33S His pET24- -29aaTrx1 His

	pET24-Trx1K79A His
	pET24 Trx1G81A His
	pET24 Trx1V84A His
	pET24 Trx1K86A His
	pSP64 His-DHFR Trx1
Trx2	pET24-Trx2His
TrR1	pET24-TrR1His
Gpx3	pSP64 His-DHFR Gpx3
bITS from Trx1	pSP64 His-DHFR bITS

3.1.5 Primers

The primers designed were obtained from Sigma-Aldrich. These primers used for protein purification and mutagenesis are listed in Table 3 and Table 4 , respectively.

Table 3 List of primers used for protein purification. This table lists the sequences of the primers used to clone the genes of interests into the corresponding plasmid. All sequences are showed in a 5'→3' orientation. The N-terminal deletions primers were paired with the Reverse primer of the full length Trx1. The C-terminal deletions primers were paired with the Forward primer of the full length Trx1.

	Primer	
Plasmid	**Name**	**Sequence (5'→3')**
pET24-Trx1His	Fwd Trx1 XBaI	GCTCTAGAATGGTTACTCAATTCAAAACTGCC
	Rev Trx1 XhoI	CCGCTCGAGAGCATTAGCAGCAATGGC
pET24 -10aaTrx1 His	Fwd Trx1 XBaI (-10aa)	GCTCTAGAATGTTCGACTCTGCAATTGC
pET24 -20aaTrx1 His	Fwd Trx1 XBaI (-20aa)	GCTCTAGAATGGTTGTCGTAGATTTCTACG
pET24 -29aaTrx1 His	Fwd Trx1 XBaI (-29aa)	GCTCTAGAATGTGCGGTCCATGTAAAATG
pET24 -34aaTrx1 His	Fwd Trx1 XBaI (-34aa)	GCTCTAGAATGATTGCTCCAATGATTG

pET24-HisXhoI -13aa	Rev Trx1 XhoI (-13aa)	CCGCTCGAGGTTGGCACCAACAAC
pET24-HisXhoI -23aa	Rev Trx1 XhoI (-23aa)	CCGCTCGAGACCGTTCTTGAATAGAAGC
pET24-HisXhoI -29aa	Rev Trx1 XhoI (-29aa)	GATATACCGCTCGAGAAGCAAAGTTGGCATAGCG

Table 4 List of primers used for single substitution mutagenesis. This table lists the sequences of the primers used to mutagenize single amino acids in Trx1 to alanine. All sequences are showed in a 5'→3' orientation.

	Primer	
Plasmid	**Mutagenesis**	**Sequence**
pET24-Trx1His	Fwd Trx1 K79A	GCTTCTATTCGCTAACGGT
	Rev Trx1 K79A	AAAGTTGGCATAGCGAAAC
	Fwd Trx1 G81A	ATTCAAGAACGCTAAGGAA
	Rev Trx1 G81A	AGAAGCAAAGTTGGCATAG
	Fwd Trx1 V84A	CGGTAAGGAAGCTGCAAAG
	Rev Trx1 V84A	TTCTTGAATAGAAGCAAAGTTGGC
	Fwd Trx1 K86A	GGAAGTTGCAGCCGTTGTTGGTGC
	Rev Trx1 K86A	TTACCGTTCTTGAATAGAAG

3.1.6 Bacterial strains

The *Escherichia coli* (*E. coli*) strains used to clone our genes of interest as well as for plasmid propagation were DH5α cells. Two different strains were used for the expression of recombinants proteins:

- BL21 (DE3): fhuA2 [lon] ompT gal (λ DE3) [dcm] ΔhsdS
  λ DE3 = λ sBamHIo ΔEcoRI-B int::(lacI::PlacUV5::T7 gene1) i21 Δnin5

- Origami 2 (DE3) pLysS: Δ(ara-leu)7697 ΔlacX74 ΔphoA PvuII phoR araD139 ahpC galE galK rpsL F'[lac$^+$ lacI^q pro] (DE3) gor522::Tn10 trxB pLysS (Cam^R, Str^R, Tet^R)

3.1.7 Yeast strains

The *Saccharomyces cerevisiae* strains that were used in this work are described in Table 5.

Table 5 Yeast strains The different yeast strains and their phenotypes used are listed. A short description with information relevant to each strain is given.

Yeast	Genotype	Description	Source
D2763-10B	MATα mal	Strain used for mitochondrial studies, constructed in the Sherman lab	(Sherman, 1964)
BY4741	MATa, his3Δ1, leu2Δ0, met15Δ0, ura3Δ0	Wild type (WT) strain	(Brachmann et al., 1998)
ΔZwf11 (Δ*g6pd*)	MATa his3Δ1 leu2Δ0 met15Δ0 ura3Δ0	Strain KO for the endogenous *Zwf1* gene, encoding glucose-6-phosphate dehydrogenase (g6pd)	Dharmacon GE healthcare
Δ*trx*1/2	MATa ura3-52 leu2-3112 trp1-1 ade2-1 his3-11 can1-100.	CY302 background. Strain KO for the cytosolic forms of Trx: Trx1 and Trx2	(Draculic et al., 2000)
Δ*trr*1	MATa his3Δ1 leu2Δ0 met15Δ0 ura3Δ0	Strain KO for the endogenous *trr1* gene, encoding thioredoxin reductase 1	Dharmacon GE healthcare
Δ*gsh*1	MATa, his3Δ1, leu2Δ0, met15Δ0, ura3Δ0	Strain KO for the endogenous *gsh1* gene, encoding Gamma glutamylcysteine synthetase1. Requires external GSH to grow.	Dharmacon GE healthcare

TsTom40	Matα ade2-101 his3-Δ200 leu2-Δ1 ura3-52 trp1-Δ63 lys2-801 tom40::ADE2 pFL39-Tom40 (CEN, TRP)	Temperature sensitive strain to knock down the levels of Tom40. This is a control strain in which the yeast was transformed with an empty vector.	(Becker et al., 2011)
TsTm40-25	Matα ade2-101 his3-Δ200 leu2-Δ1 ura3-52 trp1-Δ63 lys2-801 tom40::ADE2 pFL39-Tom40 (CEN, TRP)	Temperature sensitive strain to knock down the levels of Tom40.	(Wenz et al., 2014)
TsTom40-34	Matα ade2-101 his3-Δ200 leu2-Δ1 ura3-52 trp1-Δ63 lys2-801 tom40::ADE2 pFL39-Tom40 (CEN, TRP)	Temperature sensitive strain to knock down the levels of Tom40.	(Becker et al., 2011)
yTHCTom40	URA3::CMV-tTA MATa his3-1 leu2-0 met15-0	R1158 background. Strain for the knock down of Tom40 using doxycycline.	Dharmacon GE healthcare
yTHCSam50	URA3::CMV-tTA MATa his3-1 leu2-0 met15-0	R1158 background. Strain for the knock down of Sam50 using doxycycline.	Dharmacon GE healthcare

3.1.8 Media

3.1.8.1 Bacterial growth media

Cells were grown at 37°C in Luria-Bertani (LB) media containing 1% (w/v) bactotryptone, 0.5% (w/v) yeast extract and 1% (w/v) NaCl. Solid media was prepared by also adding 2% agar. The media was sterilised for 15min at 121°C before use.

For the preparation of selective media, 100 μg/ml ampicillin or 30μg/ml kanamycin were added to the media for selection of pSP and pET plasmids, respectively.

3.1.8.2 Yeast growth media

Yeast cells were grown in rich (YPD or YPlac) media at 30°C. The media contained 2% (w/v) carbon source (glucose for YPD and lactic acid for YPLac), 1% (w/v) yeast extract and 2% (w/v) peptone. In the case of YPlac, the pH was adjusted to pH 5.5 to ensure conversion of the acid species to lactate. Additionally, the media was supplemented with 76 mg/L methionine for the growth curve, growth spot tests and isolation of mitochondria from Δ*g6pd* and Δ*trx*1/2 yeast. The media was sterilised for 15min at 121°C before use.

3.2 Methods

3.2.1 Molecular biology assays

3.2.1.1 Competent cell preparation

All the cloning procedures were performed using competent *E. coli* DH5α cells. An o/n preculture was diluted 1:50 on LB and left to grow at 30°C until OD_{600} reached 0.2-0.4. The cells were recovered, resuspended in TFBI buffer (KOAc 30mM, $MnCl_2$ 50mM, KCl 100mM, $CaCl_2$ 10mM and glycerol 15%) and incubated with gentle shaking at 4°C for 2h. Afterwards, the cells were recovered again and resuspended in TFBII buffer (MOPS-KOH pH7 10mM, KCl 10mM, $CaCl_2$ 75mM and glycerol 15%). Finally, 100μl aliquots of the cells were stored at -80°C until its use.

3.2.1.2 Cloning

All clones were prepared through PCR amplification of the inserts using yeast genomic DNA as a template. Afterwards, the PCR products and plasmids were digested at 37°C for 1h with the desired restriction enzymes and the resulting products were purified by PCR clean-up (Qiagen) or gel extraction. For the gel extraction, digested products were separated by electrophoresis at 60V for 90min on 1% agarose gel and the desired fragment was purified with the QIAquick Gel Extraction Kit (Qiagen) following the supplier's protocol. This was followed by ligation with T4 DNA ligase (NEB) at room temperature for 1h of the two digested components at different ratios (plasmid:insert-1:0, 1:3, 1:6, 1:9) depending on the size of the insert relative to the size of the plasmid. The quantities used in every case were calculated using the following equation:

$$\frac{(ng\ vector)(bp\ insert)}{bp\ vector} = ng\ insert$$

The ligation product was then transformed into *E. coli* DH5α competent cells. For the transformation, the ligated product was added to 100µl of competent cells (3.2.1.1) and incubated on ice for 30min. Then, the cells were placed on a water bath at 42°C for 45 seconds followed by the addition of 900µl of LB media (3.1.8.1). The bacterial cells were incubated at 37°C for 1h with gently shaking to allow them to express the plasmid and thus, the resistance gene. Afterwards the cells were separated by centrifugation at 13000g on a Sigma 1-14 bench centrifuge. Finally, the cells were plated onto LB agar plates with the corresponding antibiotic selection and left to grow at 37°C overnight (o/n).

3.2.1.3 Mutagenesis

The plasmid containing the sequence to be mutated was used as template for PCR. The high fidelity Pfu polymerase (Promega) was used. The primers pair specific for each point mutation was added at a final concentration of 0.5µM. After the plasmid amplification with PCR, the reaction was treated with 1µl of DpnI (10U/µl) at 37°C for 1h. This enzyme digests the non-mutated, supercoiled, double stranded parental plasmid DNA, but not the PCR product which contains the mutation. These digested PCR mixes were transformed into DH5α competent bacterial cells following the same transformation procedure described in section

3.2.1.2. The mutated colonies that grew on the selective plates were confirmed as described in section 3.2.1.4.

3.2.1.4 Sequencing

The positive colonies, i.e. the ones that grew under selective conditions, were analysed by PCR. Then, the plasmids were isolated from these cells and sent for sequencing analysis (GATC Biotech). The sequencing results were compared to the desired WT sequence using the CLC Genomics workbench program (Qiagen Bioinformatics).

3.2.2 *In organello* assays

3.2.2.1 Isolation and purification of yeast mitochondria

Mitochondria were isolated and purified from the yeast strains D273-10B, Δ*g6pd*, Δ*trx*1/2, Δ*trr*1 and Δ*gsh*1. The cells (10L-15L) were grown o/n at a starting OD_{600} of 0.1 (to allow harvesting at log phase) at 30°C using lactate as non-fermentable carbon source to promote respiration, stop energy production via glycolysis (Turcotte et al., 2010) and increase the mitochondrial yield. The isolation of mitochondria was done accordingly to a protocol previously described (Glick, 1991). In this protocol, yeast cells were collected and washed with 300ml water by 5min centrifugation at 5000rpm and 3500rpm, respectively. Then, walls were broken by adding 50ml Tris-DTT buffer (0.1M Tris-SO_4 pH 9.4, 10mM DTT) and incubated for 30min at 30°C with gentle shaking. Partially broken cells were collected by centrifugation at 3500rpm for 5min and washed twice with 40ml 1.2 M sorbitol buffer (1.2M sorbitol, 20mM KPi pH 7.4). Then, to completely break the cell wall, yeasts were resuspended in 1.2M sorbitol buffer (5ml/cell g) + zymolase (3.5mg/cell g) and incubated at 30°C for 1h with gentle shaking. The resulting spheroblasts were recovered by 5min centrifugation at 5000rpm at 4°C. From now on, all steps were done on ice and centrifugations at 4°C unless otherwise stated. The spheroblasts were then washed twice with 40ml 1.2M sorbitol buffer and spinned down for 5min at 5000rpm. The cells were resuspended in 100ml breaking buffer pH 6.0 (0.6M sorbitol, 20mM MES-KOH pH 6.0) + 2mM PMSF and this solution was dounced 15 times to mechanically break the cells. Non-broken material was recovered by centrifugation at 3500rpm for 5min. The supernatant containing mitochondria was poured in a beaker and

another douncing step of the pellet resuspended in breaking buffer pH 6.0 with 2mM PMSF was carried out. The mitochondrial fraction was finally combined with the previous supernatant and then was spinned down at 10000 rpm for 10min and recovered as pellet. This resulting pellet was resuspended in 100ml breaking buffer pH 6.0 w/o PMSF and centrifuged 5min at 3500rpm. Supernatant fraction was recovered and spinned down at 10000rpm for 20min. The pellet containing mitochondria was then resuspended in 0.5ml breaking buffer pH 6 and the concentration was calculated using a conversion factor as follows: 10mg/ml mitochondrial protein = 0.21 $OD_{\lambda=280nm}$. Further purification of mitochondria was achieved by overlaying 5ml 14.5% Nycodenz on top of 5ml 20% Nycodenz and adding 1ml mitochondrial solution on top of the Nycodenz gradient. Then, the gradients were centrifuged for 30min at 40000rpm at 2°C using a SW40 rotor. Then, mitochondria were recovered from an interphase between both Nycodenz solutions and were diluted with 5 volumes of breaking buffer pH 7.4 (0.6M sorbitol, 20mM HEPES-KOH pH 7.4) and recovered by 10min centrifugation at 10000rpm. Finally, the concentration was calculated using the conversion factor: 10mg/ml mitochondrial protein = 0.12 $OD_{\lambda=280nm}$. Aliquots were prepared at a final concentration of 25mg/ml mitochondrial protein + 10mg/ml BSA fatty acid free in breaking buffer pH 7.4 and stored at -80°C until further use.

Following the isolation and purification processes, the mitochondria can be stored at -80°C after the addition of fatty-acid free bovine serum albumin (BSA) (Sigma-Aldrich) at a final concentration of 10mg/ml as a preservative for the mitochondria.

3.2.2.2 Protein precipitation

Pure proteins or protein content from yeast cells or mitochondria were precipitated with either ammonium sulfate ($(NH_4)_2SO_4$ or trichloroacetic acid (TCA).

- $(NH_4)_2SO_4$ precipitation: The desired amount of protein was calculated and precipitated by adding 3 volumes of ice-cold saturated $(NH_4)_2SO_4$. After 30min incubation on ice and 30min spin at 25000g at 4°C, the pellet was resuspended in the buffer required for each particular analysis.

- TCA precipitation: The desired amount of protein was calculated and precipitated by adding ice-cold TCA to a final concentration of 10%. The sample was incubated 30°C on ice and centrifuged at 25000g at 4°C. The resulting pellet was washed two times with 100µl of 100% ice-cold acetone followed by 20min incubation at room temperature to ensure the complete evaporation of the acetone. Finally, the pellet was resuspended in the required buffer.

3.2.2.3 Radioactive labelling of proteins using TNT SP6-coupled transcription/translation system

^{35}S-Methionine radiolabelled protein precursors were produced using the transcription/translation (TNT®) SP6 Coupled Reticulocyte Lysate System (Promega) according to the supplier instructions. The system translates the proteins and incorporates ^{35}S- radiolabelled methionine into each protein precursor. The TNT mix is incubated at 30°C for 90min and then, the precursors are separated from the ribosomes by centrifuging the samples in a Optima TLX centrifuge (Beckman) using a TLA100 rotor at 55000rpm at 4°C for 16min.

3.2.2.4 Import of proteins into isolated yeast mitochondria

Mitochondria were resuspended in import buffer (600mM sorbitol, 2mM KH_2PO_4, 50mM KCl, 50mM HEPES-KOH pH 7.4, 10mM $MgCl_2$, 2.5mM Na_2EDTA pH7, 5mM L-methionine, 1mg/ml fatty-acid free BSA) at a final concentration of 0.5 mg/ml, in the presence of 2mM ATP and 2.5mM NADH and were equilibrated at 30°C. Then, either the desired amount of pure recombinant protein (precipitated with ammonium sulfate and resuspended in 50mM HEPES-KOH pH 7) or 5µl of the radioactive protein precursor were added to the reaction mix and the incubation at 30°C continued for the required amount of time, following each experimental set up. At the end of the incubation period, the samples were placed on ice to terminate the reaction at the desired moment. Afterwards, the mitochondria were isolated by centrifuging at 16000g at 4°C for 5min. Non-imported material was removed by resuspending the mitochondrial pellet in an isotonic buffer solution (Breaking buffer (0.6M sorbitol, 20mM HEPES-KOH pH7.4)) in the presence of 0.1mg/ml Protease K at 4°C for 30min. Then, 1mM final concentration of the protease inhibitor phenylmethylsulfonyl fluoride (PMSF) was added and the incubation at 4°C continued for further 10min. The mitochondria

were re-isolated under the same centrifugation conditions mentioned above. The supernatant was removed and the mitochondrial pellet was resuspended in 20µl of 2X Laemmli sample buffer (+/- ß-mercaptoethanol). Finally, the samples were boiled at 95°C for 10min and analysed by 12% Tris-Tricine SDS-PAGE.

For the import into mitochondria with disrupted inner membrane potential, Δψ-, NADH was omitted from the import mix. Instead, the ionophore Carbonyl cyanide m-chlorophenyl hydrazone (CCCP) was added at a final concentration of 25µM. Afterwards, the same import procedure described above was followed.

For the import into mitochondria depleted of ATP, ATP was omitted and 10µM oligomycin and 10mU/µl apyrase were added to the import mix. The mitochondria were incubated for 10min before following the same import procedure described above.

3.2.2.5 Sequential import of proteins into mitochondria

Where mentioned, the Trx system (NADPH, TrR1 and Trx1) was pre-imported into mitochondria prior to further analysis: i.e. alkylation, Δψ measurement or import of radiolabelled precursors. Depending on the experiment to follow, 50µg or 100µg of pure isolated mitochondria were dissolved in import buffer (3.2.2.4) at a final concentration of 0.5mg/ml in the presence of 2mM ATP and 2.5mM NADPH and were equilibrated at 30°C for 5min. Then, 10µg or 20µg of recombinant pure His-tagged Trx1 were added to the import reaction for 5min more. Afterwards, 10µg or 20µg of TrR1 were added to the same import mix and incubated for a further 5min. Finally, the import mix containing mitochondria and both Trx1 and TrR1 were incubated at the same temperature (30°C) for an extra 5min to assure maximum import of both proteins into mitochondria (Figure 3.1). Non-imported material was removed by centrifugation of the import mix at 15000g and 4°C for 5min on a refrigerated Sigma bench centrifuge. The resulting pellet was resuspended and treated according to the required analysis.

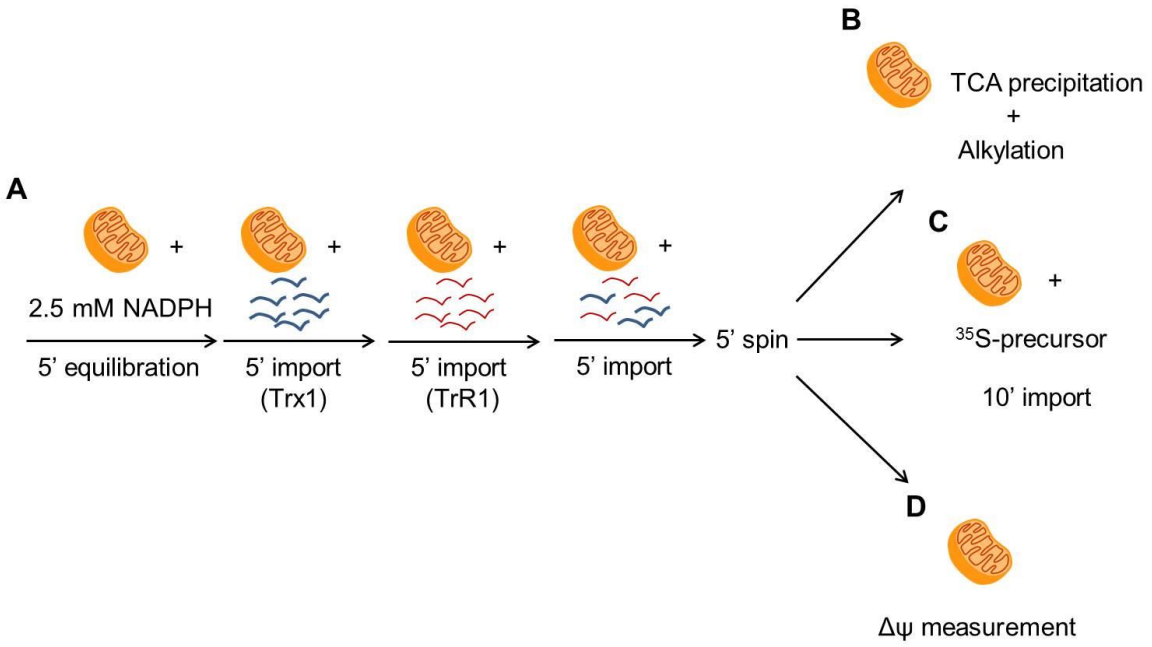

Figure 3.1 Sequential import of proteins into mitochondria. Schematic representation of **(A)** pre-import of the Trx system into mitochondria prior to **(B)** protein alkylation, **(C)** import of 35-S radiolabelled protein precursor or **(D)** inner membrane Δψ measurement.

3.2.3 Biochemical assays

3.2.3.1 NADP/NADPH measurement

The measurement of the individual levels of $NADP^+$ and NADPH was made using the NADP/NADPH-Glo™ Assay kit (Promega). Yeast cells from WT, Δ*g6pd*, Δ*trx*1/2, Δ*trr*1 and Δ*gsh*1 strains were growth on YPD o/n. Triplicates with $1X10^5$ cells were plated in a white 96-well luminometer plate. The number of cells was estimated considering the relation factor: OD_{600} 0.1=$1X10^6$ cells/ml. The cells were separated from the media by centrifugation at 15000g at 4°C and the pellet was resuspended in 12.5µl of PBS. Then, 12.5µl of lysis buffer (1% (v/v) Dodecyltrimethylammonium bromide (DTAB (Sigma)) in 0.2N NaOH) was added to the cell suspension. The sample was divided in two and 6.25µl of 0.4N HCl (for $NADP^+$ measurement) or nothing (for NADPH measurement) were added. The reduced NADPH or oxidised $NADP^+$ species are destroyed under acidic conditions or basic conditions, respectively, allowing the individual measurement of the remaining dinucleotide form. The plate was incubated at 60°C for 15min and the reaction was stopped by neutralisation with either 6.25µl of 0.5M Trizma base (Sigma) for $NADP^+$ or 12.5µl HCl/Trizma (equal volumes of 0.4N HCl and 0.5M Trizma) for NADPH for 10min at room temperature. Then, 25µl of NADP/NADPH-

Glo™ detection reagent were added to each well and the light signal produced, which is proportional to the amount of $NADP^+$ or NADPH, was recorded using a plate reader.

3.2.3.2 Tris-Tricine SDS-PAGE

Samples were resuspended in 2X Laemmli sample buffer (diluted from 6X Laemmli sample buffer: 375mM Tris-HCl pH 6.8, 9% SDS, 40% glycerol and 0.03% bromophenol blue) in the presence or absence of β-mercaptoethanol and were boiled at 95°C for 10min prior to loading on gels. The gels used in this work were 12% or 14% Tris-Tricine SDS gels and were prepared as mentioned on Table 6. The samples were separated by electrophoresis at 120V for 20min to allow them to travel past the stacking gel and then at 170V for ~70min more. The resulting gels were either stained with Coomassie blue or treated for western blot.

Table 6 Tris-Tricine gels recipe. Formula to prepare Tris-Tricine stacking and 12% and 14% separating gels.

	Stacking gel	Separating gel	
	5%	12%	14%
Acryl/Bis-acrylamide (40%)	0.375ml	3ml	3.5ml
Tricine Gel buffer	0.75ml	3.3ml	3.3ml
87% Glycerol	-	1.3ml	1.3ml
dH_2O	1.82ml	2.29ml	1.79ml
10% APS	3µl	100µl	100µl
TEMED	3µl	10µl	10µl
Total volume	3ml	10ml	10ml

3.2.3.3 Coomassie blue staining

For Coomassie staining of the proteins, the gels were soaked in Coomassie solution (30% methanol, 10% acetic acid, 0.2% Coomassie blue R-250) and left agitating to stain for 5 minutes on a Stuart SSL4 see-saw rocker. Then, the stained gel was soaked in destaining buffer (15% methanol, 10% acetic acid) and left agitating o/n until the dye was washed away.

3.2.3.4 Western blot

For western blot, the proteins were transferred onto nitrocellulose membrane (Fisher) with transfer buffer using the BioRad Semi-Dry transfer System at 25V for 25min. The membrane was block with 5% skimmed-milk powder in TBST buffer at room temperature for 1h and then incubated with the desired Ab diluted to working conditions (Table 1) in 5% skimmed-milk powder in TBST buffer at 4°C o/n or room temperature for 1:30h. The membrane was then washed with TBST (5X5min washes) to remove non-bound primary Ab. Afterwards, the membrane was incubated at room temperature for 1h with the correspondent secondary Ab. Secondary Abs were either horseradish peroxidase (HRP)-labelled or fluorescence-labelled. Both Ab were diluted to working concentration of 1:10000 in 5% skimmed-milk powder in TBST, for HRP-conjugated Abs, or TBSTalone, for fluorescence Abs. Then, the membranes were washed with TBST (5X5min washes) when the HRP-conjugated secondary Ab was used and with (4X5min washes) plus an extra 10min wash with dH_2O for the fluorescence-conjugated secondary Ab. For the HRP-Ab, blots were visualised using X-ray films (Carestream), while for the fluorescent-conjugated Ab, the LI-COR Odyssey CLx quantitative fluorescence system was used.

3.2.3.5 Large scale expression of recombinant proteins

The recombinant proteins were cloned into pET24-6XHis or pET22-6XHiss tagging vectors and were expressed in either *E. coli* BL21 (DE3) or *E. coli* Origami 2 (DE3) pLysS cells. The plasmid-insert constructs were transformed as described in 3.2.1.2 and single colonies were used to inoculate 20ml LB cultures supplemented with the appropriate antibiotic (3.1.8.1) for selection. The cells were grown at 37°C o/n and were then diluted 1:50 into fresh LB cultures. These cultures were incubated until they reached log growth phase (OD_{600} 0.4-0.7). At this point, 0.4mM IPTG was added and the cells were incubated either at 16°C o/n or room temperature for 4h. After the induction, the cell pellets were collected by centrifugation at 4°C and 5000g for 15min and were used for purification of the proteins.

3.2.3.6 Purification of 6XHis-tagged recombinant proteins

The cell pellets obtained in 3.2.3.5 were resuspended in buffer A (300mM NaCl, 50mM HEPES-KOH pH 7, 10% glycerol) supplemented with 5mM imidazole, 1mg/ml lysozyme and 10µg/ml DNAse in a relation of 5ml/gram of cell pellet and the solution was incubated at 4°C for 15min. The cells were ruptured by passing them through a French press for two cycles at 1000psi. The broken cells were centrifuged at 21000g at 4°C for 30min. Then, the supernatant was separated from the pellet and loaded onto a column containing Ni-NTA beads (Qiagen). The beads were previously equilibrated with buffer A. The solution was left to pass through the column by gravity. The bound material was washed once with buffer A supplemented with 5mM imidazole and then 2 times with washing buffer (50mM NaCl, 50mM HEPES-KOH pH 7, 10% glycerol) and increasing amounts of imidazole (wash2: 20mM imidazole and wash3: 40mM imidazole). All the fractions were collected in 50ml conical tubes. Finally, the bound proteins were eluted from the beads by adding 30ml of elution buffer (50mM NaCl, 50mM HEPES-KOH pH 7, 25% glycerol and 200mM imidazole). All the purification steps were performed at 4°C.

3.2.3.7 Measurement of the inner mitochondrial membrane potential (Δψ) of isolated yeast mitochondria

The measurement of the inner mitochondrial membrane potential in pure isolated yeast mitochondria was measured using the fluorescent dye $DiSC_3(5)$ (Gartner et al., 1995). Mitochondria were resuspended in breaking buffer to a concentration of 10µg/µl. The measurements were performed using a Horiba JobinYvonFL-1039/40 Fluorimeter at 25°C at 622nm excitation wavelength and 670nm emission wavelength. Each measurement was carried out by adding 1ml of Δψ buffer (0.6M sorbitol, 0.1% fatty-acid free BSA, 10mM $MgCl_2$, 0.5mM EDTA, 20mM KPi pH 7.4) to set a measurement base line for 50 seconds. Then 2mM final concentration of $DiSC_3(5)$ dye was added and the fluorescent signal was left to stabilise for 25 seconds prior to the addition of 100µg of mitochondria and the fluorescence was recorded for another 125 seconds. The dye gets internalised into mitochondria depending on the mitochondrial Δψ and its fluorescence is different when in the buffer or when entrapped in mitochondria. This difference allows the indirect measurement of mitochondrial Δψ. The reaction is

terminated by adding the ionophore valinomycin (Sigma) at a final concentration of 1mM.

3.2.3.8 Cross-linking between proteins

The cross-linking experiments were performed using the unspecific cross-linker glutaraldehyde (GA) which creates covalent bonds mainly between Lys residues between proteins. For the cross-linking reactions 1μg of Trx1 or Trx2 or Trx1C30/33S was mixed with 1μg of Mia40 in the presence of 0.1% final concentration of GA. Additionally, the individual proteins were treated or not with 0.01% final concentration of GA The reactions occurred at room temperature for 20seconds, 5min or 10min and were stopped by quenching of the GA with 285mM final concentration of Tris-HCl pH 8. Finally, 10μl of 6X Laemmli sample buffer +ß-mercaptoethanol were added.

3.2.3.9 Alkylation shift assay

The alkylation shift assay was performed using mal-PEG 5000 (Sigma). First, 100μg of mitochondria were precipitated with 10% final concentration ice cold TCA (section 3.2.2.2). The protein pellet was resuspended with 8μl 15mM final concentration of mal-PEG in HES buffer (50mM HEPES-KOH pH 7.4, 10mM EDTA and 3% SDS) or only with HES buffer and cover from light with aluminium foil. Samples were incubated at 30°C for 30min and then at 37°C for 30min more. Finally, 17μl of 4X Laemmli sample buffer were added to the reaction.

3.2.4 *In vivo* assays

3.2.4.1 Drop-test assay

Solid growth YPD and YPlac media was prepared as mentioned in section 3.1.8.2. Yeast cells were grown in YPD broth o/n at 30°C with gentle shaking. The cells were then diluted to an OD_{600} of 0.02 in 1ml final volume in sterile dH_2O. Serial 1:10 dilutions were prepared on sterile dH_2O and 3μl of each dilution were plated onto YPD or YPlac agar plates and incubated at either 30°C or 37°C for 48h.

3.2.4.2 Growth kinetics

Yeast cells were grown on YPD at 30°C o/n with gentle shaking. The cells were then diluted to an OD_{600} of 0.05 in 10ml of either YPD or YPlac. Afterwards, yeasts were grown at 30°C or 37°C with gentle shaking and samples to measure the OD_{600} to follow the growth kinetics were taken at 4h, 8h, 12h, 24h, 28h and 48h.

Chapter 4 Phenotypic determination of yeast strains with affected reducing capacity

4.1 Introduction

The yeast *Saccharomyces cerevisiae* (*S. cerevisiae*) is a single cell model eukaryotic organism widely used in research. Its genome was the first eukaryotic genome to be sequenced and it shares 23% homology with the human genome. Both human and yeast diverged from a common ancestor about 1 billion years ago and the conserved function between some of their genes have been shown by the regain of yeast viability after the insertion of human homologues into knock out (KO) yeast for essential genes (Douzery et al., 2004, Kachroo et al., 2015, Liu et al., 2017). Besides this trait, another important characteristic of yeast is that they can grow under fermentable and non-fermentable carbon sources, rendering this organism ideal to study aerobic oxidative phosphorylation and mitochondrial function uncoupling it from cytosolic glycolysis.

The two principal aims of this chapter were, first to characterise the effects that mutations of the main cytosolic reductive pathways in yeast have under respiratory and non-respiratory growth conditions. The second aim was to determine mitochondrial integrity and the $NADP^+$/NADPH ratios to further analyse if any of these characteristics affects the import of proteins into mitochondria.

4.1.1 Fermentable and non-fermentable carbon sources for yeast growth

The preferred carbon source for growth of *S. cerevisiae* is glucose. This preference is due to the fact that *S. cerevisiae* possess a glucose repression system that down regulates the expression of transporters and catabolic enzymes involved in the metabolism of other carbon sources when glucose is present (Kayikci and Nielsen, 2015, Rolland et al., 2002). The central component of the glucose repression system is the Sucrose non-fermenting kinase 1 (Snf1), which is negatively regulated in the presence of glucose (Carlson et al., 1981). This kinase phosphorylates the transcription factor Mig1, thus inhibiting its activity (Treitel et al., 1998). Mig1 together with the corepressors Ssn6-Tup1

repress genes involved in catabolism of carbon sources different to glucose (Treitel and Carlson, 1995, Treitel et al., 1998). Snf1 is member of the SNF1/AMPK family and is present in the form of a heterotrimeric kinase complex formed by a catalytic subunit, one of three different regulatory ß-subunits (Gal83, Sip1 and Sip2) and a regulatory γ-subunit. Under absence of glucose Snf1 is activated by phosphorylation in threonine 210 (McCartney and Schmidt, 2001) by the kinases Pak1, Tos3 or Elm1 (Hong et al., 2003). Accordingly, yeasts show a $Snf1^-$ phenotype when the three kinases are knocked out (Sutherland et al., 2003). The catalytic activity of Snf1 is regulated by three different mechanisms. The γ-subunit of the complex, encoded by the SNF4 gene, binds to the regulatory domain of Snf1 under low glucose, preventing it from binding the catalytic domain thus leaving Snf1 active (Jiang and Carlson, 1996). The cellular localisation also regulates the activity of Snf1 and this depends on the ß-subunit present in the complex, upon glucose depletion Gal83 localises to the nucleus, Sip1 to the vacuolar membrane and Sip2 remains in the cytoplasm (Schmidt and McCartney, 2000, Vincent et al., 2001, Yang et al., 1994). The third mechanism depends on the Reg1-Glc7 complex, which in the presence of glucose promotes a conformational change on Snf1 that inhibits its catalytic domain (Sanz et al., 2000). When glucose is limited or absent, the genes involved in the utilisation of non-fermentable carbon sources are derepressed. The non-fermentable carbon sources mainly used by *S. cerevisiae* are acetate, ethanol, glycerol and lactate, all of which can be converted into acetyl coenzyme A (CoA) to be used by the mitochondrial respiratory electron chain or for biomolecule synthesis. Acetate passively diffuses into the cell, although the membrane protein Adyp2 was shown to be involved in its uptake (Paiva et al., 2004). Like acetate, ethanol enters cells by passive diffusion (Kotyk and Alonso, 1985), once inside it is metabolised to acetaldehyde and acetate by the enzymes alcohol dehydrogenase and acetaldehyde dehydrogenase, respectively. Acetate is then converted into acetyl CoA by two isoforms of the acetyl CoA synthase (van den Berg et al., 1996). Unlike acetate and ethanol, glycerol is transported into yeast by the symporter sugar transporter-like protein (Stl1) (Ferreira et al., 2005) or by facilitated diffusion mediated by the Fps1 channel (Oliveira et al., 2003). Inside the cell it is transformed into glycerol-3-phosphate and then to dihydroxyacetone phosphate by glycerol kinase and a FAD-dependent glycerol-3-phosphate dehydrogenase, respectively. Then, dihydroxyacetone phosphate can

follow the gluconeogenic or glycolytic pathways. Finally, the uptake of lactate is through a lactate/pyruvate permease encoded by the gen *JEN1* (Casal et al., 1999); inside the cell, lactate is oxidised to pyruvate by two oxidoreductases encoded by the *DLD1* and *CYB2* genes (Lodi and Ferrero, 1993). Depending on the carbon source available, whether fermentable or non-fermentable, yeast can favour the usage of glycolysis or oxidative phosphorylation for the production of energy and the synthesis of metabolic intermediates, biomolecules and reductive power. In this regard, the reduction of $NADP^+$ into NADPH as part of some enzymatic reactions is key for the maintenance of the redox balance in the cell (Figure 4.1).

4.1.2 NADPH sources in the cell

As mentioned before, an important characteristic of *S. cerevisiae* is its ability to grow under different carbon sources due to their metabolic adaptation capacity. The latter is exemplified by the different enzymes that serve as NADPH source. The main source is the constitutively expressed enzyme g6pd (which is called Zwf1 in yeast but will be referred as g6pd in this work), however, it is not the only one (Minard et al., 1998) as KO yeast strains for g6pd are still viable. The cytosolic NADP-specific isocitrate dehydrogenase (Idp2), which catalyses the conversion of citrate to α-ketoglutarate, is another important source. This was shown with the loss of growth of a Δ*g6pd*Δ*idp*2 double KO strain under both endogenous and exogenous oxidative stress conditions (Minard and McAlister-Henn, 2001). Idp2 is not expressed on glucose-growth conditions but is found when cells are grown under non-fermentable media (Loftus et al., 1994). Furthermore, the oxidation of acetaldehyde to acetate also involves the reduction of $NADP^+$. This reaction is catalysed by acetaldehyde dehydrogenase (Ald6) and it was proven to be an important NADPH source since its overexpression restored the phenotypic defects of the Δ*g6pd* strain (Grabowska and Chelstowska, 2003). Nevertheless, it was not as crucial as g6pd and Idp2 for handling endogenous oxidants when yeasts were grown on non-fermentable media (Minard and McAlister-Henn, 2005).

4.1.3 Glucose-6-phosphate dehydrogenase

The first step of the pentose phosphate pathway, the oxidation of glucose-6-phosphate into 6-phosphogluconolactone, is catalysed by glucose-6-phosphate dehydrogenase (g6pd). The importance of g6pd can be seen in its involvement in various processes such as protein, nucleotide and lipid synthesis (Figure 4.1). In fact, in humans g6pd deficiency is the most common enzyme deficiency with just under 200 different mutations found so far (Minucci et al., 2012). In *S. cerevisiae*, g6pd is encoded by the gene *Zwf*1 and it is considered the main source of reductive power in the form of NADPH in the cell (Nogae and Johnston, 1990). Accordingly, g6pd is involved in the adaptive response to oxidative stress in yeast (Izawa et al., 1998). As mentioned above, its role as NADPH supplier is key for the function of the two main thiol reductive pathways in the cell.

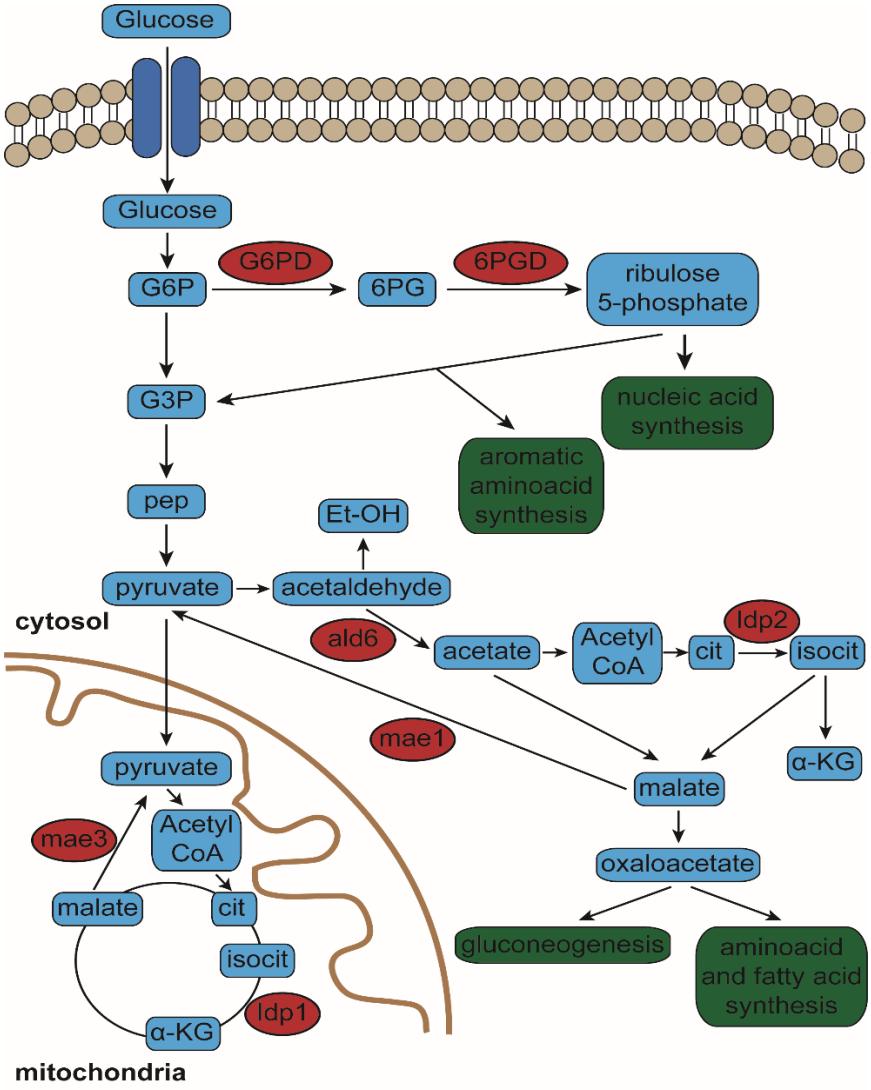

Figure 4.1 Network of NADPH producing pathways. NADPH is formed from the reduction of its oxidized form ($NADP^+$) by the pentose phosphate pathway enzymes glucose 6-phosphate dehydrogenase (g6pd) and 6-phosphogluconate dehydrogenase (6pgd), the mitochondrial, cytosolic and peroxisomal isoforms of NADP-specific isocitrate dehydrogenase (Idp1, Idp2 and Idp3 respectively), the cytosolic acetaldehyde dehydrogenase, the malic enzyme and the transhydrogenase. The NADPH producing enzymes are shown in red ovals, intermediates of the different metabolic pathways are shown in blue and final products in green.

In order to study the effects of altered NADPH levels in the cell in mitochondria biogenesis and to attempt to elucidate the presence and properties of a reductive pathway in the mitochondrial IMS, we first determined phenotypic characteristics of Δ*g6pd*, Δ*trx*1/2, Δ*trr*1 and Δ*gsh*1 yeast strains. First, the growth of these strains in fermentable and non-fermentable media at both permissive and non-permissive temperature was monitored. Then, the levels of $NADP^+$ and NAPDH were measured to relate this with the growth phenotypes.

Finally, in order have an idea of the mitochondrial integrity, Δψ was measured in isolated mitochondria of the aforementioned yeast strains.

4.2 Yeast phenotype of Δ*g6pd*, Δ*trx*1/2, Δ*trr*1 and Δ*gsh*1 strains

4.2.1 Growth curve and spot test assay of Δ*g6pd*, Δ*trx*1/2, Δ*trr*1 and Δ*gsh*1 yeast

Before more specific *in organello* and *in vitro* analysis of the KO strains, its general effects in the organism were determined. Yeast from WT, Δ*g6pd*, Δ*trx*1/2, Δ*trr*1 and Δ*gsh*1 strains were grown on complete, broth or solid, YP media containing D-glucose (YPD) or lactate (YPlac) as carbon source at 30°C or 37°C. Both YPD and YPlac media were supplemented with 76 mg/L methionine as yeast becomes auxotroph for this amino acid in Δ*g6pd* (Thomas et al., 1991) and Δ*trx*1/2(Muller, 1991). Growth kinetics was measured in broth cultures at different time points until 48h while colony growth was analysed in solid culture 48h after plating. When grown on YPD, no difference was observed for any of the five yeast strains at either 30°C or 37°C (Top panel A Figure 4.2).On the other hand, under YPlac growth at 30°C the Δ*trr*1 strain entered exponential growth phase after 8h while the rest did so after 12h, but all strains started stationary phase after 28h growth (left bottom panel A Figure 4.2). Unlike growth on YPlac at 30°C, at 37°C all yeast strains grew slower as seen by the final OD reached in both temperature conditions. Furthermore, Δ*g6pd* and Δ*trx*1/2 delayed 28h to enter exponential growth phase while WT and Δ*gsh*1 did so after 12h (right bottom panel A Figure 4.2). Beside the growth curves, colony growth formation was tested by growing serial dilutions of each yeast strain in solid media. When grown on YPD at both 30°C and 37°C no significant differences were observed between yeast strains (top panel B Figure 4.2). In the presence of lactate Δ*trx*1/2 and Δ*gsh*1 showed a growth defect which was more dramatic in Δ*g6pd* (bottom panel B Figure 4.2).

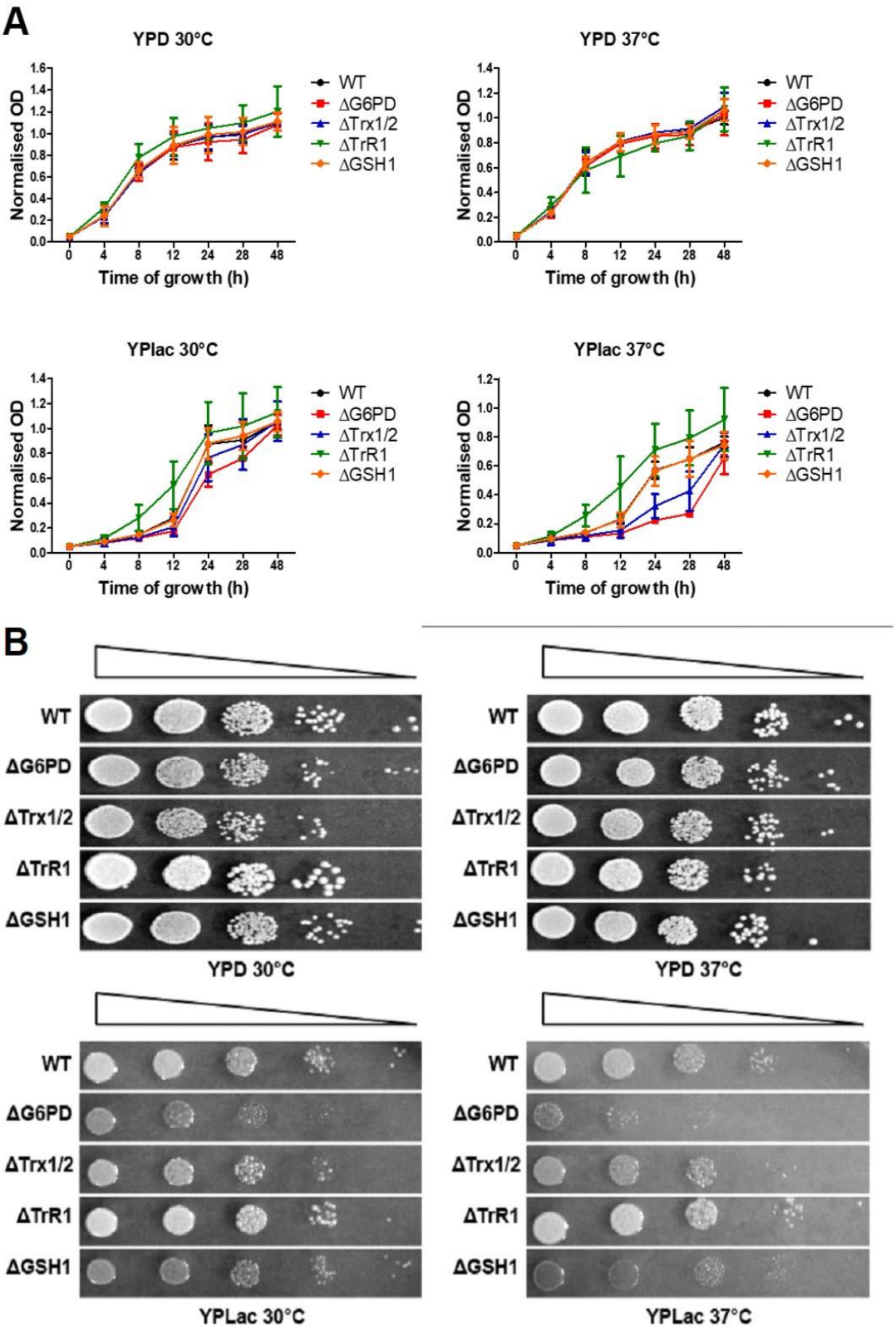

Figure 4.2 Growth curve and growth spot test of WT, Δ*g6pd*, Δ*trx*1/2, Δ*trr*1 and Δ*gsh*1 yeast. **A** Kinetics of the growth of WT (black), Δ*g6pd* (red), Δ*trx*1/2 (blue), Δ*trr*1 (green) and Δ*gsh*1 (orange) yeast under fermentable (YPD) and non-fermentable (YPlac) broth media at 30 °C and 37 °C was measured at 0h, 4h, 8h, 12h, 24h, 28h and 48h. OD_{600} values of yeast were normalised as 0.5 for time 0h. The results are shown as the mean OD_{600} of three independent measurements +/- SEM. **B** Spot test growth of WT, Δ*g6pd*, Δ*trx*1/2, Δ*trr*1 and Δ*gsh*1 yeast. Serial dilutions (1:10) of the different yeast were grown for 48h on solid fermentable (YPD) and non-fermentable (YPlac) media at either 30 °C and 37 °C. Results are representative of three independent experiments.

4.2.2 NADP+/NADPH ratio levels in Δ*g6pd*, Δ*trx*1/2, Δ*trr*1 and Δ*gsh*1 yeast

The Δ*g6pd*, Δ*trx*1/2, Δ*trr*1 and Δ*gsh*1 yeast are KO strains for elements involved in maintaining the reductive power of the cell. In this sense, NADPH represents an important pool of reducing power in the cell. Hence, measurements of the levels of both NADPH and $NADP^+$ were performed. Briefly, $1X10^5$ cells of each strain were lysed and treated with either 0.2N NaOH or 0.4N HCl to measure NADPH or $NADP^+$ respectively, using the NADP/NADPH-Glo Assay kit (Promega). Over the course of 40 minutes data were recorded and the results, displayed as the mean of two measurements, showed that NADPH was higher in every mutant strain than those of the WT: Δ*trr*1>Δ*trx*1/2>Δ*gsh*1>Δ*g6pd* (Left panel A Figure 4.3). Likewise, the levels of $NADP^+$ were higher for the mutants: Δ*trx*1/2>Δ*trr*1>Δ*gsh*1>Δ*g6pd* (Right panel A Figure 4.3). However, when comparing the $NADP^+$/NADPH ratio of each mutant strain against WT, all the mutants but Δ*g6pd* had a different ratio than the WT. The Δ*trx*1/2 and Δ*gsh*1 ratios were higher, with the Δ*gsh*1 strain having the lowest NADPH levels compared to $NADP^+$. The $NADP^+$/NADPH ratio in the Δ*trr*1 was lower and that of Δ*g6pd* showed no difference to WT.

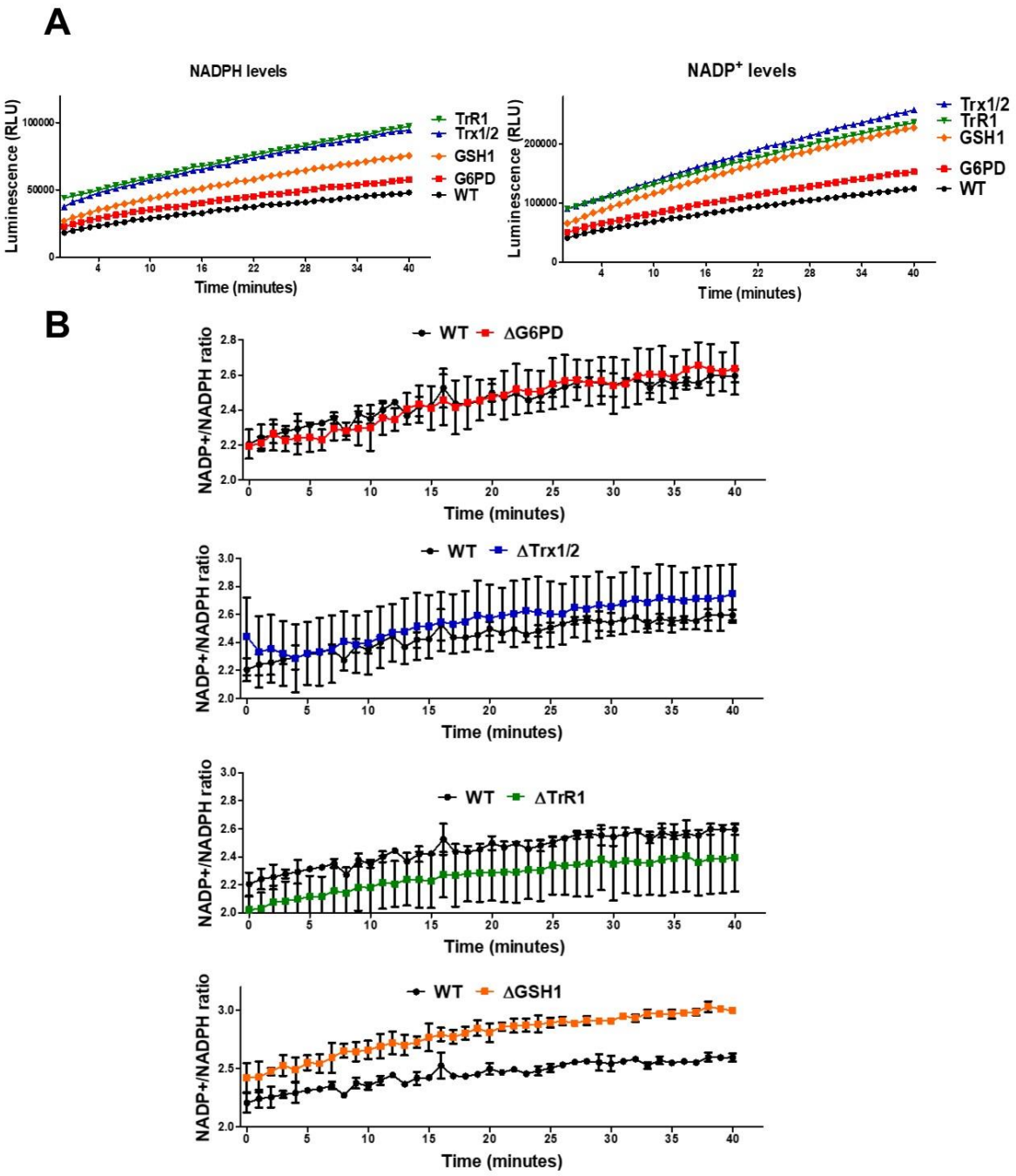

Figure 4.3 NADPH, NADP+ and NADP+/NADPH ratio measurements. Individual levels of NADPH or $NADP^+$ **(A)** and the $NADP^+$/NADPH ratio **(B)**. **A** Measurement of $NADP^+$ and NADPH levels from $1X10^5$ cells of each yeast strain (WT (black), Δ*g6pd* (red), Δ*trx*1/2 (blue), Δ*trr*1 (green) and Δ*gsh*1 (orange)) using the NADP/NADPH-Glo assay kit (Promega) for 40 minutes. The results are shown as the mean of two wells. **B** Results obtained in **(A)** were used to determine the $NADP^+$/NADPH ratio of each yeast strain. The results are presented as the mean +/- SEM of two different wells.

4.2.3 Mitochondrial inner membrane potential (Δψ) measurement of Δ*g6pd*, Δ*trx*1/2, Δ*trr*1 and Δ*gsh*1 yeast mitochondria

In order to have a general view of the mitochondrial integrity, mitochondrial IM potential Δψ of each mutant strain was measured and compared to WT. Briefly, the fluorescent dye $DiSC_3(5)$ gets internalised and retained into isolated mitochondria in the presence of Δψ but released out of mitochondria in the buffer in the absence of a Δψ. The fluoroscence of the dye is different in a buffer or when it is entrapped in mitochondria, allowing us to use this as a measure of mitochondrial internalisation and therefore (indirectly) the level of the IM potential. A drop in the fluorescence indicates a change in the environment of the dye because of internalisation into mitochondria. The fluorescence baseline emission by $DiSC_3(5)$ was the maximum value recorded before the addition of mitochondria and this value was taken as 100% to normalise the measurements for each one of the samples. The experiment was stopped with the addition of the uncoupler valinomycin (which abolishes the IM potential) after ~130s. As shown on Figure 4.4 the Δ*g6pd* mutant has similar IM Δψ to that of WT mitochondria with only 8% difference of their maximum point of dye internalisation. By sharp contrast to Δ*g6pd*, Δ*trx*1/2 and Δ*trr*1 showed a defect in IM Δψ of 20% and 40%, respectively, compared to the WT values (Figure 4.4). These results show an effect of the Δψ in all the mutants used which suggests there may be problems in the import capacity in these mitochondria and these could be correlated with the growth phenotypes observed for Δ*g6pd,* Δ*trx1/2* and Δ*gsh1* in Figure 4.2.

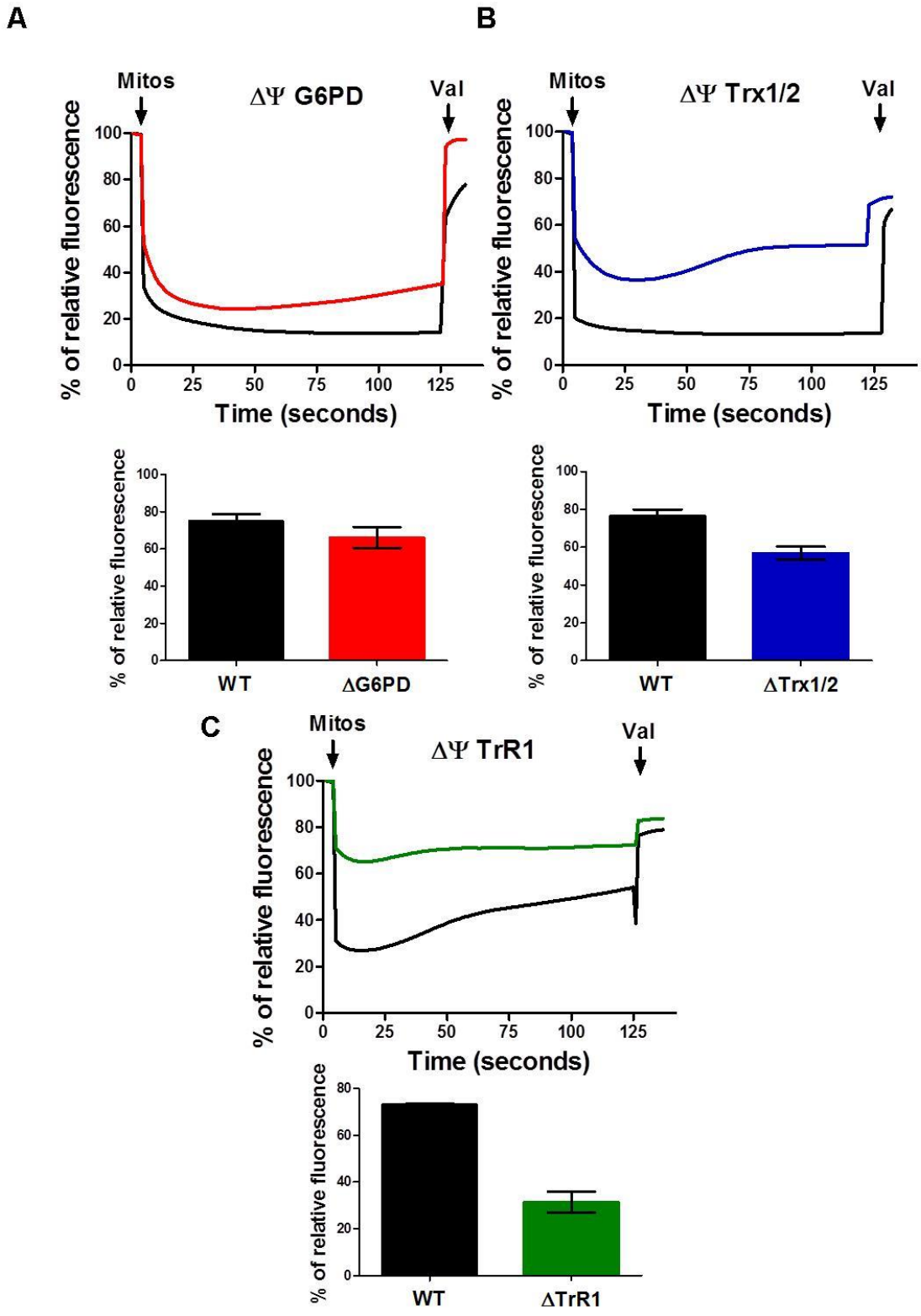

Figure 4.4 Mitochondrial membrane potential (Δψ) of WT and yeast mutant strains. Mitochondrial membrane potential measured from WT (black), **(A)** Δ*g6pd* (red), **(B)** Δ*trx*1/2 (blue), **(C)** Δ*trr*1 (green) isolated mitochondria. The top histogram of each panel shows the fluorescence of the $DiSC_3(5)$ molecule over ~130 seconds. The maximum fluorescence for each experiment was considered as 100% of relative fluorescence. The arrows indicate the time of addition of either 100 µg of mitochondria (mitos) or 1mM valinomycin (Val) were added. The results are representative of at least three different experiments. The histograms on the bottom of each panel represent the quantitative analysis of the percentage of maximum $DiSC_3(5)$ internalisation. The results are presented as the mean +/- SEM of at least three different experiments.

4.3 Discussion

In this chapter, phenotypical analysis of yeast with mutations affecting the main thiol reductive pathways (Δ*trx*1/2, Δ*trr*1 and Δ*gsh*1) or their main cytosolic NADPH source (Δ*g6pd*) were performed. First, the growth on both fermentable and non-fermentable carbon sources of these mutant strains was compared with that of the WT. In agreement with previous reports no growth defect was observed in any of the strains when cells were grown on YPD at either 30°C or 37°C (Lee et al., 2001, Muller, 1991, Muller, 1994, Minard and McAlister-Henn, 2005). Furthermore, colony growth defect in Δ*g6pd* Δ*trx*1/2 and Δ*gsh*1 strains was observed when respiratory conditions (i.e. growth on YPLac) were present (bottom panel B Figure 4.2). Therefore, the latter confirms the involvement of these enzymes or its products in the cell response to oxidative stress (Izawa et al., 1998, Lee et al., 2001, Muller, 1991, Okada et al., 2014). The growth defect shown in Δ*gsh*1 on solid YPLac growth but not on broth YPLac culture is due to the minimal amounts of GSH needed for yeast to grow normally, which are consistently provided by the YPD media. However, the serial dilutions to spot the yeast on solid media were made in water, which mimic washing conditions of GSH in previous studies (Trotter and Grant, 2003). The sharpest growth defect was observed in the Δ*g6pd* mutant probably due to its NADPH-producing role, which feeds with electrons to both the Trx and Grx systems (Fernandes and Holmgren, 2004, Lu and Holmgren, 2014). Additional controls to these growth experiments in which an exogenous reducing source (e.g. DTT, GSH or ascorbate) is added to the media to test if the growth defects are restored, or an external source of oxidative stress is added would reinforce the implication of the enzymes or their products in the response against oxidative stress.

The $NADP^+$/NADPH ratio and the NAD^+/NADH ratio are indicators of the redox state of the cell. The $NADP^+$/NADPH ratio of Δ*trx*1/2 and Δ*gsh*1 yeast strains is higher than the WT. This higher ratio indicates higher $NADP^+$ in comparison to NADPH, which could be used to compensate the absence of any of the two thiol-reducing systems (i.e. Trx and Grx). It has been shown that both thiol-reducing systems are important in the antioxidant response and that they have overlapping roles in handling oxidants (Trotter and Grant, 2005, Grant, 2001). Consistent with this polarisation towards the oxidised form of the dinucleotide the GSH/GSSG ratio has been shown to be more oxidised in Δ*trx*1/2 yeast, which

in this case also shows that the Grx system takes over the reducing role (Garrido and Grant, 2002, Trotter and Grant, 2002, Trotter and Grant, 2003). Conversely, the Δ*trr*1 $NADP^+$/NADPH ratio was lower, meaning increased relative amounts of the reduced form NADPH are present. The Δ*trr*1 yeast has been shown to have similar reductive environment to that of WT as the GSH/GSSG ratio is similar in these two strains (Garrido and Grant, 2002, Trotter and Grant, 2002). However, the $NADP^+$/NADPH ratio was not measured directly but calculated from the individual $NADP^+$ and NADPH values obtained with the NADP/NADPH-Glo Assay kit. These individual measurements were made following the destruction of one of the two NADP species, a process that might impact the total value of either of the two NADP species, thus affecting the value of the $NADP^+$/NADPH ratio. Another consideration to note is that the assay is a cycling reaction where NADP is the limiting reagent. Hence, the results form a sigmoidal curve and the correct measurement should be that of the curve slope. In the results shown on 4.1.2, the saturation plateau was never reached, and the graphs were compared directly between the WT and the mutants.

The state of the mitochondrial IM Δψ is indicative of mitochondrial integrity. Unlike the growth results, Δψ in Δ*g6pd* showed similar dye internalisation than that of the WT, but Δψ values of Δ*trx*1/2, and Δ*trr*1 were considerably lower with regard to WT. Despite g6pd being an important source of NADPH, it has been shown that other sources are crucial for NADPH production (Grabowska and Chelstowska, 2003, Minard et al., 1998, Minard and McAlister-Henn, 2001, Minard and McAlister-Henn, 2005). Indeed, as shown in the results section of chapter 5 the import of proteins that depend on Δψ like the Subunit 9 (Su9) of the F0 ATPase is not affected in Δ*g6pd* mitochondria. Disruptions in the Δψ are normally associated with the accumulation of ROS. The Δ*trx*1/2 and Δ*trr*1 strains are more sensitive to ROS as they lack key effectors in any of these two reductive pathways which can explain their disrupted Δψ (Grant, 2001) Unlike these mutants, the Δ*g6pd* strain does have the effectors of these reductive pathways and, as mentioned before, other sources of NADPH which might help to keep functional scavenging of endogenous ROS at levels that are not detrimental for Δψ. However, as seen in the bottom panel B of Figure 4.2, this mutant strain had the most dramatic growth defect when a respiratory substrate was present. In this regard, the pleiotropic nature of NADPH effects needs to be considered as it

might, directly or indirectly, affect different pathways important for cell growth. Accordingly, the different pathways that contribute to the NADPH pool are shown in Figure 4.1 which highlights the very wide network this cofactor is involved in. The fact that either form of NADP can be found bound to proteins and thus, not able to be detected needs to also be taken into account. Taken together, the yeast strains missing effectors of one of the main thiol-reductive pathways, as well as a strain lacking one of the main NADPH sources have lower $\Delta\psi$ and are not able to grow under respiratory conditions.

Chapter 5 Protein levels and import capacity of yeast strains with affected reducing capacity

5.1 Introduction

In the previous chapter it was shown that the Δ*g6pd* and Δ*trx*1/2 yeast mutants have growth defects when exposed to a non-fermentable carbon source and that these mutants together with the Δ*gsh*1 strains have lower Δψ than that of WT. Also, Δ*g6pd* has a similar NADP+/NADPH ratio than the WT but this is different in the rest of the mutants. It has been shown that Δψ is an indication of mitochondrial dysfunction and is vital for the import of proteins into the matrix or insertion at the inner membrane via the TIM23 and the TIM22 complexes respectively (Demishtein-Zohary and Azem, 2017, Endres et al., 1999). The yeast *S. cerevisiae* has extensively been used for import experiments as it shares high homology with the mammalian mitochondria biogenesis. In the last three decades the import of proteins into mitochondria has been elucidated and with that, its complexity and importance in mitochondrial integrity as well as in health have become evident.

In this chapter, we analysed the impact that redox disturbances in the cell have on the import of protein into mitochondria, in particular to the mitochondrial IMS. This is important as a growing number of diseases have been related to defects on the protein import into mitochondria.

5.1.1 Importance of protein import into mitochondria

The main import pathways have been described in detail in the main introduction (section 1.2). Disruption of protein import into mitochondria has been shown to affect yeast adaptability to stress conditions, growth impairment and even loss of viability. In humans, a growing set of diseases associated with problems in the mitochondrial import machinery has been identified.

One of the earliest reports of mitochondrial import impairment associated with disease described a single base mutation in the MTS of the E1α subunit of the pyruvate dehydrogenase (PDH) complex, resulting in lower levels of the protein in the patient's sample (Takakubo et al., 1995). PDH deficiency is a common

cause of lactic acidosis in children and is involved in central nervous system abnormalities (Robinson et al., 1987, Robinson et al., 1980). The lower protein levels in the patient were attributed to decreased import capacity of the protein due to an R10P substitution in the MTS. The latter was seen after preforming import experiments of the matrix protein ornithine transcarbamylase fused with either the WT or the R10P MTS into mitochondria (Takakubo et al., 1995). Another disease associated with defects in the import machinery is the deafness dystonia syndrome (DDS), also known as Mohr-Tranebjaerg syndrome, which is characterised by deafness and dystonia in various severity levels and can cause mental deterioration, paranoia and cortical blindness. This disease is caused by the incapability of the deafness dystonia peptide (DPP) 1, the human homologue of yeast Tim8, to form the heteromultimeric complex with Tim13 in the IMS. The complex formation impairment is due to a mutation of a cysteine in the CX_3C twin motif of DDP1, which has been shown to affect the DDP1-Tim13 interaction, but not the targeting or localisation into the IMS of the protein (Koehler et al., 1999, Roesch et al., 2002, Sabine Hofmann, 2002). The DDP1-Tim13 complex assists the targeting of proteins into their correspondent mitochondrial compartments and thus, its wide involvement in mitochondrial biogenesis is believed to be the cause of DDS.

In this chapter, we verified the levels of mitochondrial proteins and the import capacity of the Δ*g6pd* yeast strain in order to know if the mitochondrial import pathways were affected.

5.2 Mitochondrial protein levels in WT and Δ*g6pd* yeast

5.2.1 Steady state levels of mitochondrial proteins in WT and Δ*g6pd* mitochondria

Following the general phenotypic effects found in the Δ*g6pd*, Δ*trx*1/2, Δ*trr*1 and Δ*gsh*1 as described in the previous chapter, we now wanted to look in more detail and find out if the mitochondrial import pathways were affected in Δ*g6pd* as its effects should be upstream to the specific Trx or Grx mutant strains. Thus, as a first approach we analysed the protein levels in isolated mitochondria from this strain and compared them to WT. In order to detect the proteins, rabbit polyclonal antibodies (Ab) raised against recombinant purified proteins were

used to perform western blots. Different amounts of mitochondria (20 µg, 40 µg and 80 µg) were analysed by Tris-Tricine SDS-PAGE where the membrane was incubated with the corresponding primary Ab and detected by chemiluminescence. As shown in Figure 5.1, no difference in protein levels was seen for either the matrix targeted protein Hsp70 (Voos and Rottgers, 2002), the OM proteins Tom70 (Wu and Sha, 2006), Tom40 (Hill et al., 1998) and porin (Blachly-Dyson et al., 1997) or the IM protein Tim23 (Guiard, 1985). The levels of the IM anchored Mia40 (Chatzi et al., 2013) and the IMS sulfhydryl oxidase Erv1 (Mesecke et al., 2005) were also not affected. However, the levels of the IMS protein Cytochrome c (Guiard, 1985) (second last rectangle Figure 5.1) were slightly less in the Δ*g6pd* and considerably decreased for the IM protein Tim22. Furthermore, a more dramatic difference was seen for the Mia40 substrates Tim10 and Tim9 (Vial et al., 2002) (Bottom rectangle Figure 5.1). These results suggest specific alterations on IMS proteins that depend on the Mia40 pathway and IM proteins that depend on the TIM22 complex for their import.

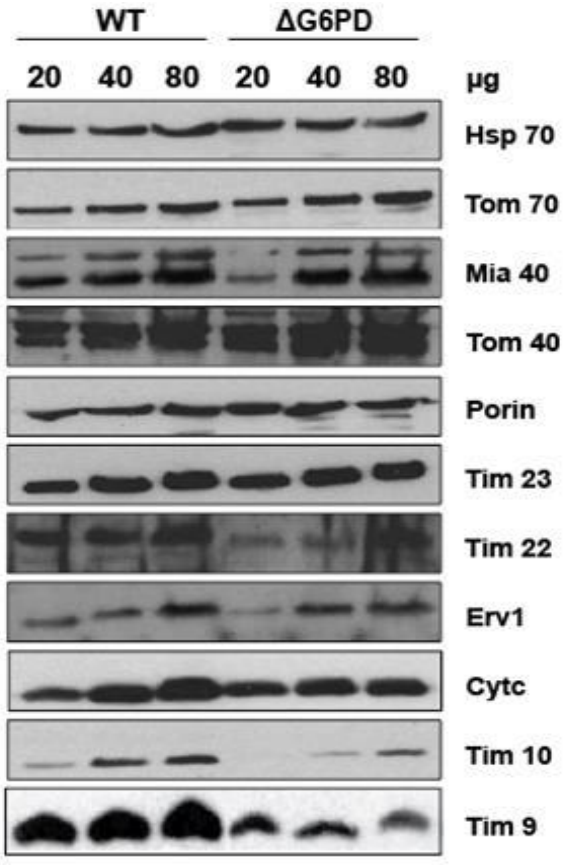

Figure 5.1 Mitochondrial protein levels in WT and Δ*g6pd* pure mitochondria. Western blot analysis of 20 µg, 40 µg and 80 µg of WT and Δ*g6pd* pure mitochondria for the detection of the mitochondrial proteins Hsp70 (matrix), Tom70 (OM), Mia40 (IM anchored) porin (OM), Tim23 (IM), Tim22 (IM), Erv1 (IMS), cytochrome c (cytc) (IMS) and the Mia40 substrates Tim10 and Tim9 (IMS).

5.2.2 Protein import capacity of WT and Δ*g6pd* mitochondria

The lower steady Tim10 levels in Δ*g6pd* mitochondria shown in Figure 5.1 could be due to either decreased protein translation, or increased degradation after translation and import or decreased protein import capacity. To distinguish between these different possibilities, the import capacity of Δ*g6pd* mitochondria was assessed by presenting different protein precursors into mitochondria isolated from the Δ*g6pd* strain ((Glick, 1991) and section 3.2.2.1) and comparing their import levels to those in WT mitochondria. *In vitro* translated ^{35}S-Methionine radiolabelled protein precursors were synthesised using a rabbit reticulocyte lysate transcription and translation (TNT) system (Promega) (section 3.2.2.3). The precursors were then presented to 50 µg of mitochondria and incubated at 30°C for 15 minutes. The resulting mitochondrial pellet was resuspended and treated with Proteinase K (PK) to remove non-imported material. In parallel, in order to make sure that the PK actually cleaved the material that was not protected by mitochondria an import sample was treated concomitantly with both the detergent Triton X-100, to solubilize mitochondria and expose all their protein content, and the proteinase (denoted as 'TX' lanes in all panels Figure 5.2). Additionally, 10% of the total protein input used for the import reaction was loaded (first lane in all panels Figure 5.2). The resulting samples were analysed by Tris-Tricine SDS-PAGE and visualised by autoradiography. The results show that the import of the OM auxiliary protein Tom5 (Dietmeier et al., 1997), the matrix targeted Su9-DHFR (Ooi et al., 1985) and the IMS localised protein Erv1 (Mesecke et al., 2005) was not affected (panels A, B and D Figure 5.2). On the other hand, the import of Mia40 itself in Δ*g6pd* was lower than in WT (panel C Figure 5.2). Furthermore, the import of the small Tim proteins Tim12, Tim10 and Tim9 which are classical Mia40 substrates (Sideris and Tokatlidis, 2007) was severely impaired in the mutant strain (Panels E-G Figure 5.2). Strikingly, the import of the IM protein Tim11 was also affected (Panel H Figure 5.2). The results in Figure 5.2 indicate that the effect of the Δ*g6pd* mutation, although it could be thought as global (Figure 4.2), in terms of mitochondria biogenesis is in fact specific to the MIA import pathway.

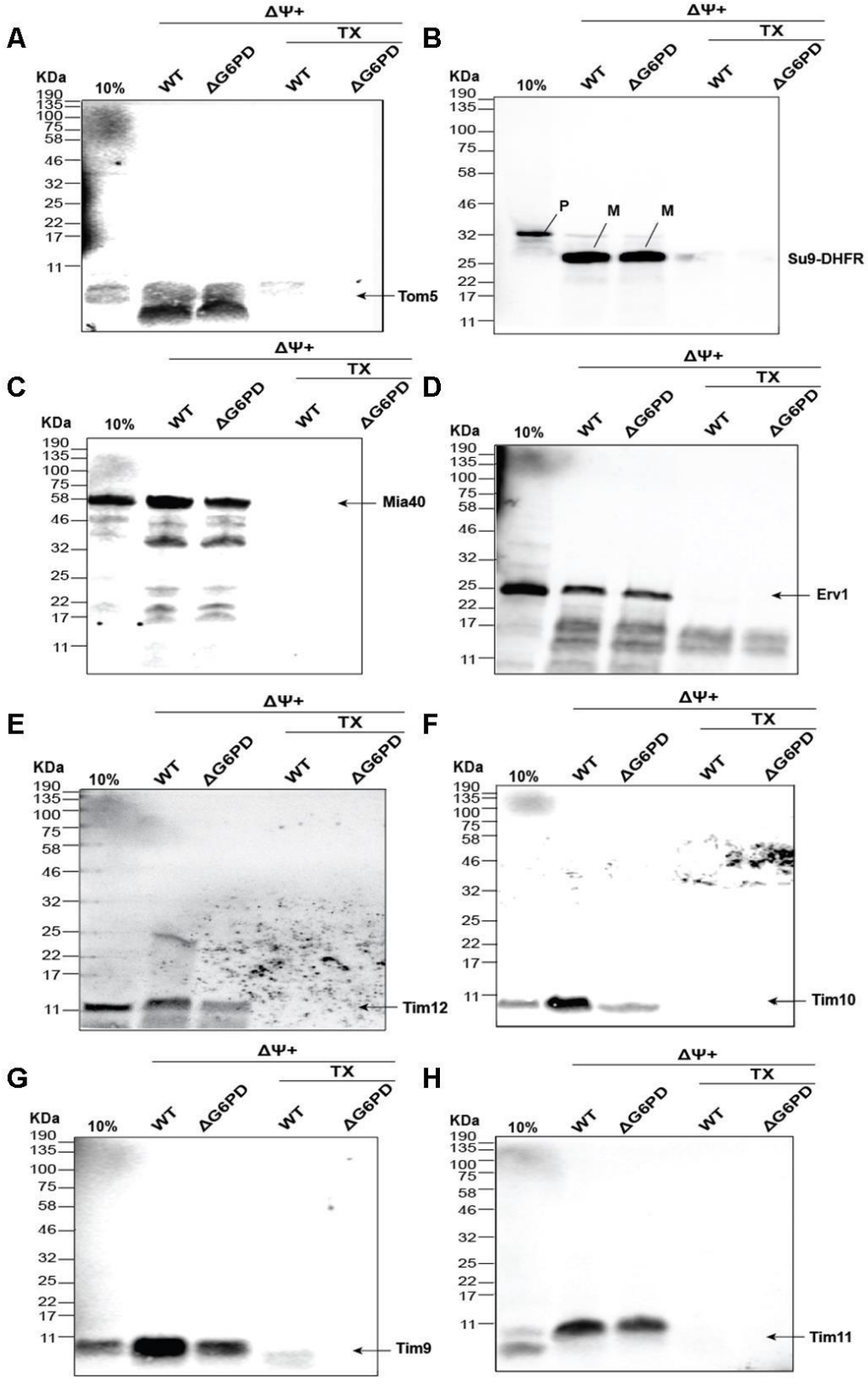

Figure 5.2 Import capacity of WT and Δ*g6pd* mitochondria. Autoradiography of the import of mitochondrial proteins into WT and Δ*g6pd* pure mitochondria. Import of radiolabelled protein precursors for **(A)** Tom5 (OM), **(B)** Su9-DHFR (matrix), **(C)** Mia40 (IMS), **(D)** Erv1 (IMS), **(E)** Tim12 (IMS), **(F)** Tim10 (IMS), **(G)** Tim9 (IMS) and **(H)** Tim11 (IMS) in the presence of membrane potential ($\Delta\psi^+$). First lane in each panel represents 10% of total precursor presented to mitochondria. The results are representative for at least three different biological replicates. TX: Triton X-100.

5.2.3 Oxidative state of Mia40 in WT and Δ*g6pd* mitochondria

The effect of the Δ*g6pd* mutation was more dramatic for substrates of the MIA pathway and despite no apparent difference in the $NADP^+$/NADPH ratio (Figure 4.3), g6pd is important to the redox balance (Izawa et al., 1998). We reasoned that these g6pd-dependent redox effects at the level of mitochondrial protein import could be exerted via a direct influence of the redox state of Mia40 in mitochondria. Under physiological conditions, Mia40 must exist in a balanced state between its reduced and oxidized forms to function properly (Erdogan et al., 2018). Thus, I examined directly the redox state of Mia40 in WT and Δ*g6pd* via an alkylation shift assay. Briefly, the molecule mal-PEG binds to free reduced (SH-) but not oxidised (S-S) thiols adding 5 kDa per free thiol group. As a result, the alkylated (reduced) protein can be detected as higher bands than the oxidised ones after Tris-Tricine SDS-PAGE and western blot analysis. As a control, one sample was treated with the reducing agent DTT to reveal that the maleimide had bound (first and fourth lane in Figure 5.3). For this experiment, rabbit polyclonal anti Mia40 antisera was used and detected by fluorescence. The core of Mia40 possesses 6 cysteines residues, 4 structural ones engaged in two very stable intramolecular disulphide bonds buried internally in the folded core of Mia40 and 2 present in its surface-exposed, active site CPC motif (Banci et al., 2009), which can readily shift from the reduced to the oxidized (disulphide-bonded) state and are prone to be easily alkylated by the mal-PEG molecule. The results in Figure 5.3 showed that the redox state of Mia40 in Δ*g6pd* mitochondria is more oxidised (70kDa band lane 6 Figure 5.3) compared to a more balanced state between the reduced and oxidised forms in WT mitochondria (lane 3 Figure 5.3). Therefore, the altered redox balance of Mia40 towards an oxidised state compromises the import of classical MIA pathway substrates.

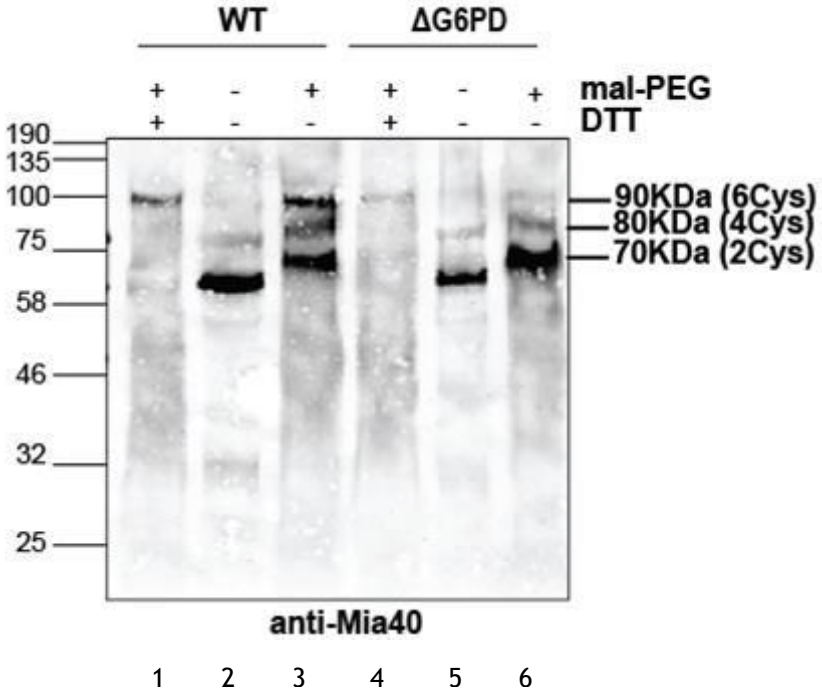

Figure 5.3 Redox state of Mia40 in WT and Δ*g6pd*. Proteins from pure isolated mitochondria from WT and Δ*g6pd* yeast were precipitated with 10% TCA and treated (lanes 3 and 6) or not (lanes 2 and 5) with mal-PEG or mal-PEG+DTT (lanes 1 and 4). Immunodecoration with anti-Mia40 Ab and fluorescence detection. The size of each band was determined by linear regression of a pattern curve created with the distance travelled of each molecular weight marker. The results are representative of at least three different biological replicates.

5.3 Discussion

The aim of this chapter was to determine if the absence of g6pd was affecting the levels of mitochondrial proteins and if such an effect was due to reduced import capacity of mitochondria isolated from this yeast strain. Despite the fact that a decreased oxidative stress response and methionine auxotrophy are known effects of Δ*g6pd* yeast (Izawa et al., 1998, Thomas et al., 1991), no information was available at the start of this thesis on how the deficiency of this enzyme may influence mitochondrial protein levels or mitochondria biogenesis. The Δ*g6pd* yeast strain has normally been used to determine NADPH sources in the cell under different conditions (Izawa et al., 1998, Minard and McAlister-Henn, 2005). Even studies of its deficiency in humans have neglected to look on how it might influence mitochondria, mainly because this deficiency is associated to haemolytic anaemia which affects red blood cells, a cell type that loses mitochondria and other organelles as these cells mature (Bubp et al., 2015, Ho et al., 2007). However, as mentioned in the introduction of this chapter the import impairment into mitochondria is associated to certain diseases. Given the

fact that this mutation is the most common enzyme deficiency in humans (Ho et al., 2007), the study of its effects on mitochondria biogenesis is of major importance. From the results in Figure 5.1 and Figure 5.2 we can conclude that the presequence pathway, the sorting of ß-barrel proteins and the pathway dependent on the TIM22 complex are not affected in Δ*g6pd* yeast. On the other hand, a specific effect in the mutant strain on the main import pathway of the IMS, the MIA pathway, is observed.

The presequence pathway, responsible for the import of most mitochondrial proteins that are targeted to the matrix (Tamura et al., 2009a) appears not to be defective. This is supported by the similar mitochondrial Δψ between Δ*g6pd* and WT yeast (Panel A Figure 4.4) as it is known that this pathway depends on Δψ as the main import driving force (Geissler et al., 2000, Pfanner et al., 1987). In addition, the levels of the channel forming protein Tim23 (Truscott et al., 2001) and the mitochondrial chaperone Hsp70 (Chacinska et al., 2009), both essential for the functioning of this pathway were not affected (Figure 5.1). Neither was the import of the Su9-DHFR precursor (Panel B Figure 5.2), a matrix targeted precursor. Furthermore, the import of Mia40, which also depends on Tim23 (Chatzi et al., 2013), was only slightly affected. Likewise, the SAM sorting pathway (Wiedemann et al., 2003), which is responsible for the insertion of ß-barrel proteins in the OM also remains unaffected. Although the levels of the small Tims are affected in the mutant strain and these proteins are also involved in the sorting of ß-barrel proteins (section 1.2.4), the remaining proteins might be enough to fulfil their function. These non-affected pathways can be seen in Figure 5.1 and panels A-D of Figure 5.2 as a variety of proteins steady state and import levels are not affected in the mutant. Since the OM ß-barrel protein Tom40 is the entry gate of such proteins (Hill et al., 1998) and its levels are normal in the yeast mutant (Figure 5.1), we can infer that it is properly inserted and active. Moreover, the levels of another abundant ß-barrel protein, porin (Lee et al., 1998) are also normal in Δ*g6pd*. On the other hand, the so-called carrier pathway (for polytopic integral membrane proteins of the inner membrane) appears to be affected, even though the levels of Δψ (the main energy source for this pathway) are not substantially affected ((Panel A Figure 4.4) (Pfanner and Neupert, 1985, Pfanner and Neupert, 1987)) and the levels of the main import receptor Tom70 for this pathway (Sollner et al., 1990, Young et

al., 2003) are also similar to the WT. The fact that the essential component of the TIM22 complex, the protein Tim22 (Kerscher et al., 1997, Kovermann et al., 2002) is considerably affected suggests that import via this pathway is impaired.

The most intriguing and exciting result in this chapter is that the import of proteins into the IMS which is mediated primarily by the MIA pathway (Backes and Herrmann, 2017, Chatzi et al., 2016, Fischer et al., 2013) is clearly and specifically affected. Despite the fact that the steady-state levels of Mia40 and Erv1, the two key players of the this pathway (Banci et al., 2013, Banci et al., 2009, Chatzi et al., 2016, Chatzi et al., 2013, Mesecke et al., 2005) are similar in the mutant and the WT, the import of these proteins does not or not fully depend on the MIA system.

The classical substrates of this pathway include the small Tim proteins, i.e. Tim8, Tim9, Tim10, Tim12 and Tim13 (Koehler, 2004, Sideris and Tokatlidis, 2007). Therefore, the decreased protein levels and import of Tim9, Tim10 and Tim12 seen in Figure 5.1 and panels E-G of Figure 5.2 indicate a specific and considerable effect of the Δ*g6pd* mutation on the MIA pathway. Intriguingly, the import levels of the IM associated protein Tim11 (Arnold et al., 1997, Tokatlidis et al., 1996), which engages in a yet unknown import mechanism, were also decreased in the Δ*g6pd* yeast mutant. One explanation for this is that Tim11 has a very active cysteine, which might be affected because of the reductive alterations in this yeast mutant (Tokatlidis et al., 1996).

The MIA pathway relies on the oxidative folding capacity of the oxidoreductase Mia40 which oxidises cysteine residues in its substrates via an active CPC motif (Banci et al., 2009). Since growth on respiratory conditions of yeast is affected and the MIA pathway impaired because of the absence of g6pd, we hypothesised that the redox state of Mia40 was altered. In fact, Mia40 from Δ*g6pd* is more oxidised than its WT counterpart, where it has the capacity to remain in a balanced redox state (Figure 5.3). This balance between reduced and oxidised state of WT Mia40 is in agreement with previous studies (Erdogan et al., 2018, Kojer et al., 2012). In summary, the results of this chapter showed a clear and specific defect on the import capacity of IMS proteins that depend on the MIA pathway and that this decreased import is due to the unbalanced redox state of Mia40 towards the oxidative form.

Chapter 6 The thioredoxin system in the IMS of yeast mitochondria

6.1 Introduction

The data shown in the previous chapters provide evidence that the Δ*g6pd* yeast strain cannot grow under respiratory (Figure 4.2) conditions, i.e. increased ROS-producing conditions. Furthermore, this mutant has decreased import capacity specifically for IMS proteins that depend on the MIA pathway (Figure 5.2) because, at least in part, of a more oxidised state of Mia40 (Figure 5.3). The latter suggests that a reducing pathway must be present in the IMS to keep the redox state of Mia40 in a balanced manner because this is needed for its proper function. This idea is supported by the presence of not only oxidative but also reductive pathways in every other cellular compartment similar to the mitochondrial IMS that houses a full oxidoreductase machinery, *i.e.* the ER and the bacterial periplasm (Cardenas-Rodriguez and Tokatlidis, 2017, Herrmann and Riemer, 2014). In this context, the two main thiol-reductive systems (Trx and Grx) are good candidates to fulfil this role. In fact, a recent publication on an updated version of the yeast mitochondrial IMS proteome identified both protein components of the cytosolic Trx system to be present in this sub-mitochondrial compartment (Vögtle et al., 2012). Thus, we hypothesised that the Trx system is the reductive pathway in the IMS responsible for keeping Mia40 in a functional reduced/oxidised state.

6.1.1 The Thioredoxin super family: The Thioredoxin fold

As mentioned in the introduction, the yeast cytosolic Trx isoforms (Trx1 and Trx2) are members of the thioredoxin protein family. This superfamily includes a wide range of proteins playing different roles in the cell such as thiol disulphide oxidoreductases (Holmgren, 1995), glutathione S-transferases (Nishida et al., 1998) and disulphide isomerases (Kemmink et al., 1997). Additionally, proteins containing this motif are widely conserved as they have been found in a vast range of species from bacteria (Holmgren et al., 1975) and yeast (Trotter and Grant, 2002) to humans (Watson et al., 2003).

The members of this family share a motif called the thioredoxin fold, consisting in four central ß-sheets flanked by three α-helices (Ren et al., 2009). The strictly conserved redox active CXXC site is present within a loop connecting a ß-sheet with an α-helix (Figure 6.1, (Holmgren et al., 1975)). Noteworthy, the residues between the two active cysteines influence the redox potential of these proteins giving them their oxidant or reductant nature. In particular, both the Trx1 and Trx2 yeast proteins have a Cys-Gly-Pro-Cys motif (Figure 6.1). This sequence is shared with both the human and the *Escherichia coli* cytosolic Trx (Figure 6.1). In particular, the *E. coli* Trx1 has been found to be its strongest reductant (Krause et al., 1991). This is important to consider given the highly similar structure and the identical redox active site between *S. cerevisiae* and *E. coli*. Hence, Trx1 is indeed a good candidate to be a reductant in the oxidising environment of the mitochondrial IMS.

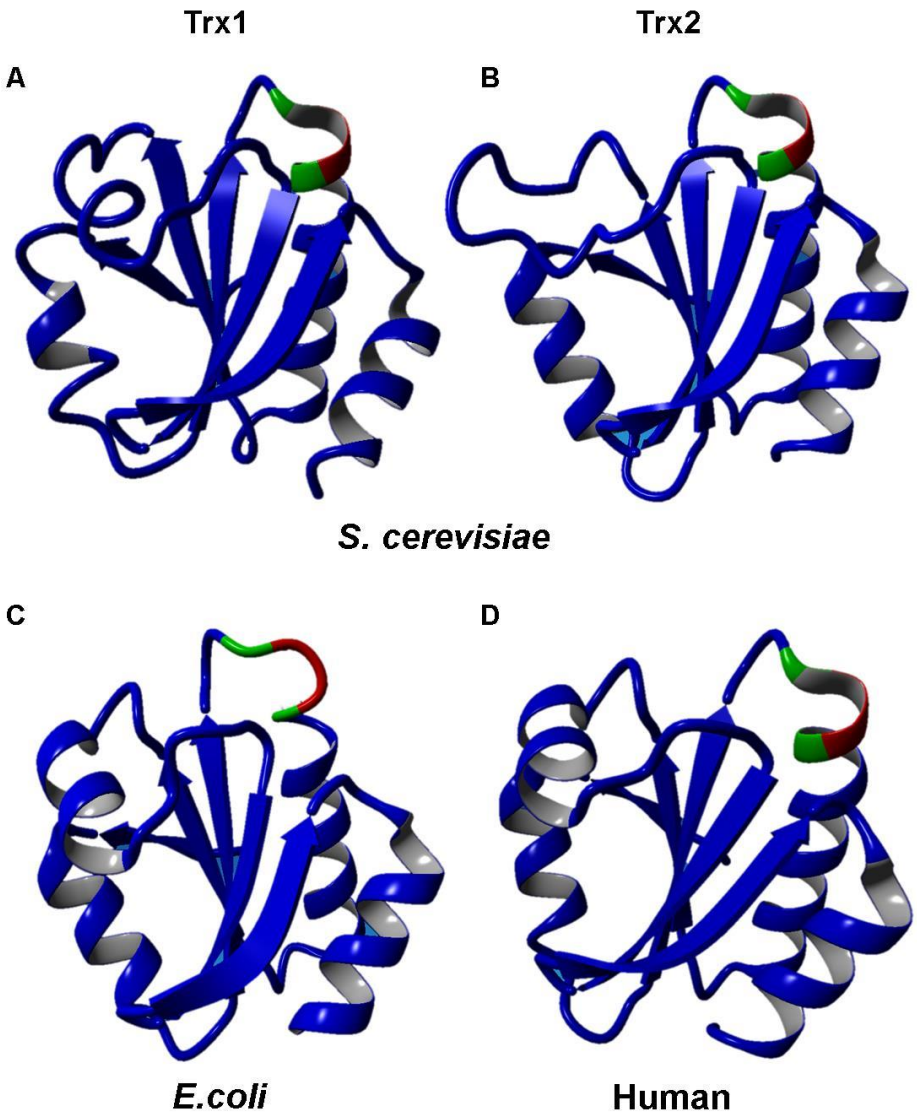

Figure 6.1 Thiol-reductant thioredoxin is widely conserved among species. Crystal structures of thioredoxin 1 from both cytosolic isoforms of *Saccharomyces cerevisiae*: **(A)** Trx1 (PDB id: 2n5a) and **(B)** (Trx2) (PDB id: 2fa4), **(C)** *Escherichia coli* (PDB id: 5hr1) and **(D)** human (PDB id: 5dqy). The characteristic exposed redox active site shared by the four proteins is highlighted as green: Cys and red: Gly-Pro.

In this chapter we first confirmed that the components of the cytosolic Trx system, Trx1, Trx2 and TrR1, can be imported into WT and Δ*g6pd* mitochondria. Furthermore, the *in vitro* and *in organello* interaction between Mia40 and Trx was shown. Finally, the inner membrane potential Δψ (as a measure of a functional defect in mitochondria) and the import capacity of Δ*g6pd* mitochondria (as a direct measure of an effect on the biogenesis capacity for mitochondria) were assessed after the exogenous addition of NADPH, Trx1 and TrR1.

6.2 Influence of the thioredoxin system localisation in the IMS on the import of other proteins imported into the IMS of mitochondria

6.2.1 Import of Trx1 and TrR1 into WT and Δ*g6pd* isolated mitochondria

The first step before testing if the Trx system can act as the missing reductive pathway in the IMS was to make sure that Trx1, Trx2 and TrR1 can be imported into WT and Δg6pd mitochondria. To achieve this, import of 10 µg of recombinant His-tagged Trx1 (Manganas, 2017), Trx2 (Subramanian, 2018) or TrR1 (Manganas, 2017) were presented to 50 µg of isolated WT or Δg6pd mitochondria. The import reaction was carried out for 15 min at 30°C, non-imported material was removed by exogenous protease treatment, mitochondria were re-isolated by centrifugation and analysed for their imported material by Tris-Tricine SDS-PAGE and immunoblotting followed by chemiluminescence as previously described (section 3.2.3.2 and Figure 5.2). Where mentioned, ß-mercaptoethanol (lanes 2 and 6 Figure 6.2) was omitted and ATP (lanes 4 and 8 Figure 6.2) or inner membrane potential Δψ (lanes 5 and 9 Figure 6.2) were depleted in order to test if the import depends on any of those factors. A sample representing 2% of the total protein used for the import reaction was added (first lane Figure 6.2). The results about the import into WT confirmed previous data from our lab indicating that the import of Trx1 and TrR1 does not depend on the presence of either ATP or inner Δψ (Figure 6.2). Additionally, the import of the other cytosolic isoform of yeast thioredoxin, Trx2, was also not affected by any of these conditions (bottom Figure 6.2). Likewise, the proteins Trx1, Trx2 and TrR1 can get imported into mitochondria from Δg6pd yeast and for the case of TrR1 it is increased when ATP and the inner Δψ are depleted (top Figure 6.2). Additionally, bands of lower molecular weight can be seen in the TrR1 blot, these bands might be degraded products resulting from the import of the protein Therefore, with the information showed in Figure 6.2 we can conclude that Trx1, Trx2 and TrR1 get imported into Δg6pd mitochondria independent on Δψ and ATP.

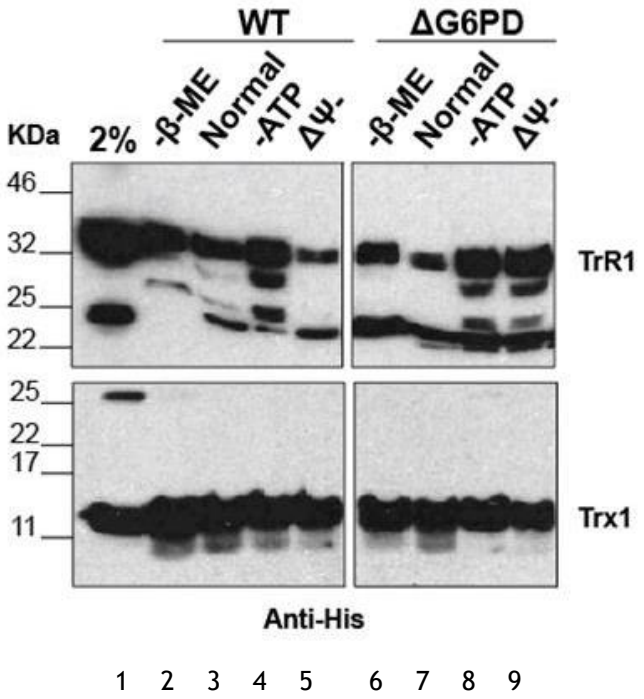

Figure 6.2 TrR1 and Trx1 import into WT and Δ*g6pd* mitochondria. Western blot analysis for the import of recombinant His-tagged TrR1, Trx1 and Trx2 into WT and Δ*g6pd* pure mitochondria. Mouse anti-His Ab was used to detect imported proteins. First lane represents 2% of the total protein presented to mitochondria. -β-ME: absence of β-mercaptoethanol in the sample buffer, -ATP: depletion of ATP with oligomycin (10μM) and apyrase (10mU/μl) and Δψ-: depletion of inner Δψ with valinomycin (1mM). Results are representative of at least three different experiments.

6.2.2 *In vitro* interaction between Mia40 and Thioredoxin

The cytosolic protein components of the yeast Trx system can not only be imported into mitochondria, but it also has been shown to localise to the IMS of mitochondria (Manganas, 2017). Furthermore, it was demonstrated that the Trx system reduces Mia40 *in vitro* and that Trx1 pulls down Mia40 after its import into mitochondria (Manganas, 2017). Here we wanted to expand on the interaction between Trx and Mia40. In order to do that, cross-linking experiments between Mia40 and Trx1, Trx2 or the mutant Trx1 C30/33S using the non-specific cross-linker glutaraldehyde (GA) were performed. Briefly, 1μg of recombinant His-tagged Mia40 was added to 1μg of recombinant His-tagged Trx1 (panel A Figure 6.3) or Trx2 (panel B Figure 6.3) or Trx1 C30/33S (panel C Figure 6.3) in the presence (lanes 6-8 Figure 6.3) or not (lane 5 Figure 6.3) of 0.1% GA for up to 10 minutes at room temperature. The gels were then analysed by Tris-Tricine SDS-PAGE, immunoblotting and chemiluminescence. In parallel, as controls each individual C-terminal 6XHis-tagged protein was treated with or without GA (lanes 1-4 in each panel Figure 6.3). The results in Figure 6.3 show the monomers of Trx1, Trx2 and Trx1 C30/33S at 12 kDa and oligomers of about

27 kDa, 35 kDa and 52 kDa in the three proteins. Higher species are seen for both Trx2 and the Trx1 cysteine mutant but not Trx1 (lane 2 in all panels Figure 6.3). The other control, Mia40, runs at 20 kDa and forms an oligomer of 33 kDa (lanes 3 and 4 in all panels Figure 6.3). When only the two proteins were added, both monomers but no other bands can be seen (lane 5 Figure 6.3). Finally, after the addition of GA in the presence of both proteins all the bands in the controls are observed, but also an extra band at 30 kDa (arrow in all panels Figure 6.3), which is likely Mia40-Trx1 intermolecular adduct. These results indicate that *in vitro* Mia 40 can interact with both Trx1 and Trx2 as well as the mutant Trx1 C30/33S, which suggests that the Mia40-Trx1 interaction is independent of the Cys residues on Trx1. The interaction monitored by X-linking as used in this assay is based on the vicinity of interacting surfaces between Mia40 and Trx1. The fact that we still see the interaction to persist even with the Cys mutants of Trx1 means that these are not affected structurally to an extent that would affect the interacting surface of Trx1 with Mia40. GA is a crosslinker creating covalent bonds between Lys residues between proteins, and therefore not very specific. A more detailed analysis of the interacting surfaces between Mia40 and Trx1 would require either trypsinolysis and mass spectrometry analysis after the crosslinking, or a high resolution structural analysis of the complex (via NMR or X-ray crystallography).

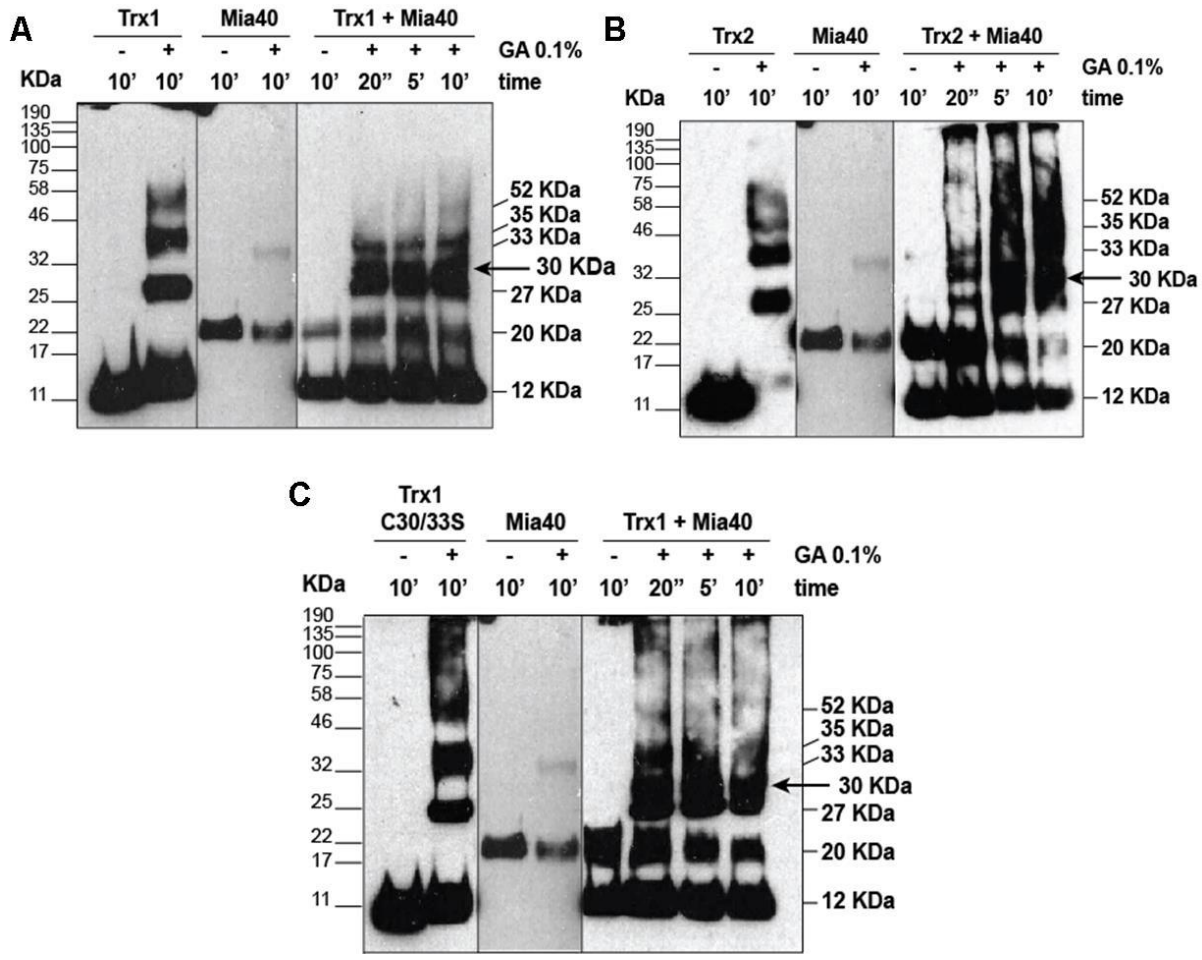

Figure 6.3 Cross-link between different Trx and Mia40. Recombinant His-tagged proteins Mia40 and **(A)** Trx1 or **(B)** Trx2 or **(C)** Trx1 C30/33S were treated or not with 0.1% glutaraldehyde (GA) for 20'', 5' or 10'. Samples were analysed by Tris-tricine SDS-PAGE and western blot using mouse anti-His Ab. Controls using the individual proteins treated or not with GA (lanes 1-4 in all panels). The results are representative of at least three different experiments.

6.2.3 Import of the Trx system to restore the inner membrane potential Δψ and the import capacity of Δ*g6pd* mitochondria

In the previous chapters we have concluded that the import capacity of the MIA substrates in the Δ*g6pd* mitochondria was specifically affected because Mia40 redox balance was perturbed and Mia40 stayed in a more oxidised form than it would under physiological conditions. Hence, Mia40 must interact with a reductive pathway, the lack of which in the g6pd mutant forced the protein to stay aberrantly oxidised. In this matter,
Figure 6.2 and Figure 6.3 show that Trx1, Trx2 and TrR1 can get imported into Δ*g6pd* mitochondria and that both Trx1 and Trx2 interact with Mia40 *in vitro*. Therefore, we checked whether the import of the Trx system can restore the unbalanced redox state of Mia40 and subsequently recover the import capacity of mitochondria isolated from Δ*g6pd* yeast.

As a first step we tested if the Trx system imported into the IMS can interact functionally with Mia40 in the same compartment. Thus, 100 µg of Δ*g6pd*

mitochondria were equilibrated with 2.5mM NADPH (to make sure that they have enough NADPH as a reducing power) and incubated first with 20µg of Trx1 for 5' at 30°C and then with 20µg of TrR1 for a further 10' at the same temperature. In parallel, the same amount of WT or Δ*g6pd* mitochondria were equilibrated with NADPH and incubated for 20' at 30°C. The mitochondria were then treated or not with Mal-PEG as previously described in Figure 5.3 followed by analysis on Tris-Tricine SDS-PAGE, western blotting using rabbit polyclonal anti-Mia40 antisera and fluorescence (Figure 6.5). A schematic representation of this is shown in panel A and panel B Figure 6.4.

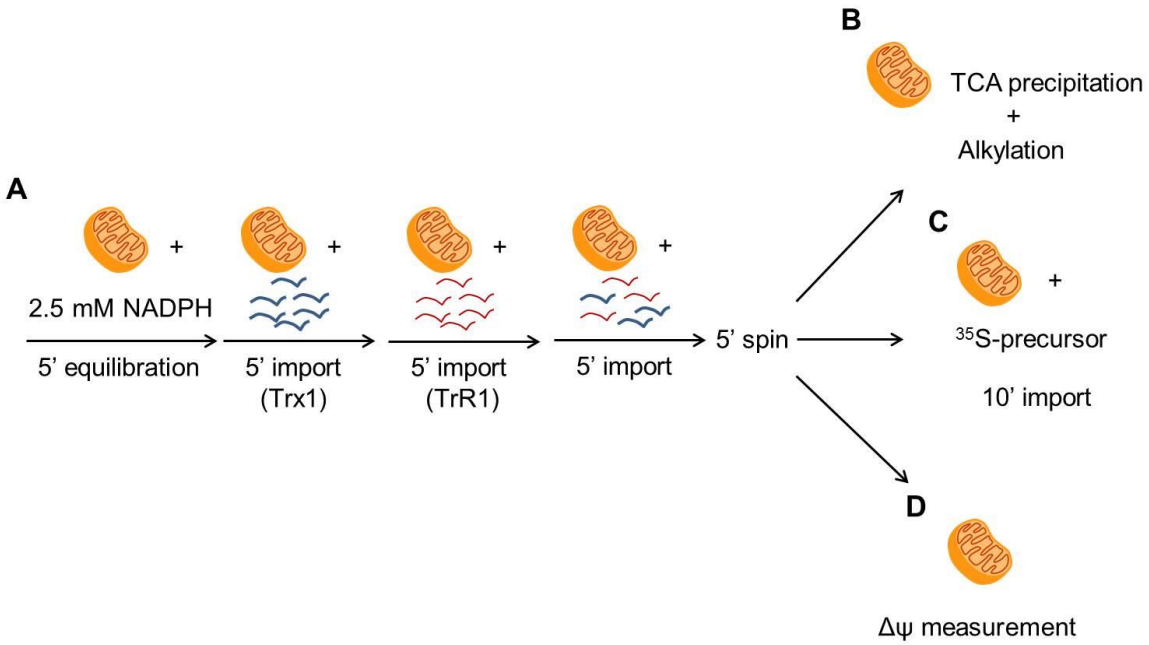

Figure 6.4 Pre-import of Trx system into mitochondria. (A) 50µg of mitochondria were equilibrated at 30°C with 2.5mM NADPH for 5 min. Then, Trx1 was imported for 5 min. Afterwards, TrR1 was added to the import mix and was left to import for a further 5 min. Finally, the import reaction was left for 5min more before separation of mitochondria with a 5min spin for further analysis. **(B)** The mitochondrial sample was precipitated with 10% TCA and treated for alkylation. **(C)** Import of ^{35}S-radiolabelled methionine into pre-imported Trx mitochondria. **(D)** Measurement of mitochondrial inner membrane potential.

The addition of mal-PEG reveals in this assay the reduced species of Mia40. In WT cells (lanes 1-3 Figure 6.5), Mia40 is in a mixed population of oxidised species that do not react with mal-PEG and reduced species that do react with mal-PEG (lane 3 Figure 6.5). As a control, the completely oxidised Mia40 is indicated as a single species without the addition of mal-PEG (lane 2 Figure 6.5). When DTT is added to the WT mitochondria to completely reduce Mia40 and mal-PEG is added, essentially all of Mia40 is shifted to the mal-PEG bound reduced species (lane 1 Figure 6.5). In Δ*g6pd* mitochondria, in the absence of pre-imported Trx1/TrR1 (lanes 4-6 Figure 6.5), Mia40 cannot be shifted to a reduced state by mal-PEG addition and persists in an oxidised state (compare lanes 5 and 6 for the Δ*g6pd* mitochondria to lanes 2 and 3 for the WT mitochondria Figure 6.5). Interestingly, the addition of Trx1 and TrR1 into Δ*g6pd* mitochondria (lanes 7 and 8 Figure 6.5) restores the redox balance of Mia40 to the levels of the WT mitochondria: we can now see the reduced Mia40 species revealed by an interaction with mal-PEG (lane 8 Figure 6.5) which is identical to the WT (lane 3 Figure 6.5).

These results show that Trx1 and TrR1 restores the redox balance of Mia40 after their import into mitochondria and endow the IMS with a fully functional reductive machinery. Moreover, after their import Trx1 and TrR1 interact with Mia40 as can be seen by the restored redox balanced state of Mia40 (last lane Figure 6.5) unlike the mainly oxidised state in Δ*g6pd* mitochondria where no Trx system was added (lane 6 Figure 6.5). Therefore, we conclude that the Trx system reduces Mia40 to a functional redox-balanced state.

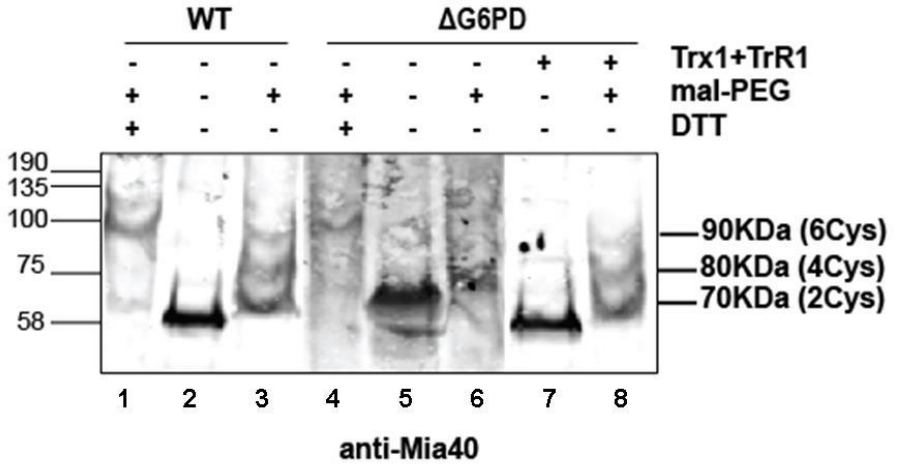

Figure 6.5 Redox state of Mia40 in WT and Δ*g6pd* after the import of the Trx system. Mitochondria isolated from WT and Δ*g6pd* yeast were equilibrated at 30°C with NADPH (5min) and then incubated for a total of 15 min with or without Trx1 and TrR1. Afterwards, mitochondria were precipitated with 10%TCA and treated (lanes 3, 6 and 8) or not (lanes 2, 5 and 7) with mal-PEG or mal-PEG+DTT (lanes 1 and 4). Immunodecoration with anti-Mia40 polyclonal Ab and fluorescence detection. The size of each band was determined by linear regression of a pattern curve created with the distance travelled of each molecular weight marker. The results are representative of three different experiments.

Since the Trx system reduces Mia40 after its import into mitochondria, we tested whether restoring Mia40 to its physiological redox balance would restore the import of Tim9, Tim10 and the human protein Cox17 (hCox17), which are widely known import substrates of the MIA pathway. Briefly, the Trx system (Trx1 and TrR1) was imported into 50 µg of Δ*g6pd* mitochondria as described in Figure 6.5. Additionally, the import of 10 µg recombinant Δ290Mia40SPS (soluble fraction of Mia40 with mutated active CPC motif) instead of the Trx system was used as control. Afterwards, samples were centrifuged to remove non-imported material and pellets were resuspended in import buffer in the presence of 2mM ATP and 2.5 mM NADH. The import of ^{35}S-Methionine radiolabelled-protein precursors (Tim9, Tim10 and hCox17) was performed as described in Figure 5.2 for 10 minutes. Samples were analysed by Tris-Tricine SDS-PAGE and visualised by autoradiography. The Trx system, but not exogenous Mia40, improved the import of Tim9 and Tim10 (panel A and B Figure 6.6) in 16% and 10%, respectively. In contrast, the import of hCox17 was ~1% less in the mutant mitochondria and no improvement was seen after pre-imported Trx system or Mia40 (panel C Figure 6.6). Interestingly, the import of Tim9, Tim10 and hCox is reduced when Mia40 was pre-imported (Mia40 lane and light grey columns Figure 6.6). Taken together, these results show that the reduction of Mia40 by the Trx system partially restores the import capacity of Δ*g6pd* mitochondria.

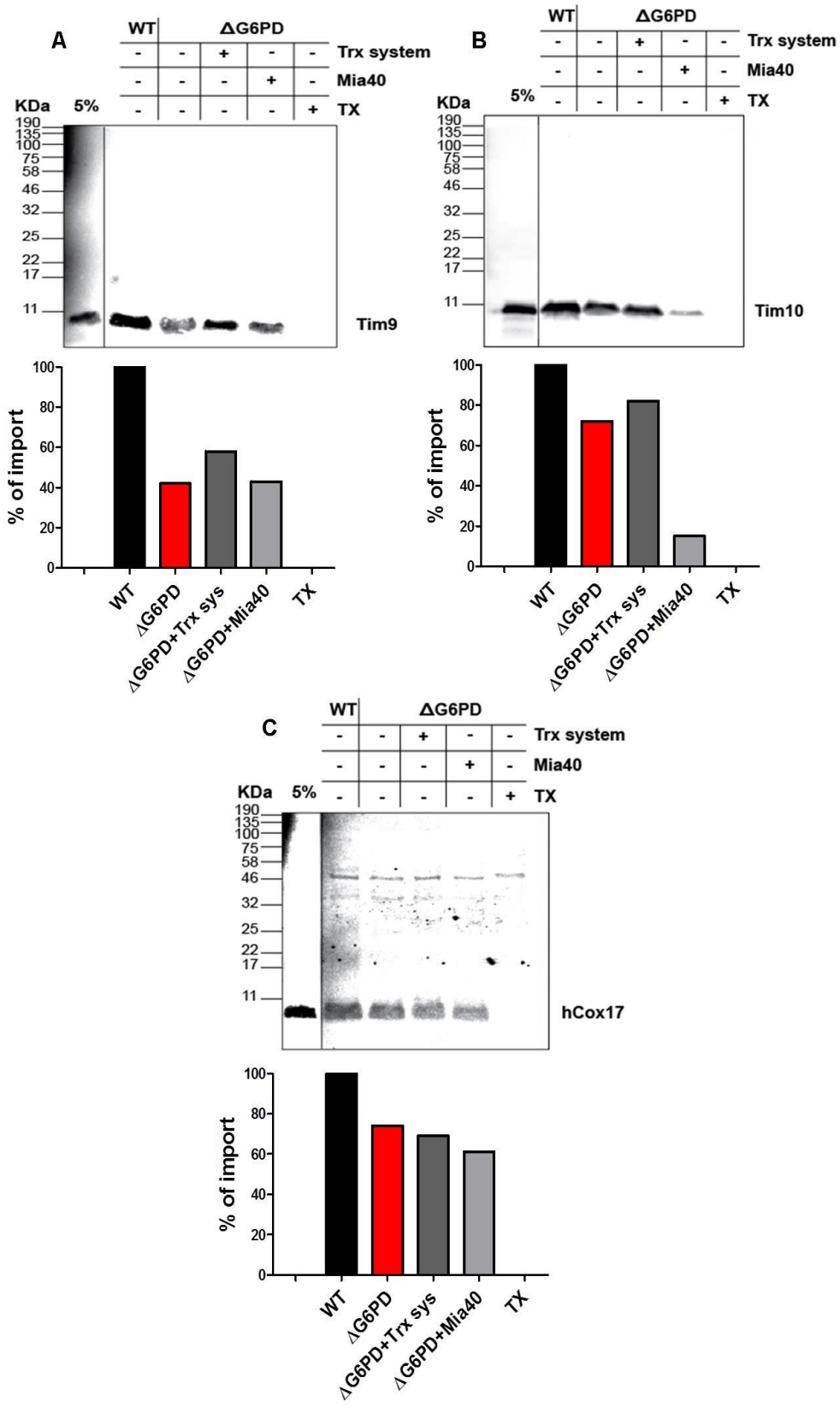

Figure 6.6 Import of Tim9, Tim10 and hCox17 into Trx-treated Δ*g6pd* mitochondria. Mitochondria isolated from WT and Δ*g6pd* yeast were equilibrated at 30°C with NADPH (5min) and then incubated for a total of 15 min with or without Trx1 (10µg) and TrR1 (10µg) or Mia40 (10µg). Afterwards, import of radiolabelled protein precursors for **(A)** Tim9, **(B)** Tim10 and **(C)** hCox17 for 10 minutes. First lane in each panel represents 5% of total precursor presented to mitochondria. The histograms on the bottom represent the relative quantification of each band.

Finally, as shown in Figure 4.4 the inner membrane potential Δψ was decreased in Δ*g6pd*, Δ*trx*1/2 and Δ*trr*1 isolated mitochondria. Given the fact that the import of the Trx system into Δ*g6pd* mitochondria re-establishes the balance in the redox state of Mia40 (Figure 6.5) and that this partially restores the protein import capacity of Mia40 substrates (Figure 6.6), we wanted to assess whether the decreased inner membrane potential Δψ in Δ*g6pd* could also be restored. Thus, we imported or not the Trx system into Δ*g6pd* and WT isolated mitochondria as mentioned for Figure 6.5. Then, the inner membrane potential Δψ was estimated by measuring the fluorescence of the inner membrane potential Δψ-dependent dye $DiSC_3(5)$ in the same way as in Figure 4.4. Intriguingly, the results in Figure 6.7 show that pre-import of the Trx system into Δ*g6pd* mitochondria did not recover the inner membrane potential Δψ defect. These results are indicative that the effects of Δ*g6pd* on the membrane potential of the IM cannot be restored by the Trx system in the IMS which seems to have a very specific effect on the Mia40 itself and as a consequence on the import pathway mediated by Mia40 but not a generic effect affecting the IM.

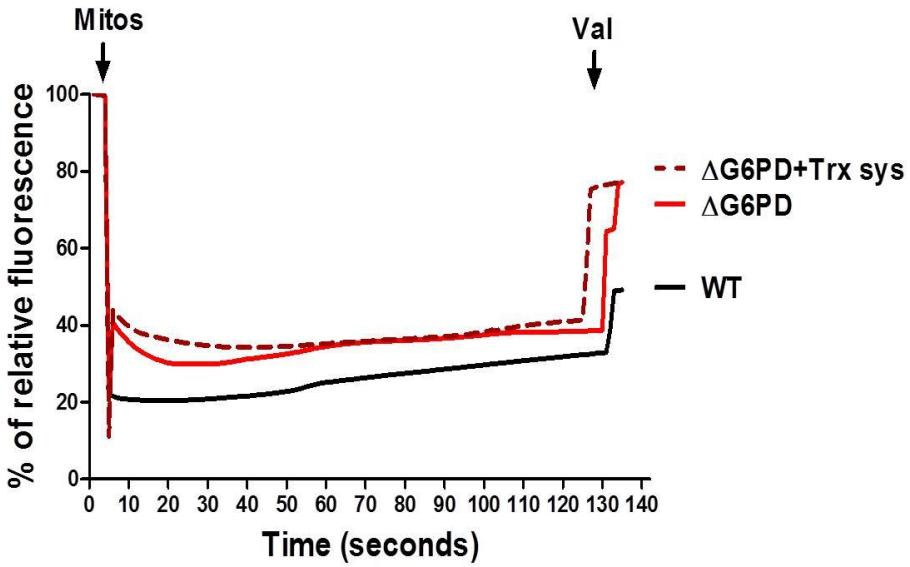

Figure 6.7 Mitochondrial membrane potential (Δψ) in Δ*g6pd* mitochondria after the import of the Trx system. Mitochondrial membrane potential measured from WT (black line), Δ*g6pd* (red line) and Δ*g6pd* pre-treated with Trx system (dark red dotted lines). The fluorescence of the $DiSC_3(5)$ molecule was measured for molecule over ~130 seconds. The maximum fluorescence for each experiment was considered as 100% of relative fluorescence. The arrows indicate the time of addition of either 100 µg of mitochondria (mitos) or 1mM valinomycin (val) were added. The results are representative of at least three different experiments.

6.3 Discussion

In the previous chapters I showed that mitochondria from Δg6pd null cells have decreased import capacity of the MIA pathway substrates (Figure 5.2). This import defect is because the balance of the redox state of Mia40 is perturbed and the Mia40 protein cannot cycle from its oxidised to the reduced state (Figure 5.3). Hence, a not yet known reductive system must be present in the mitochondrial IMS to keep the optimal redox state balance of Mia40 and to regulate other important functions such as disulfide proofreading and reduction of proteins to regulate their degradation or activity. Since Δg6pd is the main NADPH supplier in the cell (Minard et al., 1998) and this cofactor is the final electron donor for the thioredoxin and glutaredoxin pathways (Grant, 2001), one of these two or even both pathways could serve as the reductive force in the IMS. Accordingly, recent studies proposed the cytosolic Grx system to be such a reductive pathway (Kojer et al., 2012, Kojer et al., 2015). In these studies, the authors used a redox sensitive Grx1-roGFP2 probe, to demonstrate that the cytosolic and IMS, but not the IMS and matrix GSH pools are linked (Kojer et al., 2012). They also suggested that alterations in the cytosolic Grx system like the deletion of the glutathione reductase (Glr1), impact the redox state of Mia40. However, they saw that the redox state of Mia40 in ΔGlr1 was not significantly different to that of the WT, but only showed that when the levels of the sulfhydryl oxidase Erv1 were decreased, Mia40 becomes more reduced. The latter suggested the existence of a reductant acting on Mia40 since the balance between oxidising and reducing forms was altered by the decreased levels of Erv1 (oxidase) resulting in a reduced form of Mia40. They then proposed the Grx system given its availability in the IMS and a delayed recovery of the reduced form of Mia40 in a ΔGlr1 and Erv1 decreased strain following oxidative treatment as compared with the Erv1 decreased yeast (Kojer et al., 2012). In particular, they suggested the cytosolic isoform of Grx2 (cytoGrx2) as the active reductive component in the IMS (Kojer and Riemer, 2014). However, unlike our results showing that Trx1, Trx2 and TrR1 can be imported into mitochondria (Figure 6.2), they did not see influence of exogenous cytogrx2 when presented to mitochondria expressing an IMS-localised roGFP2 probe. Nevertheless, they argue to have found cytogrx2 in the IMS in a Δgrx1Δgrx2Δgrx8 yeast strain harbouring a plasmid that expresses cytogrx2. Yet in this experiment they only

gradually exposed mitochondrial proteins to proteinase K by solubilising mitochondrial membranes with increasing amounts of the detergent digitonin. Since the degradation of cytoGrx2 was similar to that observed for Mia40, they concluded that both proteins reside in the same compartment (the IMS). A limitation of this technique is that the proteins can behave differently to the proteinase treatment (Fountoulakis, 1995), making their comparison not reliable. In contrast, mitochondrial Na2CO3 extraction and mitoplasting have proved to be powerful tools to determine localisation of proteins in the different mitochondrial compartments (Kritsiligkou et al., 2017). In this regard, data from our lab using both mitoplasting and Na2CO3 extraction showed that both Trx1 and TrR1 localise to the IMS of mitochondria after import (Manganas, 2017). Additionally, another study using a roGFP2 probe without fused Grx1 found that the IMS was a more oxidising environment (Hu et al., 2008). However, Kojer et al reasoned that the probe used in that study could not be reduced due to the need of the entire Grx system as compared to the probe used by them where only the presence of GSH is needed for the reducing of the probe (Kojer et al., 2012). The latter pre-supposes that the glutaredoxin system is either not present in the IMS or present in small amounts or only transiently. Moreover, as mentioned before, all the components of the thioredoxin were recently identified in the IMS of S. cerevisiae (Vögtle et al., 2012), but this was not the case for the glutaredoxin system. Here we showed that both the Trx1 and TrR1 can be imported into mitochondria independent of the main known import pathways since their import does not depend on the main well-known protein import energy sources, ATP and Δψ which are crucial for targeting proteins into mitochondria by both the TIM23 and TIM22 complexes ((Geissler et al., 2000, Pfanner et al., 1987, Pfanner and Neupert, 1985, Pfanner and Neupert, 1987) and (Figure 6.2). Furthermore, the import of Trx1 and TrR1 does not depend on the MIA pathway given the fact that both proteins can be imported in mitochondria from Δg6pd yeast, which specifically has reduced import capacity for this pathway (Figure 5.2). The latter is further supported by previous results in our lab that showed that both proteins can be imported in mitochondria from cells depleted for Mia40 or Erv1 (Manganas, 2017). These results make the Trx system a better candidate to be the main, but likely not the only, reductive pathway in the IMS. Moreover, this idea is supported by the fact that Trx1 from yeast and E. coli share the same redox active site Cys-Gly-Pro-Cys (Figure 6.1).

Noteworthy, E. coli Trx1 has been found to be the strongest reductant in bacteria (Krause et al., 1991). This characteristic is important as suggests that the Trx1 is a potent reductant.

After proving that the Trx system can be imported into mitochondria, we then asked if the system interacts with Mia40. Hence, we tested the *in vitro* interaction between the recombinant proteins Mia40 and Trx1, Trx2 or the mutant Trx1 C30/33S using the non-specific cross-linker GA. As can be observed in Figure 6.3, a cross-linked product of 30 kDa between Mia40 and Trx1 (panel A Figure 6.3), Trx2 (panel B Figure 6.3) or Trx1 C30/33S (panel C Figure 6.3) is detected. The molecular weight of the product is consistent with the individual molecular weights of the proteins (Mia40: 20kDa and Trx1:12kDa). In addition, it has been shown that the Trx system reduces Mia40 in *in vitro* reconstitution experiments (Manganas, 2017). It was then crucial to test if such an interaction between Mia40 and the Trx system could take place inside the mitochondria. We reasoned that if the Trx system interacts and reduces Mia40, then the exogenous addition of the Trx system to mitochondria from Δ*g6pd* yeast cells would reverse the redox imbalance of Mia40 in the Δ*g6pd* strain (Figure 5.3) Indeed, the addition of the Trx system (which can work independent of Mia40 for its import) restores the redox balance of Mia40 to the level of WT mitochondria (compare lanes 3 and 8 Figure 6.5).

Unlike other studies that measured the redox state of Mia40 in isolated mitochondria and found a more oxidised form of the protein (Bihlmaier et al., 2007), the results presented here (Figure 5.3 and Figure 6.5) agree with the redox state of Mia40 seen in total cell extracts (Kojer et al., 2012). This information shows that functional WT Mia40 exists in a balanced state between its oxidised and reduced forms. Interestingly, Kojer *et al* did not find differences in the redox state of Mia40 in a ΔGlr1 strain which is thought to be altered in its reductive capacity. Conversely, our data shows that the MIA import pathway is specifically affected in Δ*g6pd* mitochondria (Figure 5.2). Taking these two results together with the *in vitro* (Figure 6.3) and *in organello* (Figure 6.5) interaction between Mia40 and the Trx system, we hypothesised that the exogenous addition of the system would recover the defects observed in mitochondria from Δ*g6pd* yeast, in particular the inner Δψ and the import

capacity. As can be seen in Figure 6.7, pre-treatment of Δ*g6pd* mitochondria with the Trx system does not influence the mitochondrial inner membrane potential Δψ. Thus, restoration of the balance in the redox state of Mia40 has no effect on Δψ. On the other hand, the import of Tim9 (panel A Figure 6.6) and Tim10 (panel B Figure 6.6) but not of human Cox17 (hCox17; panel C Figure 6.6) is slightly recovered after the addition of the Trx system, and not by addition of Mia40 (lane 5 in all panels Figure 6.6). In fact, the addition of Mia40 results in even less protein import. This more dramatic defect could possibly be because the import of the exogenous Mia40 saturates the already affected MIA pathway. Another possibility for this is that, since the Mia40 used was the soluble peptide, it accumulated outside mitochondria and blocked the import of the other proteins. These results show that the Trx system reduces Mia40 and that this interaction restores to some extent the decreased import capacity of mitochondria from Δ*g6pd*. The latter suggest that the Trx system represents the main but not the only reductive pathway in the IMS and cross-talk with other mechanisms must constitute the full reductive capacity in this compartment.

Chapter 7 Import pathway of Trx1 into mitochondria

7.1 Introduction

As shown before, members of the thioredoxin system, i.e. Trx1 and TrR1, were found in to be present in the mitochondrial IMS of yeast in a proteomic study (Vögtle et al., 2012). Accordingly, the results shown in the previous chapters confirm that the two proteins can be imported into mitochondria (Figure 6.2) and play an important role in the maintenance of the redox equilibrium in this important mitochondrial compartment (Figure 6.4). Furthermore, maintaining the balance between the reductive and oxidative forms of the oxidoreductase Mia40 is crucial for its function on the import of proteins targeted to the IMS (Figure 5.1 and Figure 5.2). In this respect, the exogenous addition of the Trx system into the IMS helps to restore the decreased import capacity of mitochondria from Δg6pd yeast (Figure 6.5). Thus, the presence of the Trx system in the IMS of mitochondria is essential for the proper function of the MIA pathway and possibly other reductive-regulated mechanisms important for protein targeting and degradation (Lee et al., 2013). However, besides the functional role of the thioredoxin system it is important to know how these proteins are being targeted into mitochondria. The latter is important given the fact that these proteins reside mainly in the cytosol and they are lacking a conventional mitochondrial targeting signal. Hence, in this chapter we tried to elucidate the import pathway followed by Trx1 to mitochondria.

7.1.1 Dual localised proteins: cytosol and mitochondria

In the IMS proteome reported by Vogtle *et al* in 2012 a considerable number of proteins share cytosolic and mitochondrial localisation. Furthermore, many of these proteins, like Trx1 and TrR1 are involved in redox homeostasis and oxidative stress response. The majority of these dual targeted proteins do not possess classical mitochondrial targeting sequences (Karniely and Pines, 2005). Instead, different mechanisms such as folding competition between the two compartments, e.g. the copper chaperone for superoxide dismutase (Ccs1) (Kloppel et al., 2011), and unconventional internal or N-terminal signals are responsible to drive these proteins into mitochondria. Such is the case for the

thiol peroxidase Gpx3, the major H_2O_2 sensor in yeast, which recently was shown to contain an 18 amino acid N-terminal extension that is involved in its localisation to mitochondria and in particular to the IMS (Kritsiligkou et al., 2017). It is likely that the dual localisation of proteins is linked to stress conditions in mitochondria as shown by the mitochondrial localisation of proteins involved in cellular response to stress like p53 (Zhuang et al., 2013) and the Cu/Zn superoxide dismutase (Sod1) (Sturtz et al., 2001). Hence, the elucidation of the import pathway followed by these proteins is of major importance to better understand their involvement in the protection of the cell.

The import pathway of Trx1 has not yet been elucidated but recent analysis in our lab identified an internal signal located towards the C-terminus that resembles the signal that is involved in the import of ß-barrel proteins into the mitochondria and its sorting into the mitochondrial outer membrane.

7.1.2 β-signal for the import and sorting of β-barrel proteins into the mitochondrial outer membrane

The import of ß-barrel proteins into mitochondria and the mechanism of insertion into the outer membrane has just recently started to be uncovered. In particular, a conserved C-terminal sequence among all eukaryotes was found to be responsible for the insertion of these type of proteins into the OM (Kutik et al., 2008). This ß-signal is present in the last predicted transmembrane ß-strand and is formed by a large polar residue, an invariant glycine and two hydrophobic residues (Po-X-G-X-X-Hy-X-Hy) (Kutik et al., 2008). Furthermore, the mechanism by which these ß-barrel proteins are inserted was later described. Once the ß-precursors are in the IMS of mitochondria the ß-signal interacts with the ß1 strand from the sorting and assembly machinery (SAM) core subunit, Sam50, and replaces the last ß segment of SAM50 (ß16) (Höhr et al., 2018). This induces lateral opening of SAM50 between ß1 and ß16 and the rest of the incoming ß-barrel protein strands are inserted in this opened gate as ß-hairpin-like structures (Höhr et al., 2018). However, it was shown that this signal is not enough for the targeting of ß-barrel proteins into mitochondria but only for their sorting and insertion after initial translocation across the outer membrane through the Tom40 channel (Jores et al., 2016). Instead, a ß-hairpin motif was found to be the minimal structure needed for the targeting of this type of

proteins to mitochondria and the presence of the ß-signal is dispensable for these to happen (Jores et al., 2016).

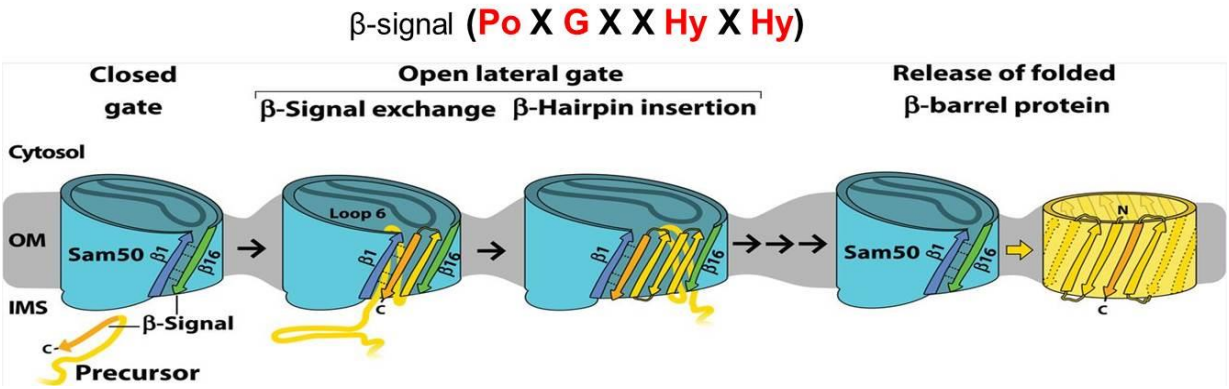

Figure 7.1 Putative model for sorting of β-barrel proteins. The insertion of β-barrel proteins in the mitochondrial OM is mediated by the recognition of the β-signal of the incoming protein by Sam50. This signal replaces the β-signal of Sam50 β16 strand creating an open gate between β1 and β16 were the rest of the incoming protein is inserted in a β-hairpin-like structure. Finally, the new folded β-barrel protein is laterally release to the OM. The sequence of the β-signal is shown on the top of the figure. Image modified from (Höhr et al., 2018).

In this chapter, we describe the identification of a conserved 'ß-signal-like signal' present in both Trx1 and TrR1 proteins and other proteins that are in the IMS but are not substrates for the Mia40 pathway. The proteins that we found sharing such a signal amount to 22% of the total IMS proteome reported in 2012 (out of a total of 51 proteins). Finally, the influence of a synthetic peptide with the sequence of this putative signal on the import of Trx1 was tested. Additionally, the construction of single point mutants of the key residues as well as a C-terminal deletion lacking the signal were attempted.

7.2 A possible novel targeting signal into the IMS: β-like IMS targeting signal (bITS)

7.2.1 Bioinformatics analysis of the β-like IMS targeting signal (bITS)

Analysis of the sequence of Trx1, Trx2 and TrR1 showed no classical targeting signal (no ITS (section 1.2.6 for the Mia40 pathway), no N18-like signal like the Gpx3 signal, and nothing like the Cytb2 bipartite presequence). So, none of the known targeting signals for the IMS were present in the sequence of Trx1, Trx2 and TrR1. After the publication of different studies that found a conserved signal (ß-signal) responsible for the insertion of ß-barrel proteins into the

mitochondrial OM (Höhr et al., 2018, Kutik et al., 2008), we found a similar sequence that is present in the thiol peroxidase Gpx3, the thiol-reducing protein Trx1 and the Trx reductase, TrR1. The typical ß-signal present in ß-barrel proteins consists of a large polar residue (Po), a conserved glycine and two hydrophobic residues (Hy) distributed in a consensus motif: Po-X-X-G-X-Hy-X-Hy. Whereas the ß-signal-like signal, which we called ß-IMS Targeting Signal (bITS), is identical to the ß-signal with the exception that is it contains a polar instead of a hydrophobic residue in the last position (panel A Figure 7.2) We then performed a detailed analysis of the sequence of all the proteins found in the IMS of *S. cerevisiae* for the presence of such a putative signal. As a result, we found that 22% of the proteins in the IMS proteome have exclusively a conserved bITS signal (panel B Figure 7.2). Noteworthy, the previously described IMS targeting signal (ITS) that is present in substrates of the MIA pathway is exclusively present in 21% and the 57% remaining share both signals (panel B Figure 7.2). It is important to note that some of the proteins with both signals do not possess the canonical signals but variations of them. Furthermore, the alignment of all the 11 proteins containing only the bITS, but not the ITS signal, show it is highly conserved (panel A Figure 7.2). It is important to mention that out of the 11 bITS proteins in the IMS, the adenylate kinase (Adk1) contain two putative bITS signals within their sequence (Figure 7.2). This bioinformatics analysis shows a highly conserved and wide spread sequence among the IMS proteins. Moreover, the import mechanism of most of these proteins is not yet known and the fact that they are involved in response to various types of stress makes the presence of the bITS signal more interesting and exciting.

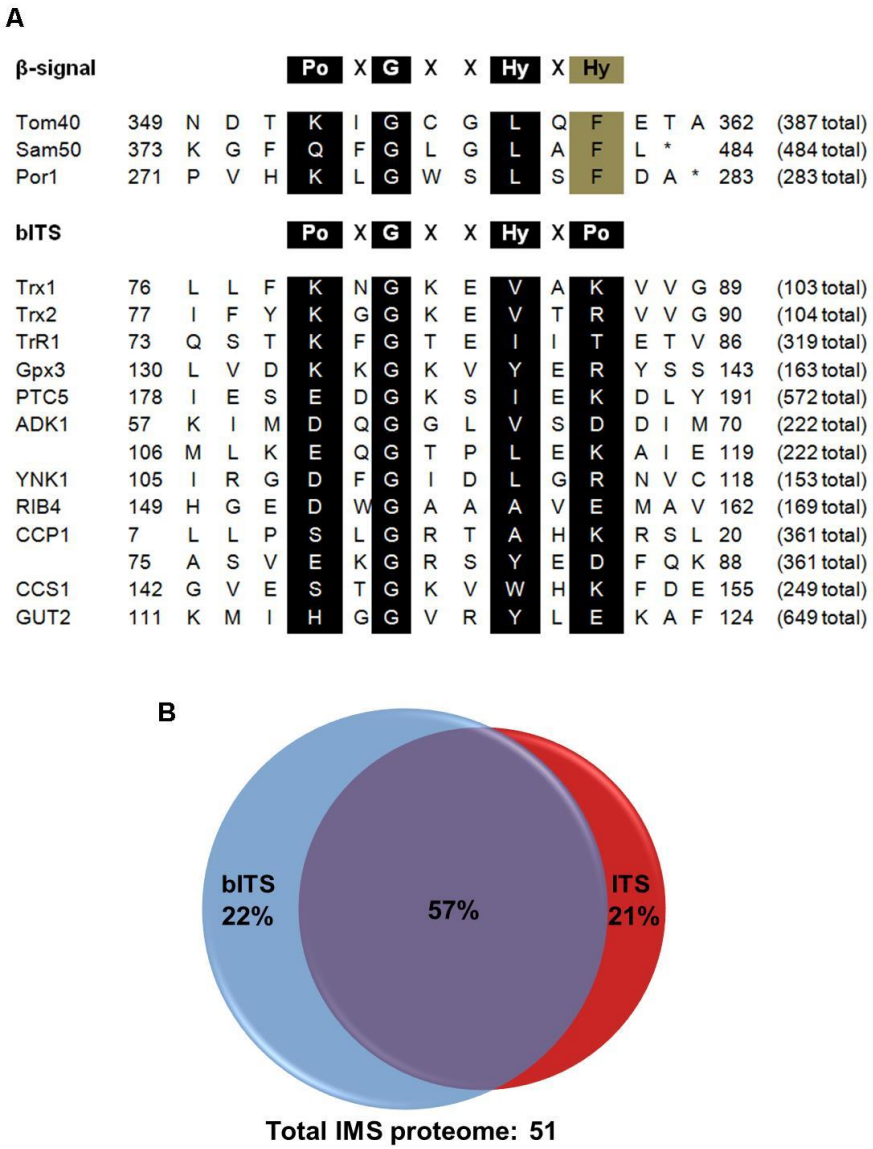

Figure 7.2 Alignment and distribution of the bITS signal among the IMS proteins. (A) Alignment of the main OM β-signal containing proteins (top) and the IMS bITS proteins (bottom). The polar (Po), glycine (G) and hydrophobic (Hy) residues are shaded in black and the Hy residue in the β-signal that differentiates both signals is shaded in golden. **(B)** Venn diagram of the distribution of both the ITS targeting signal and the putative bITS targeting signal in the proteins from the IMS of *S. cerevisiae*. The percentage of bITS and ITS containing proteins are shown in blue and red, respectively.

Likewise, it is interesting that the bITS-containing proteins differ considerably in length and do not appear to have any other sequence homology or any structural similarities between them. The latter is clearly seen when comparing the crystal structure of Trx1 (panel A Figure 7.3) and Trx2 (panel B Figure 7.3) (which are highly homologous), to the non-related peroxidase Gpx3 (panel C Figure 7.3) and TrR1 (panel D Figure 7.3). Interestingly, the alignment between these four bITS proteins confirms the presence of the signal in these proteins despite their structural differences. (panel E Figure 7.3)

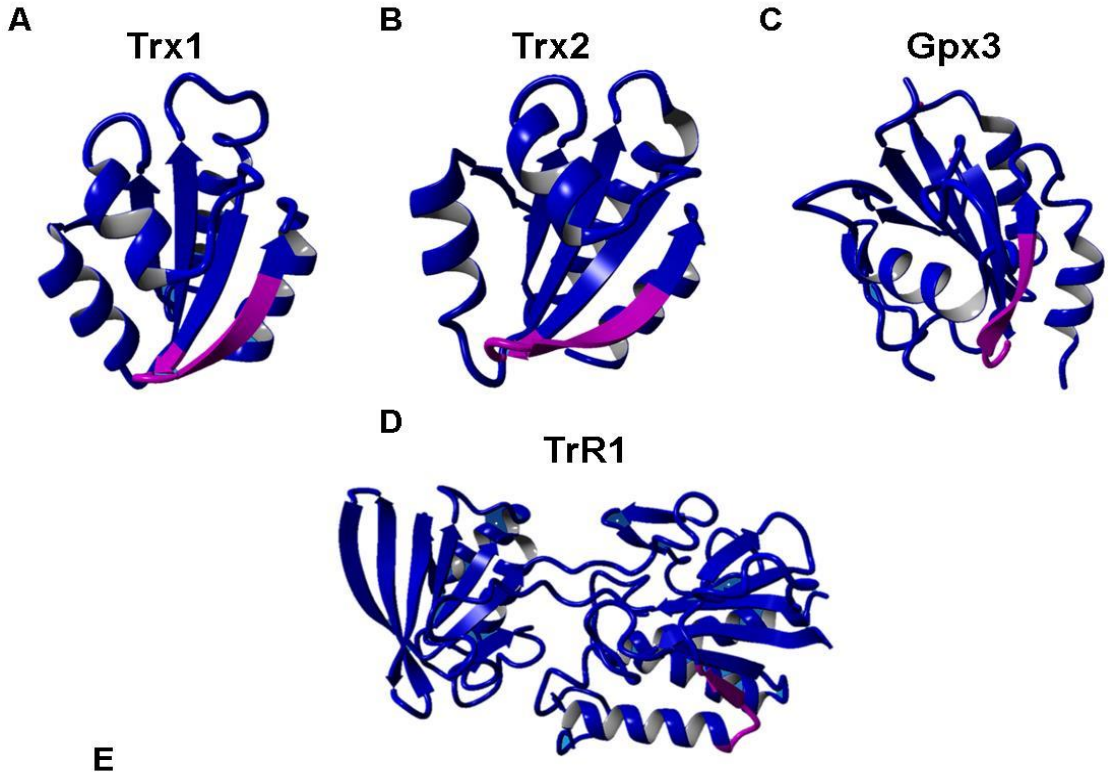

E

Trx1		MVTQFKTASE	FDSAIAQDKL	VVVDFYATWC	GPCKMIAPMI	EKFSEQYPQA	DFYKLDVD
Trx2		MVTQLKSASE	YDSALASGDK	LVVVDFFATW	CGPCKMIAPM	IEKFAEQYSD	AAFYKLDVD
Gpx3	MSEF	YKLAPVDKKG	QPFPFDQLKG	KVVLIVNVAS	KCGFTPQYKE	LEALYKRYKD	EGFTIIGFPC
TrR1		MVHNKV	TIIGSGPAAH	TAAIYLARAE	IKPILYEGMM	ANGIAAGGQL	TTTTEIENFP
Trx1		ELGDVAQKNE	VSAMPTLLLF	KNGKEVAKVV	GANPAAIKQA	IAANA*	
Trx2		EVSDVAQKAE	VSSMPTLIFY	KGGKEVTRVV	GANPAAIKQA	IASNV*	
Gpx3		NQFGHQEPGS	DEEIAQFCQL	KKGKVYERYS	SLTKPSSLSE	TIEELLKEVE*	
TrR1		GFPDGLTGSE	LMDRMREQST	KFGTEIITET	VSKVDLSSKP	FKLWTEFNED	AEPVTTDAII
Trx1							
Trx2							
Gpx3							
TrR1		LATGASAKRM	HLPGEETYWQ	KGISACAVCD	GAVPIFRNKP	LAVIGGGDSA	CEEAQFLTKY
Trx1							
Trx2							
Gpx3							
TrR1		GSKVFMLVRK	DHLRASTIMQ	KRAEKNEKIE	ILYNTVALEA	KGDGKLLNAL	RIKNTKKNEE
Trx1							
Trx2							
Gpx3							
TrR1		TDLPVSGLFY	AIGHTPATKI	VAGQVDTDEA	GYIKTVPGSS	LTSVPGFFAA	GDVQDSKYRQ
Trx1							
Trx2							
Gpx3							
TrR1		AITSAGSGCM	AALDAEKYLT	SLE*			

Figure 7.3 Crystal structures and alignment of the bITS proteins Trx1, Trx2, Gpx3 and TrR1. Comparison of the crystal structures from **(A)** Trx1 (PDB id: 2n5a), **(B)** Trx2 (PDB id: 2fa4), **(C)** Gpx3 (PDB:3cmi) and **(D)** TrR1 (PDB: 3itj). The bITS signal is highlighted in pink. **(E)** Protein sequence alignment of Trx1, Trx2, Gpx3 and TrR1, highlighted in red the conserved polar, glycine and hydrophobic residues of the bITS and in blue the polar residue in the last position which differentiates the β-signal and bITS.

The strikingly conserved presence of the bITS signal and its existence in the yeast Trx1, Trx2 and TrR1 proteins, prompted us to look for the bITS signal in these proteins across different species. Indeed, we found that the bITS sequence of both thioredoxin and thioredoxin reductase is highly conserved among humans, mice, *S. cerevisiae*, *Arabidopsis thaliana* (*A. thaliana*) and *Caenorhabditis elegans* (*C. elegans*) (panel A Figure 7.4). Looking in the 3D Xray structure of these proteins it was interesting to see that the localisation of the bITS signal in Trx was almost identical between the *S. cerevisiae* proteins Trx1, and Trx2 and the human homologue TXN (panel B Figure 7.4), i.e. comprising part of a solvent exposed ß-turn and a loop. The fact that the sequence and localisation of the bITS within different proteins is conserved in evolution suggests that it might play an important role.

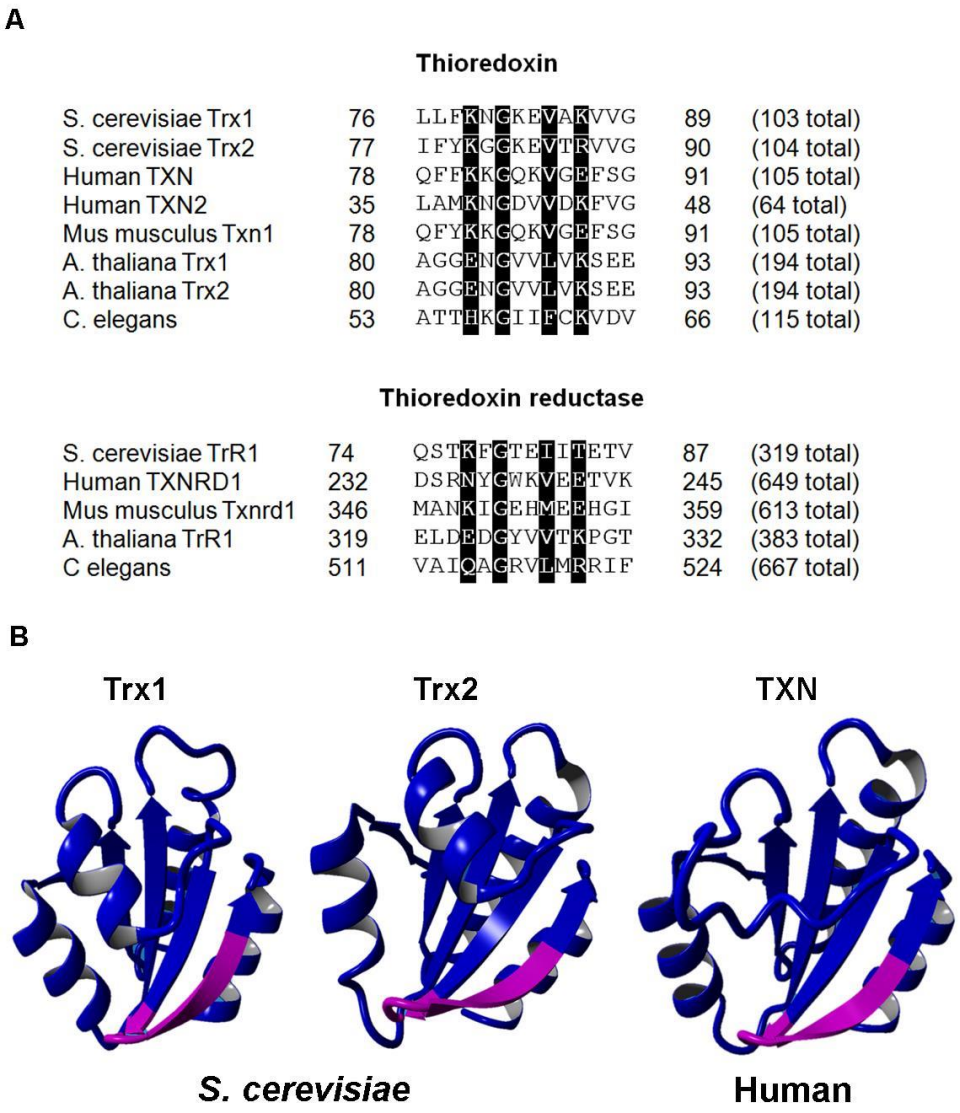

Figure 7.4 Thioredoxin and thioredoxin reductase are highly conserved among species. (A) Sequence alignment of the bITS signal of the isoforms of thioredoxin (top) and thioredoxin reductase (bottom) present in *S. cerevisiae,* human, mice, *A. thaliana* and *C. elegans.* **(B)** Crystal structures of Trx1 (PDB id: 2n5a) and Trx2 (PDB id: 2fa4) from *S. cerevisiae* and the human TXN (PDB id: 5dqy). The conserved bITS signal is shown in pink.

7.2.2 First steps for dissecting the involvement of bITS in the import of Trx1 into mitochondria

7.2.2.1 Import of Trx1 in the presence of Gpx3 bITS peptide

After the identification of bITS in many IMS proteins and its highly conserved sequence and localisation among species we started to work on elucidating its involvement, if any, on the import of Trx1. As a first approach, we commercially synthesised (GeneScript) bITS peptides from Trx1, Gpx3, the ß-signal and a scrambled version of the Trx1 bITS containing the same amino acids of the original sequence but in random positions. We reasoned that if the signal is

acting as targeting sequence, the peptide alone might compete with the protein for a potential receptor or entry gate. Thus, we performed import experiments of recombinant His-tagged Trx1 (Materials and Methods and Figure 6.2) in the presence of increasing amounts of the bITS peptide from Gpx3 (panel A Figure 7.5). We used the import of the in vitro translated 35S-Methionine radiolabelled precursor of the matrix-targeted Su9 fused to DHFR (su9-DHFR) as control, given that it is imported through the TOM complex and the TIM23 complex, any effect that the bITS peptide might exert would indicate alterations in one of the two or both pathways (panel B Figure 7.5). Additionally, it was shown that the ß-signal peptide does not affect the import of ß-barrel proteins, but it inhibits the formation of an intermediate between the ß-protein and Sam50 (Kutik et al., 2008). Thus, we used the import of porin and the ß-signal peptide as a control of the correct peptide synthesis (Figure 7.5) expecting no effect on the import of porin. Finally, the resulting samples were analysed by Tris-Tricine SDS-PAGE and either western blot, for the detection of His-tagged Trx1 using α-His Ab, or autoradiography, for the import of Su9-DHFR and porin. The results confirmed that the import of the ß-barrel protein, porin, is not affected (panel C Figure 7.5). Furthermore, the import of Su9-DHFR was not affected by any of the amounts added of the Gpx3-bITS (panel B Figure 7.5). Strikingly, the import levels of Trx1 into WT mitochondria showed a dose-dependent relation with the Gpx3 bITS peptide (panel A Figure 7.5). The latter is counterintuitive to what we hypothesised. In parallel, the membrane used to detect Trx1 was blotted again to determine that loading of the samples was not influencing the result. Detection of the abundant matrix protein Hsp70 using rabbit polyclonal anti-Hsp70 Ab was then carried out and we found that the loading was not responsible of the increased import of Trx1 in the presence of gpx3 bITS (lower panel A Figure 7.5). These results suggest that the Gpx3 bITS peptide clearly influences the import of Trx1, but in a yet unknown manner. A possibility would be that the peptide is interacting with a receptor or gate and this triggers opening of such a gate. Further analysis needs to be conducted on the mechanism of this phenomenon.

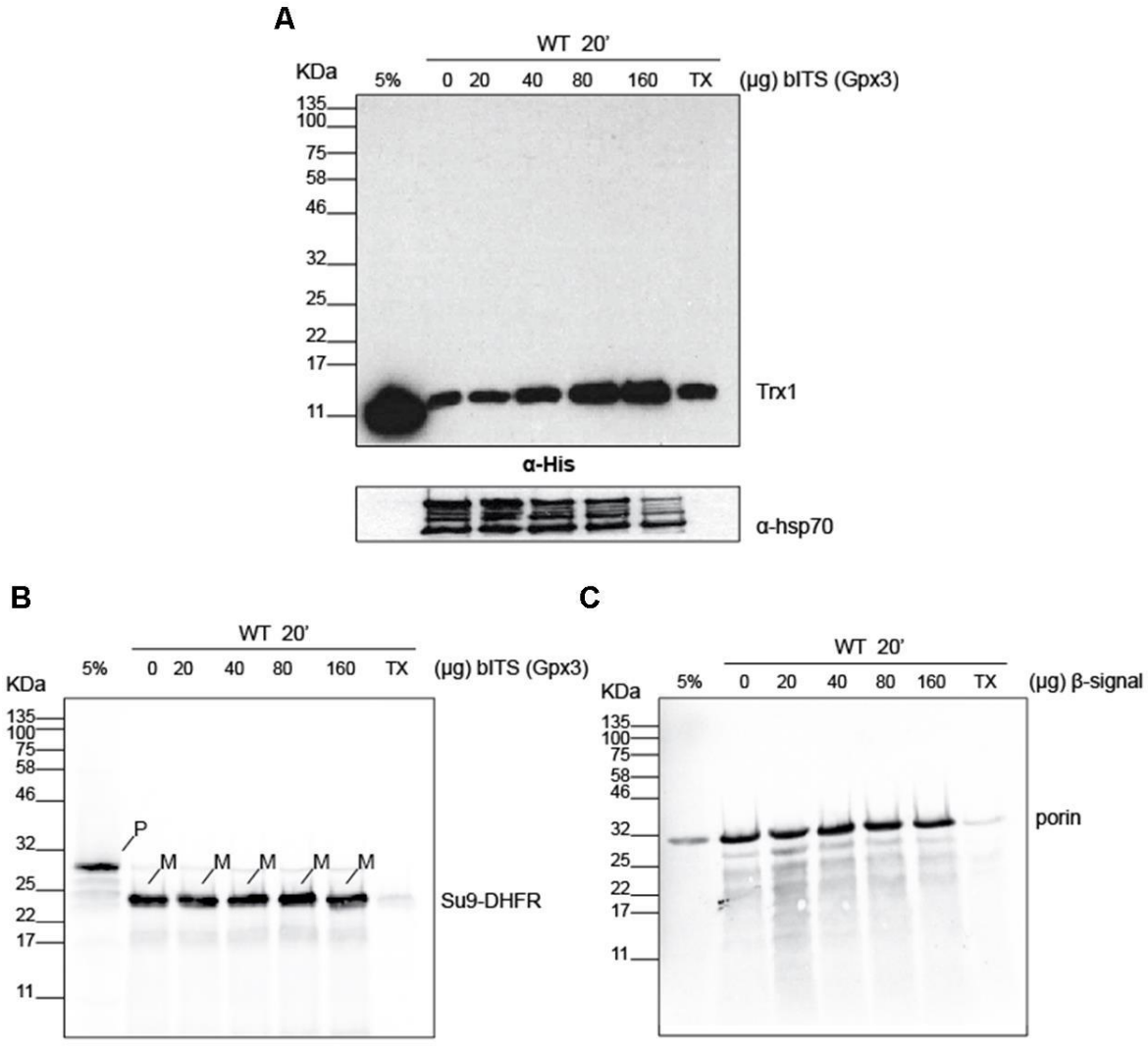

Figure 7.5 Import of Trx1 in the presence of Gpx3 bITS. (A) Import of 10µg of recombinant His-tagged Trx1 into WT pure mitochondria pre-incubated 5min with increasing amounts (0 µg, 20 µg, 40 µg, 80 µg and 160 µg) of the Gpx3 bITS peptide. Western blot was performed using α-His Ab. The lower panel shows a western blot for the detection of Hsp70 as loading control. **(B)** and **(C)** Autoradiography of the import of radiolabelled precursors for **(B)** Su9-DHFR and **(C)** porin into WT mitochondria in the presence of with increasing amounts (0 µg, 20 µg, 40 µg, 80 µg and 160 µg) of **(B)** the Gpx3 bITS peptide or **(C)** the β-signal.

Since the Gpx3 bITS peptide has an effect on the import of Trx1, we then tried to dissect the importance of the sequence in the protein import as well as that of the putative amino acids within the sequence. To achieve this, we created primers in order to chop different N- (panel A Figure 7.6) and C-(panel B Figure 7.6) terminal segments of Trx1 as well as primers for the mutation of the residues conserved in the bITS signal, i.e. K79, G81, V84 and K86 (panel C Figure 7.6).

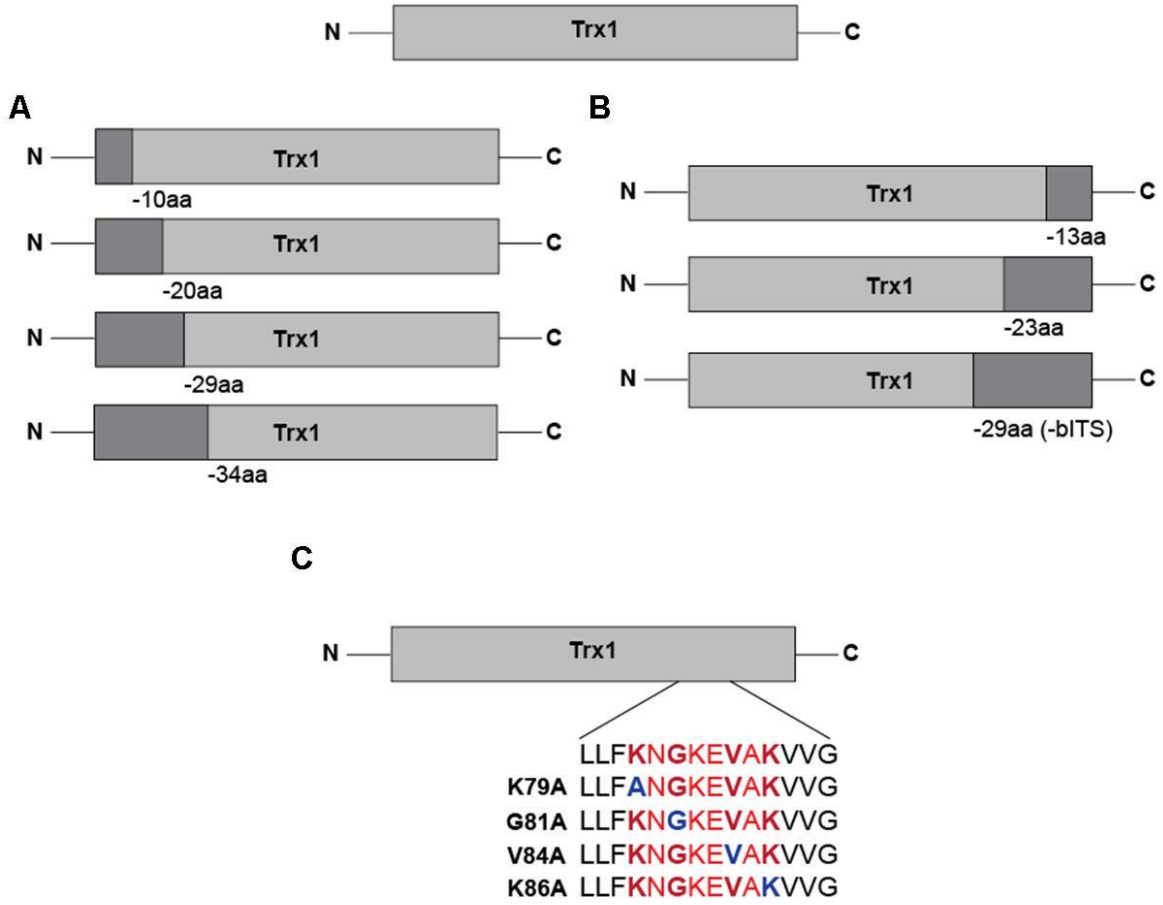

Figure 7.6 Experimental design to elucidate the importance of bITS in the import of Trx1. Schematic representation of the different truncated or mutated versions of Trx1. **(A)** N-terminal deletion (grey boxes) of -10 aa, -20 aa, -29 aa and -34 aa. **(B)** C-terminal deletion (grey boxes) of 13 aa, -23 aa and -29 aa, this last one chops out the bITS from the protein. **(C)** Mutagenesis of individual amino acids of the bITS sequence: K79A, G81A, V84A and K86A.

With this strategy we first amplified and cloned the -29 aa C-terminal version of Trx1, which removes the complete bITS signal, into the pET24b(+) (Novagen) plasmid (Materials and Methods). This plasmid allows overexpression of the C-terminal 6X His-tagged version of any protein cloned in it. The vector with the insert was then sequenced to confirm that the coding sequences did not have any mutations. Afterwards, the plasmid was used to transform BL21 (DE3) bacterial expression cells. The expression of the protein was induced by adding 0.4mM Isopropyl ß-D-1-thiogalactopyranoside (ITPG) for 4h (Material and Methods). Unfortunately, the expression was not induced as can be seen in four different colonies (Panel A Figure 7.7). We then use the plasmid containing the protein to transform another bacterial expression strain, the origami 2 (DE3) pLysS (Novagen). Unfortunately, the protein was not expressed either in this bacterial strain (Figure 7.7).

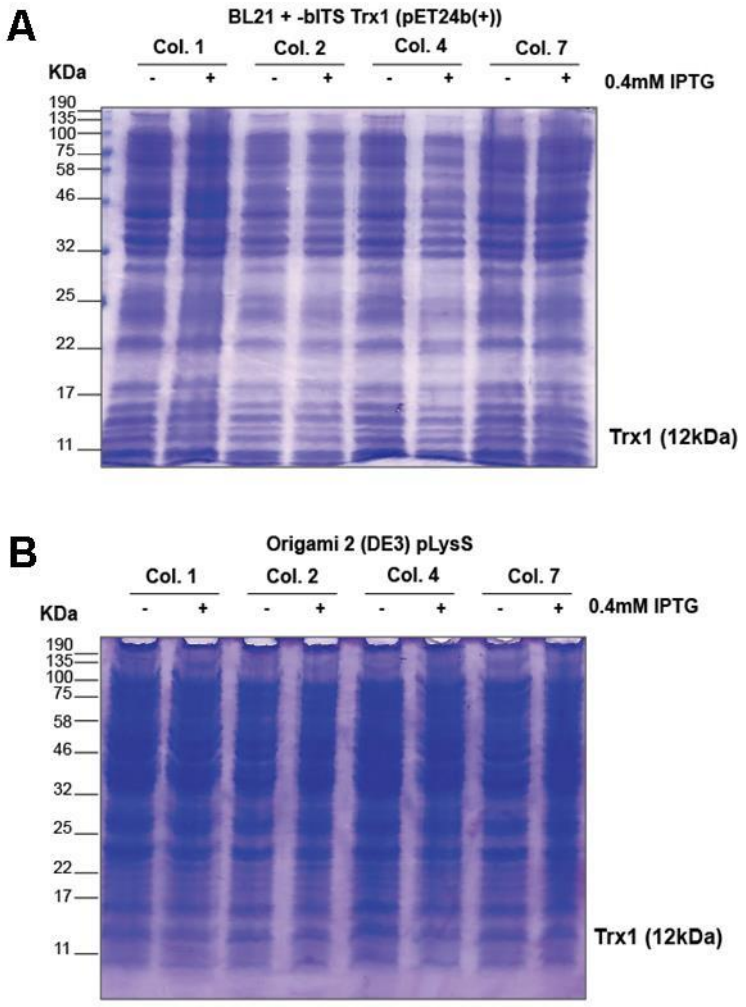

Figure 7.7 Induction of expression of N-terminal-29 aa Trx1. IPTG (0.4mM) induction of the expression of -29 aa C-terminal version of Trx1 on **(A)** BL21 (DE3) bacterial expression cells and **(B)** origami 2 (DE3) pLysS.

In parallel, mutagenesis to alanine of the individual conserved residues of the bITS signal was performed in collaboration with Marie Safner in our lab. The primers listed in (Material and Methods) were used to amplify the mutant versions of the WT Trx1 protein cloned into the pET24b(+) plasmid (panel C Figure 7.6). The sequencing results showed that three out of the four intended mutants were correct (Figure 7.8). However, we faced the same expression problem as for the C-terminal -29aa Trx1.

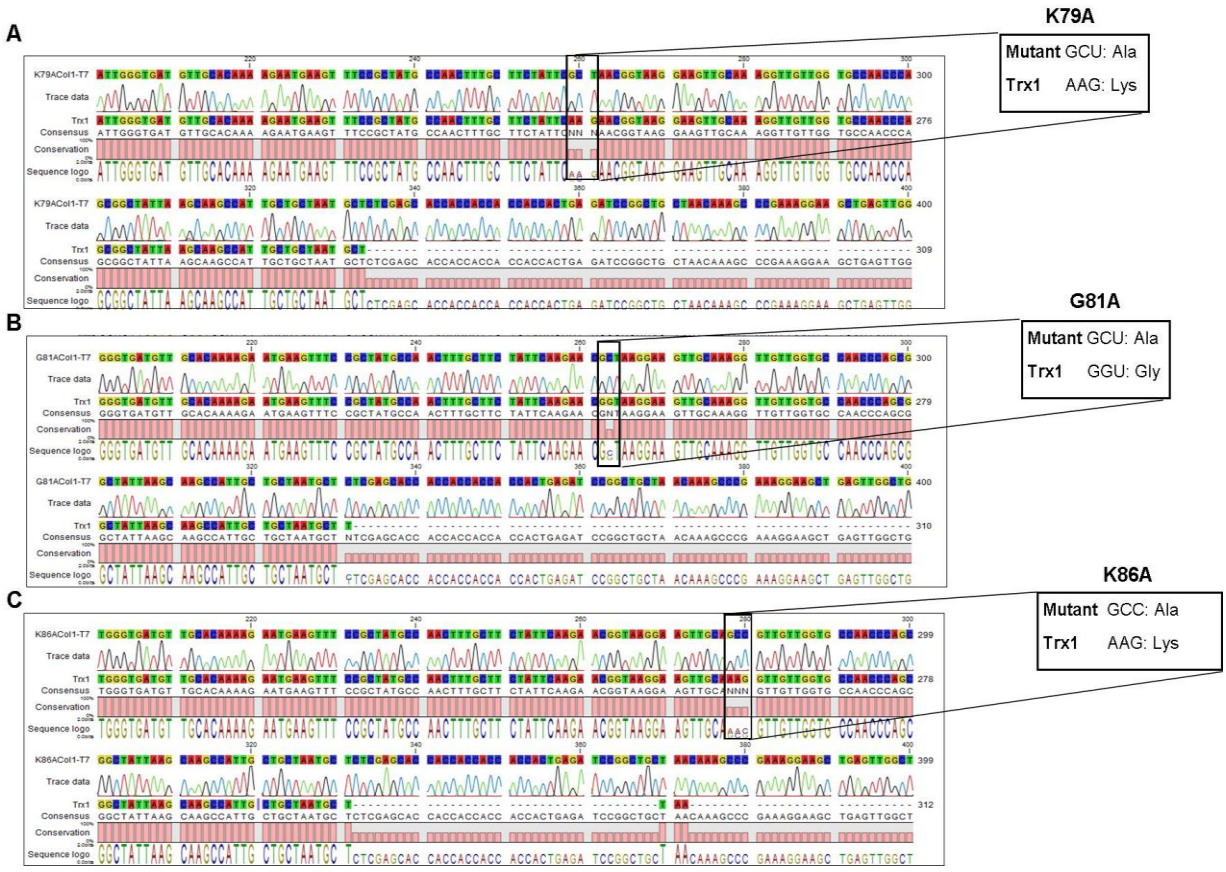

Figure 7.8 Alignment of the mutations of the conserved residues in bITS. Positive sequencing results of the mutagenesis of the individual bITS residues: **(A)** K79A, **(B)** G81A and **(C)** K86A. The C-terminal end of Trx1 is shown and the black boxes on each panel highlights the mutation and shows the original and mutated codons.

7.2.2.2 Import channel involved in the translocation of Trx1 into yeast mitochondria

In parallel with creating the tools to elucidate the sequence that drives Trx1 and potentially other proteins into mitochondria, we started to work on elucidating the channel that is involved in the translocation of this protein, and probably a considerable set of other proteins that are also targeted to the IMS. Since the bITS sequence resembles the ß-signal which interacts with the Sam50 protein, we hypothesised that this channel might also be involved in the import of Trx1. The involvement of Sam50 as a direct entry gate for any protein has not yet been demonstrated and is a challenging concept. All proteins destined for mitochondria are translocated first through the Tom40, so we wanted to explore this possibility first. We used yeast temperature sensitive (Ts) mutant strains for Tom40, gifted by Dr. Thomas Becker from Freiburg University. This *S. cerevisiase* strain (Becker et al., 2011, Wenz et al., 2014) have been transformed with a plasmid that conditions the expression of the protein of interest depending on

the temperature at which the yeast is grown. A switch to non-permissive temperature (37°C) represses the expression of the protein and decreases its levels. This is an important strategy in particular for essential proteins such as Tom40, for which a complete gene deletion in the yeast is inviable. We obtained three different yeast strains, one strain transformed with an empty plasmid to rule out any influence by the transformation or the vector in the expression of the protein. The other two strains (named 25 and 34) were different TsTom40 yeast strains generated by Dr. Becker's group. Briefly, we grew the yeast until log phase at the permissive temperature 24°C and then switched it to the non-permissive 37°C for 8h further hours as recommended by Dr. Becker. Afterwards, we isolated pure mitochondria (Materials and Methods) and performed import experiments (Materials and Methods) of ^{35}S-Methionine radiolabelled precursors of proteins that are known to depend on the Tom40 channel for their translocation. These control proteins included the matrix-targeted protein Su9-DHFR (panel A Figure 7.9) and the IMS protein Mia40 (panel B Figure 7.9). We got some variable results for these two proteins. The import of Su9-DHFR was impaired in both TsTom40 strains as expected (compare lane 2 with lanes 3 and 4 panel A Figure 7.9), but the import of Mia40 was not affected (panel B Figure 7.9). At the same time, we performed import experiments using the 6X His-tagged recombinant versions of both Trx1 (panel C Figure 7.9) and Trx2 (panel D Figure 7.9) into mitochondria from the three Tstom40 strains and found no differences on the import levels of Trx2. However, and quite unexpectedly, an increase on the import of Trx1 was observed (panel C Figure 7.9). Despite the results on the import of Trx1 and Trx2, the fact that the control of Mia40 did not work as expected made those results non-conclusive. In parallel, we performed western blot analysis to detect the steady state levels of Tom40 in the three TsTom40 mutants (WT, 25 and 34) and the non-transformed yeast parental strain D273-10B (referred as WT). Surprisingly, we saw no differences in the levels of Tom40 in these strains suggesting the expression of Tom40 was not repressed by the temperature switch.

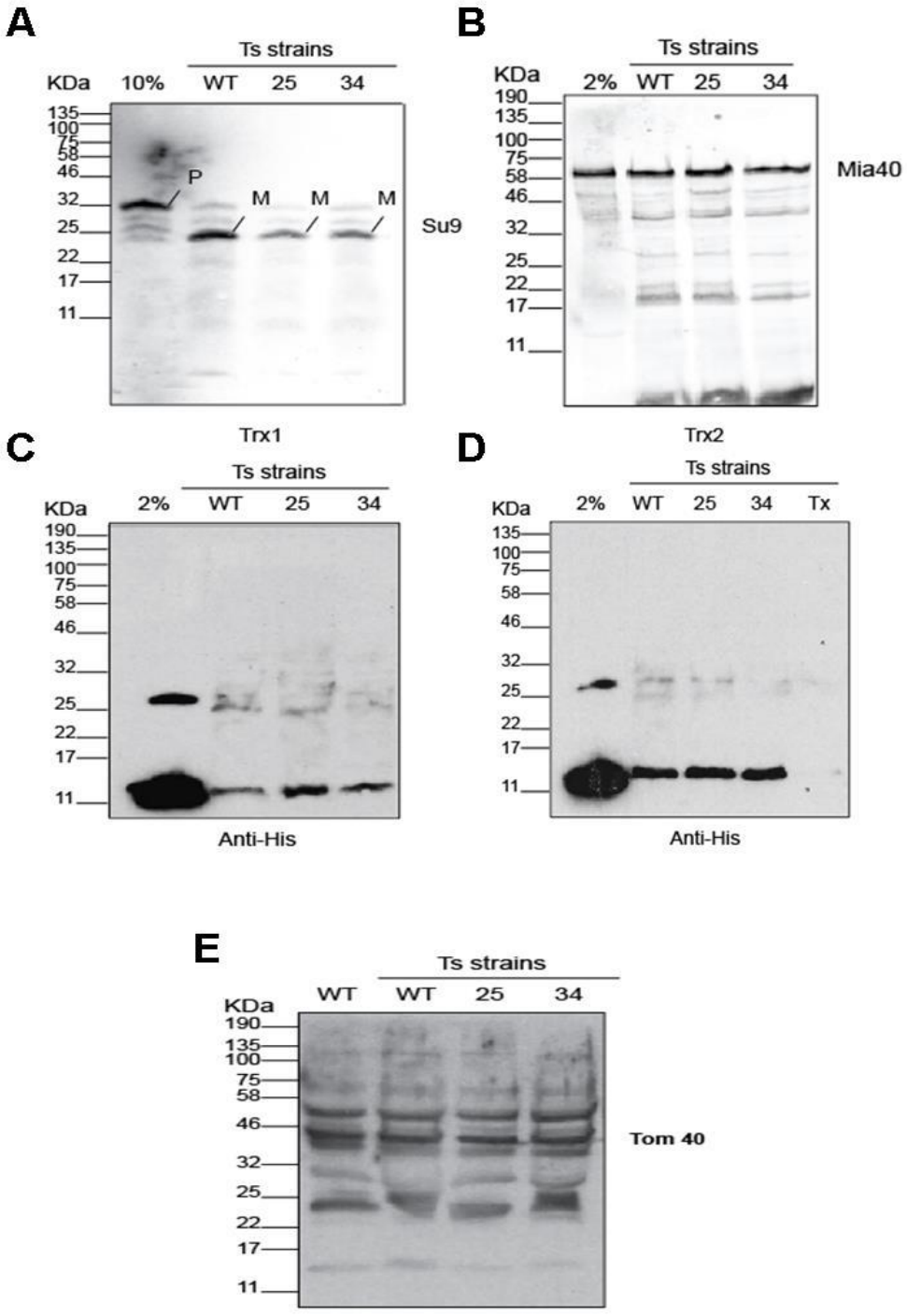

Figure 7.9 Test of a TsTom40 yeast strain. (A-B) Autoradiography of import experiments into isolated mitochondria from WT TsTom40 yeast and the two mutants 25 TsTom40 and 34 TsTom40. **(A)** Su9-DHFR and **(B)** Mia40. **(C-D)** Western blot and immunodecoration with anti-His Ab of the import into isolated mitochondria from WT TsTom40 yeast. **(C)** Trx1 and **(D)** Trx2. **(E)** Western blot analysis of mitochondria isolated from D273-10B (WT) yeast, WT TsTom40 yeast and the two mutants 25 TsTom40 and 34 TsTom40. Immunodetection with polyclonal anti-Tom40 Ab.

After the previous results where we did not get decreased expression of Tom40, we used a different, yet similar approach. We now include the Sam50 to compare the effect that the decreased expression of these two essential channel proteins have on the import of Trx1. We commercially obtained Tom40 and

Sam50 yTHC yeast strain (GE Dharmacon) in which the promoter was substituted by a Tet-promoter. This allows the gene to be switched off by adding doxycycline in the yeast growth media. As a first step, I titrated the concentration of doxycycline needed to repress the expression of Tom40 and Sam50. The yeast strains were grown in YPD (Materials and Methods) o/n to get a saturated culture. Then, both cultures were diluted to 0.05 OD and left to grow for 14h at which time different concentrations of doxycycline were added (5µg/ml, 10µg/ml and 20µg/ml). The cells were left to grow for further 8h to ensure protein repression. The results show that repression of the expression of is achieved when adding 5µg/ml (Tom40) and 20µg/ml (Sam50) of doxycycline to the media. The detection of Sam50 was indirect as we lacked an anti-Sam50 Ab, instead we use the levels of the ß-barrel protein porin, which depends on Sam50 for its insertion (Kutik et al., 2008). The expression of Tom40 was inhibited with as low as 5µg/ml doxycycline (panel A Figure 7.10), whereas the inhibition of Sam50 was observed at 20µg/ml doxycycline (panel B Figure 7.10).

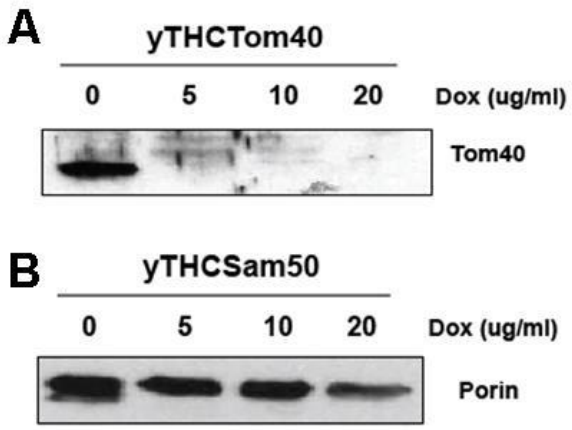

Figure 7.10 yTHCTom40 and yTHCSam50 repression strains. Doxycycline-induced repression with 0µg/ml, 5 µg/ml, 10 µg/ml and 20 µg/ml doxycycline of **(A)** Tom40 and **(B)** Sam50. Immunodecoration with Anti-Tom40 and Anti-porin (for the indirect detection of Sam50).

7.3 Discussion

In this chapter, based on the ß-signal, which drives the insertion of ß-barrel proteins into the mitochondrial OM (Kutik et al., 2008), we found a putative ß-signal- like sequence which is present in a considerable proportion (22%) of proteins residing in the mitochondrial IMS (Vögtle et al., 2017). This signal, which we call the bITS signal is identical to the ß-signal with the exception that it contains a polar instead of a hydrophobic residue in the last position. Furthermore, bioinformatics analysis showed that bITS is conserved through evolution as we found it to be present in different species from bacteria to yeast and to humans. In addition, the bITS is found in a loop in different proteins that do not share structure or function similarities. Thus, although not conclusive, the characteristics of bITS found in this analysis lead us to reasoned that it might be involved in the import and/or sorting of proteins like Trx1. We then started to test the involvement of bITS in the import of Trx1 but failed in our attempts so far to express single point mutant versions of the consensus motif in Trx1 as well as a C-terminal deletion in which the bITS signal was removed in the same protein. This result was surprising as the expression of Trx1 is used as expression enhancer for low expressed proteins. We reasoned that these mutations or deletions within the protein affect the its stability and thus, the lack of expression. Different approaches which will include the use of new primers pair and a different plasmid like pSP6 for *in vitro* translation would be performed.

In addition, we commercially synthesised bITS peptides and used them in competition import experiments. Strikingly, the addition of Gpx3 bITS signal appears to enhance the import of Trx1. As it can be seen in Figure 7.5, the control using triton-x 100 did not seem to work. However, if comparing this lane with that of the loading control, we found that the protein there, Hsp70 which resides in the matrix, cannot be detected because it was digested by the Protease K, which suggests that the protease was functional and that the band seen after the import might be due to the protein being in a tightly folded conformation.

Finally, we are looking for the influence that two major channels in the cell, Tom40 and Sam50, might exert in the import of Trx1. It is interesting to note that both channels have their own particular characteristics like the pore size,

which is wider in Sam50, but represents the entry point into mitochondria. To do so we established the optimum conditions for the inducible repression of these two essential proteins to further test if the import of Trx1 depends on one or the other channel.

The first steps on elucidating the import into mitochondria of the thioredoxin, which plays a crucial role in the regulation of import via the MIA pathway, have been made and further analysis making use of these tools will be required to achieve this task.

Chapter 8 Conclusions and future work

8.1 Summary and conclusions

This work studied the molecular and mechanistic links between redox perturbations and protein biogenesis in mitochondria. Furthermore, it investigated the localisation and function of the thioredoxin system as the main reductive pathway that controls the redox balance in the mitochondrial intermembrane space. To achieve the latter, we used mutants of the model organism yeast *S. cerevisiae*. These mutants were defective in mechanisms or intermediates involved in the reductive machinery of the cell. Hence, we used mutants of the main source of cytosolic NADPH, the glucose-6-phosphate dehydrogenase (Δzwf1, here called Δ*g6pd*), the two cytosolic thioredoxins (Δ*trx*1/2), the cytosolic Trx reductase (Δ*trr*1) and the first enzyme involved in the synthesis of GSH (Δ*gsh*1).

In the first chapter we characterised the yeast mutant strains. It was shown that Δ*g6pd*, Δ*trx*1/2 and Δ*gsh*1 had growth defects when incubated on the non-fermentable media YPLac (Figure 4.2). This result confirmed that the yeasts were defective in handling respiratory conditions, in which ROS are generated (Lee et al., 2001, Minard and McAlister-Henn, 2005). Noteworthy is that the sharpest growth defect observed was in Δ*g6pd*, probably due to the fact that NADPH feeds the two main thiol-reductive pathways, the Grx and Trx systems, which make this yeast strain more sensitive to respiratory conditions (Fernandes and Holmgren, 2004, Lu and Holmgren, 2014). In this sense, the levels of $NADP^+$ and NADPH were also measured and it was found that the individual levels of both dinucleotides are increased as compared to those of WT. However, when the $NADP^+$/NADPH ratio were compared between the different yeast strains we found did not find differences between the WT and the Δ*g6pd* yeast. Unlike Δ*g6pd* yeast, Δ*trx*1/2 and Δ*gsh*1 had higher ratio than that of WT which means higher presence of the oxidised form of NADP in relation to the reduced form and is consistent with the overlapping role of the proteins deleted in both strains (Grant, 2001, Trotter and Grant, 2005). Conversely, the $NADP^+$/NADPH ratio in Δ*trr*1 yeast was lower which indicates that is polarised towards the reduced form of NADP. An explanation for this is that under these conditions Trx might be more oxidised and the cell is sensing this and attempts to equilibrate this

oxidative state of Trx by increasing the relative amounts of NADPH. However, the determination of the redox state of Trx1, Trx2 and Trx3 is needed to probe if this is assumption is true.

Finally, as an indication of the mitochondrial function, the inner membrane Δψ was measured in the yeast mutant strains. The results showed that Δ*g6pd*, Δ*trx*1/2 and Δ*trr*1 yeast have lower Δψ than the WT which is consistent with the fact that disruptions on Δψ have been reported to be associated with accumulation of ROS and these strains are not effective in handling such species (Grant, 2001, Minard et al., 1998, Minard and McAlister-Henn, 2005). Taken together the results on this characterisation chapter showed that the Δ*g6pd*, Δ*trx*1/2 and Δ*gsh*1 mutant yeast strains are sensitive to respiratory conditions, which is an indirect indication of reduced capacity to handle ROS challenge.

Afterwards, we chose the yeast strain with the sharpest growth defect, the Δ*g6pd* strain, as representative of a wider reductive imbalance to test the levels of proteins and the import capacity of mitochondria isolated from this strain. We found that specifically steady state levels and import levels of substrates of the MIA import pathway into the mitochondrial IMS were decreased. In addition, we found that the redox state of the main effector of this import pathway, the oxidoreductase Mia40, was unbalanced towards the oxidised form These results lead us to conclude that mitochondria derived from Δ*g6pd* have reduced import capacity for classical substrates of MIA pathway because the redox state of Mia40 is polarised towards the oxidative form. The latter is supported by the fact that both yeast Mia40 and its human homolog (CHCHD4) is in a balanced state between the reductive and oxidative forms (Erdogan et al., 2018, Kojer et al., 2012). Furthermore, these results meant that a reductive mechanism in the IMS must interact and regulate the redox state of Mia40.

Hence, based on the recent identification of members of the Trx system in the mitochondrial IMS (Vögtle et al., 2012) we hypothesised that this system was such a reductive pathway. Indeed, the results in Chapter 6 show that both Trx1 and TrR1 are imported into mitochondria and interact both *in vitro and in organello* with Mia40 as seen by cross-linking experiments and the reduction of Mia40 in Δ*g6pd* mitochondria back to WT Mia40 redox balanced state when the Trx system was pre-imported into mitochondria. We also found that the pre-

import of the Trx system in the mitochondria with decreased import capacity helps, in some extent, to restore this altered import capacity. Thus, we suggest that the Trx system is the main import system in the mitochondrial IMS.

Finally, we tried to discover and characterise the import mechanism of Trx1 into mitochondria. We found a putative signal present in Trx1 and share with 22% of the total (51) IMS proteome. This signal resembles the signal that drives the insertion of ß-barrel proteins into the mitochondrial OM with the difference that the last amino acid of that ß-signal and the signal that we found (which we call bITS) is hydrophobic (ß-signal) instead of polar (bITS). Bioinformatics analysis revealed that this signal is conserved among species and is shared by proteins with no structural similarity. Furthermore, preliminary results showed that the bITS signal might have an effect on the import of Trx1 into mitochondria. Interestingly, another bITS-protein, the peroxidase Gpx3 appears to drive the import into mitochondria of a folded cargo. However, more work on this needs to be done.

In addition, we propose a model of redox regulation of the import of proteins targeted to the mitochondrial IMS in which the redox state of Mia40 serves as a sensor for the import or not of these proteins. The schematic representation of such a model is shown in Figure 8.1. We propose that under normal conditions (panel A Figure 8.1), the cytosolic Trx system aids the translocation of protein precursors (Durigon et al., 2012). Once in the IMS, the precursors are oxidised and folded by Mia40 as previously described (Banci et al., 2009, Chacinska et al., 2004, Mesecke et al., 2005, Sideris et al., 2009). The latter is possible in a scenario where Mia40 resides in a balanced state between its reducing and oxidising forms due to the interaction with Erv1, Gpx3 and Hot13 (oxidising form) and the Trx system probably with cooperation from GSH (reducing form). However, under conditions where the redox state of Mia40 is mainly oxidised (panel B Figure 8.1), the import of these proteins is blocked. Even though, the protein precursors might also be affected in the cytosol, it has been shown that other NADPH-sources take over the generation of NADPH in the absence of g6pd (Grabowska and Chelstowska, 2003, Minard et al., 1998, Minard and McAlister-Henn, 2001, Minard and McAlister-Henn, 2005). Furthermore, our results showed no differences between the NADP+/NADPH ratio of Δ*g6pd* yeast and that of WT

yeast. In addition, we showed that the import capacity of Mia40 is affected when more oxidised in a system that bypasses the need of the cytosolic machinery (*in organello*).

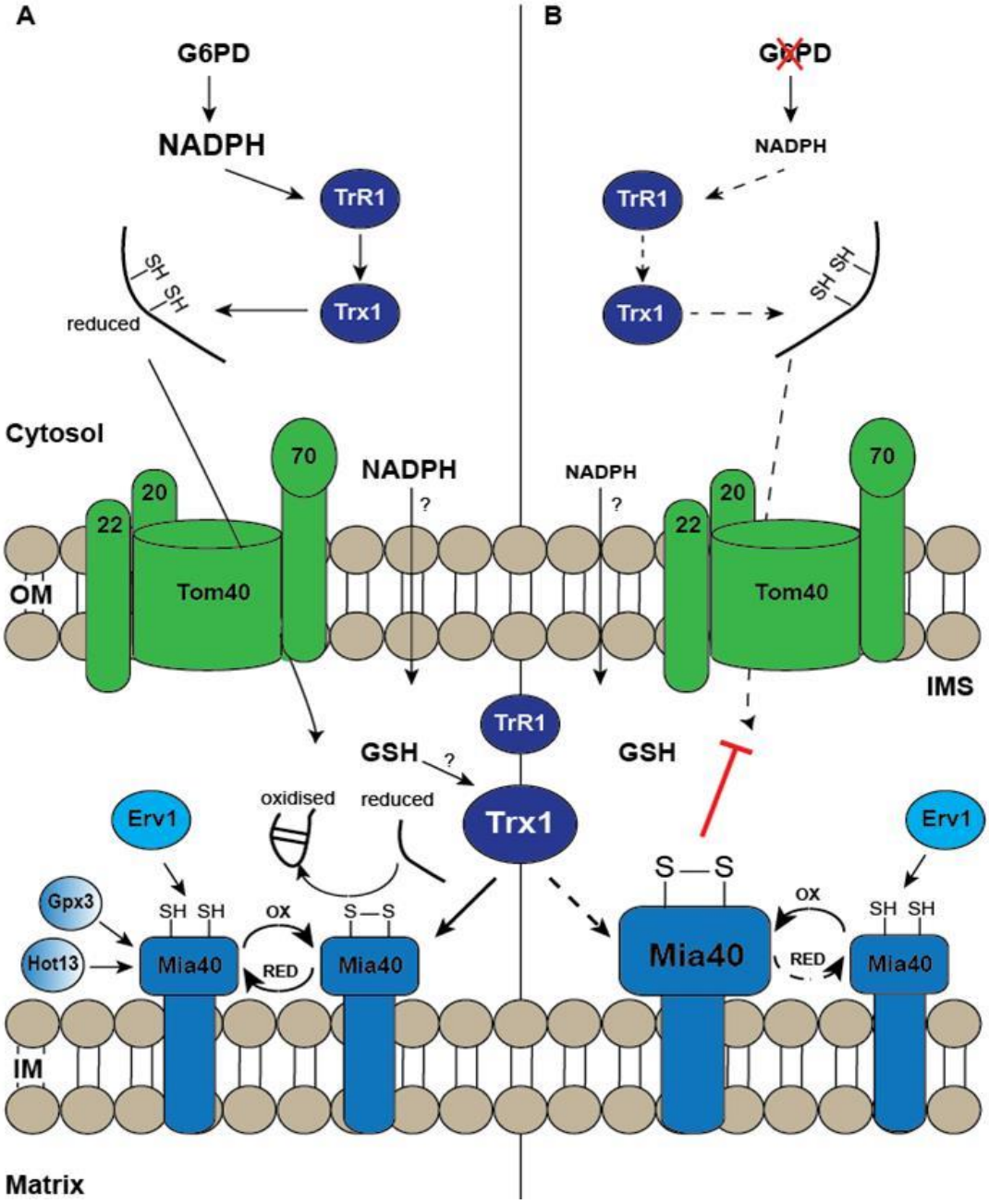

Figure 8.1 Proposed model for the regulation of protein import by the redox state Mia40. (A) Under normal conditions, protein precursors are helped by cytosolic thioredoxins to translocate into the mitochondrial IMS where they are oxidised and folded by the interaction with Mia40 which is kept in a functional balanced state between its oxidising (by Erv1, Gpx3 and Hot13) and reducing forms (by the Trx system). **(B)** When glucose-6-phosphate dehydrogenase is depleted, the import capacity of mitochondria is decreased because Mia40 is in a polarised redox state towards the oxidising form. Thus, the redox state of Mia40 acts as a sensor for the regulation of the import of proteins into the IMS.

8.2 Future work

In order to support the model proposed, a more detailed analysis of the interacting surfaces between Mia40 and Trx1 would require either trypsinolysis and mass spectrometry analysis after the crosslinking, or a high-resolution structural analysis of the complex. Furthermore, optimisation of the determination of import capacity after pre-imported Trx system is crucial to test how this system affects not only the redox state of Mia40, but also that of other proteins such as members of the Trx system itself. Additionally, the construction of probes like the ones used by Kojer *et al* but with the thioredoxin reductase might be a powerful tool to determine the levels of NADPH in the different cellular compartments and if this cofactor can be transported through the mitochondrial OM.

Another important tool would be the expression of an exclusively IMS-targeted version of Trx1 to show if such a model is true *in vivo*. The latter would be complemented with the expression of the human version of Trx1 to test if the effect is conserved.

The elucidation of the import mechanism by which Trx1 is targeted into the mitochondria represents a major challenge. However, the successful expression and purification of recombinant proteins to test the involvement of the proposed bITS sequence is critical. Alongside with that, blue native gels after the import of Trx1 to determine if it is associated to an import complex. In addition, pulldown experiments with Cys trap mutants of Trx1 to possibly confirm an interaction with Mia40 would be of major importance.

In addition, import experiments of Trx1 in the conditional Tom40 and Sam50 mutants to determine the influences of both channels in the translocation of Trx1 across the OM. Another important experiment would be to test the influence of the small Tims complex as they are involved in sorting of proteins into the IMS and the outer and inner membrane.

Appendix

List of Publications

- CARDENAS-RODRIGUEZ, M., CHATZI, A. & TOKATLIDIS, K. 2018. Iron–sulfur clusters: from metals through mitochondria biogenesis to disease. *JBIC Journal of Biological Inorganic Chemistry*, 23, 509-520.

- CARDENAS-RODRIGUEZ, M. & TOKATLIDIS, K. 2017. Cytosolic redox components regulate protein homeostasis via additional localisation in the mitochondrial intermembrane space. *FEBS Lett*, 591, 2661-2670.

List of References

AALTONEN, M. J., FRIEDMAN, J. R., OSMAN, C., SALIN, B., DI RAGO, J.-P., NUNNARI, J., LANGER, T. & TATSUTA, T. 2016. MICOS and phospholipid transfer by Ups2–Mdm35 organize membrane lipid synthesis in mitochondria. *The Journal of Cell Biology,* 213**,** 525-34.

ABE, Y., SHODAI, T., MUTO, T., MIHARA, K., TORII, H., NISHIKAWA, S., ENDO, T. & KOHDA, D. 2000. Structural basis of presequence recognition by the mitochondrial protein import receptor Tom20. *Cell,* 100**,** 551-60.

ADEMOWO, O. S., DIAS, H. K. I., BURTON, D. G. A. & GRIFFITHS, H. R. 2017. Lipid (per) oxidation in mitochondria: an emerging target in the ageing process? *Biogerontology,* 18**,** 859-79.

AGLEDAL, L., NIERE, M. & ZIEGLER, M. 2010. The phosphate makes a difference: cellular functions of NADP. *Redox Rep,* 15**,** 2-10.

AON, M. A., STANLEY, B. A., SIVAKUMARAN, V., KEMBRO, J. M., O'ROURKE, B., PAOLOCCI, N. & CORTASSA, S. 2012. Glutathione/thioredoxin systems modulate mitochondrial H₂O₂ emission: An experimental-computational study. *The Journal of General Physiology,* 139**,** 479-91.

ARNOLD, I., BAUER, M. F., BRUNNER, M., NEUPERT, W. & STUART, R. A. 1997. Yeast mitochondrial F1F0-ATPase: the novel subunit e is identical to Tim11. *FEBS Lett,* 411**,** 195-200.

BACKES, S. & HERRMANN, J. M. 2017. Protein Translocation into the Intermembrane Space and Matrix of Mitochondria: Mechanisms and Driving Forces. *Front Mol Biosci,* 4**,** 1-11.

BANCI, L., BERTINI, I., CALDERONE, V., CEFARO, C., CIOFI-BAFFONI, S., GALLO, A., KALLERGI, E., LIONAKI, E., POZIDIS, C. & TOKATLIDIS, K. 2011. Molecular recognition and substrate mimicry drive the electron-transfer process between MIA40 and ALR. *Proc Natl Acad Sci U S A,* 108**,** 4811-6.

BANCI, L., BERTINI, I., CEFARO, C., CIOFI-BAFFONI, S., GAJDA, K., FELLI, I. C., GALLO, A., PAVELKOVA, A., KALLERGI, E., ANDREADAKI, M., KATRAKILI, N., POZIDIS, C. & TOKATLIDIS, K. 2013. An intrinsically disordered domain has a dual function coupled to compartment-dependent redox control. *J Mol Biol,* 425**,** 594-608.

BANCI, L., BERTINI, I., CEFARO, C., CIOFI-BAFFONI, S., GALLO, A., MARTINELLI, M., SIDERIS, D. P., KATRAKILI, N. & TOKATLIDIS, K. 2009. MIA40 is an oxidoreductase that catalyzes oxidative protein folding in mitochondria. *Nat Struct Mol Biol,* 16**,** 198-206.

BARDWELL, J. C., LEE, J. O., JANDER, G., MARTIN, N., BELIN, D. & BECKWITH, J. 1993. A pathway for disulfide bond formation in vivo. *Proc Natl Acad Sci U S A,* 90**,** 1038-42.

BECKER, T., BOTTINGER, L. & PFANNER, N. 2012. Mitochondrial protein import: from transport pathways to an integrated network. *Trends Biochem Sci,* 37**,** 85-91.

BECKER, T., WENZ, L.-S., KRÜGER, V., LEHMANN, W., MÜLLER, J. M., GORONCY, L., ZUFALL, N., LITHGOW, T., GUIARD, B., CHACINSKA, A., WAGNER, R., MEISINGER, C. & PFANNER, N. 2011. The mitochondrial import protein Mim1 promotes biogenesis of multispanning outer membrane proteins. *The Journal of Cell Biology,* 194**,** 387-95.

BECKMAN, J. S., CHEN, J., ISCHIROPOULOS, H. & CROW, J. P. 1994. Oxidative chemistry of peroxynitrite. *Methods Enzymol,* 233**,** 229-40.

BERTHOLD, J., BAUER, M. F., SCHNEIDER, H.-C., KLAUS, C., DIETMEIER, K., NEUPERT, W. & BRUNNER, M. 1995. The MIM complex mediates preprotein translocationacross the mitochondrial inner membrane and couples it to the mt-Hsp70/ATP driving system. *Cell,* 81**,** 1085-93.

BEVERLY, K. N., SAWAYA, M. R., SCHMID, E. & KOEHLER, C. M. 2008. The Tim8-Tim13 complex has multiple substrate binding sites and binds cooperatively to Tim23. *J Mol Biol,* 382**,** 1144-56.

BIEN, M., LONGEN, S., WAGENER, N., CHWALLA, I., HERRMANN, J. M. & RIEMER, J. 2010. Mitochondrial disulfide bond formation is driven by intersubunit electron transfer in Erv1 and proofread by glutathione. *Mol Cell,* 37**,** 516-28.

BIHLMAIER, K., MESECKE, N., TERZIYSKA, N., BIEN, M., HELL, K. & HERRMANN, J. M. 2007. The disulfide relay system of mitochondria is connected to the respiratory chain. *J Cell Biol,* 179**,** 389-95.

BLACHLY-DYSON, E., SONG, J., WOLFGANG, W. J., COLOMBINI, M. & FORTE, M. 1997. Multicopy suppressors of phenotypes resulting from the absence of yeast VDAC encode a VDAC-like protein. *Mol Cell Biol,* 17**,** 5727-38.

BOVERIS, A. 1984. Determination of the production of superoxide radicals and hydrogen peroxide in mitochondria. *Methods in Enzymology.* Academic Press.

BRACHMANN, C. B., DAVIES, A., COST, G. J., CAPUTO, E., LI, J., HIETER, P. & BOEKE, J. D. 1998. Designer deletion strains derived from Saccharomyces cerevisiae S288C: a useful set of strains and plasmids for PCR-mediated gene disruption and other applications. *Yeast,* 14**,** 115-32.

BRAGOSZEWSKI, P., GORNICKA, A., SZTOLSZTENER, M. E. & CHACINSKA, A. 2013. The ubiquitin-proteasome system regulates mitochondrial intermembrane space proteins. *Mol Cell Biol,* 33**,** 2136-48.

BRAGOSZEWSKI, P., WASILEWSKI, M., SAKOWSKA, P., GORNICKA, A., BOTTINGER, L., QIU, J., WIEDEMANN, N. & CHACINSKA, A. 2015. Retro-translocation of mitochondrial intermembrane space proteins. *Proc Natl Acad Sci U S A,* 112**,** 7713-8.

BUBP, J., JEN, M. & MATUSZEWSKI, K. 2015. Caring for Glucose-6-Phosphate Dehydrogenase (G6PD)-Deficient Patients: Implications for Pharmacy. *P t,* 40**,** 572-4.

BUSHWELLER, J. H., ASLUND, F., WUTHRICH, K. & HOLMGREN, A. 1992. Structural and functional characterization of the mutant Escherichia coli glutaredoxin (C14----S) and its mixed disulfide with glutathione. *Biochemistry,* 31**,** 9288-93.

CARDENAS-RODRIGUEZ, M., CHATZI, A. & TOKATLIDIS, K. 2018. Iron–sulfur clusters: from metals through mitochondria biogenesis to disease. *JBIC Journal of Biological Inorganic Chemistry,* 23**,** 509-20.

CARDENAS-RODRIGUEZ, M. & TOKATLIDIS, K. 2017. Cytosolic redox components regulate protein homeostasis via additional localisation in the mitochondrial intermembrane space. *FEBS Lett,* 591**,** 2661-70.

CARLSON, M., OSMOND, B. C. & BOTSTEIN, D. 1981. Mutants of Yeast Defective in Sucrose Utilization. *Genetics,* 98**,** 25-40.

CASAL, M., PAIVA, S., ANDRADE, R. P., GANCEDO, C. & LEÃO, C. 1999. The Lactate-Proton Symport of Saccharomyces cerevisiae Is Encoded by JEN1. *Journal of Bacteriology,* 181**,** 2620-23.

CHACINSKA, A., KOEHLER, C. M., MILENKOVIC, D., LITHGOW, T. & PFANNER, N. 2009. Importing mitochondrial proteins: machineries and mechanisms. *Cell,* 138**,** 628-44.

CHACINSKA, A., PFANNSCHMIDT, S., WIEDEMANN, N., KOZJAK, V., SANJUAN SZKLARZ, L. K., SCHULZE-SPECKING, A., TRUSCOTT, K. N., GUIARD, B., MEISINGER, C. & PFANNER, N. 2004. Essential role of Mia40 in import and assembly of mitochondrial intermembrane space proteins. *EMBO J,* 23**,** 3735-46.

CHATZI, A., MANGANAS, P. & TOKATLIDIS, K. 2016. Oxidative folding in the mitochondrial intermembrane space: A regulated process important for cell physiology and disease. *Biochim Biophys Acta,* 1863**,** 1298-306.

CHATZI, A., SIDERIS, D. P., KATRAKILI, N., POZIDIS, C. & TOKATLIDIS, K. 2013. Biogenesis of yeast Mia40 - uncoupling folding from import and atypical recognition features. *FEBS J,* 280**,** 4960-9.

CLAYPOOL, S. M., OKTAY, Y., BOONTHEUNG, P., LOO, J. A. & KOEHLER, C. M. 2008. Cardiolipin defines the interactome of the major ADP/ATP carrier protein of the mitochondrial inner membrane. *The Journal of Cell Biology,* 182**,** 937-50.

COLLET, J. F. & BARDWELL, J. C. 2002. Oxidative protein folding in bacteria. *Mol Microbiol,* 44**,** 1-8.

CUNNINGHAM, G. M., FLORES, L. C., ROMAN, M. G., CHENG, C., DUBE, S., ALLEN, C., VALENTINE, J. M., HUBBARD, G. B., BAI, Y., SAUNDERS, T. L. & IKENO, Y. 2018. Thioredoxin overexpression in both the cytosol and mitochondria accelerates age-related disease and shortens lifespan in male C57BL/6 mice. *Geroscience,* 40**,** 453-68.

CUNNINGHAM, G. M., ROMAN, M. G., FLORES, L. C., HUBBARD, G. B., SALMON, A. B., ZHANG, Y., GELFOND, J. & IKENO, Y. 2015. The paradoxical role of thioredoxin on oxidative stress and aging. *Arch Biochem Biophys,* 576**,** 32-8.

CURRAN, S. P., LEUENBERGER, D., LEVERICH, E. P., HWANG, D. K., BEVERLY, K. N. & KOEHLER, C. M. 2004. The role of Hot13p and redox chemistry in the mitochondrial TIM22 import pathway. *J Biol Chem,* 279**,** 43744-51.

DE KROON, A. I., DOLIS, D., MAYER, A., LILL, R. & DE KRUIJFF, B. 1997. Phospholipid composition of highly purified mitochondrial outer membranes of rat liver and Neurospora crassa. Is cardiolipin present in the mitochondrial outer membrane? *Biochim Biophys Acta,* 1325**,** 108-16.

DEMISHTEIN-ZOHARY, K. & AZEM, A. 2017. The TIM23 mitochondrial protein import complex: function and dysfunction. *Cell and Tissue Research,* 367**,** 33-41.

DIETMEIER, K., HONLINGER, A., BOMER, U., DEKKER, P. J., ECKERSKORN, C., LOTTSPEICH, F., KUBRICH, M. & PFANNER, N. 1997. Tom5 functionally links mitochondrial preprotein receptors to the general import pore. *Nature,* 388**,** 195-200.

DOUZERY, E. J., SNELL, E. A., BAPTESTE, E., DELSUC, F. & PHILIPPE, H. 2004. The timing of eukaryotic evolution: does a relaxed molecular clock reconcile proteins and fossils? *Proc Natl Acad Sci U S A,* 101**,** 15386-91.

DRACULIC, T., DAWES, I. W. & GRANT, C. M. 2000. A single glutaredoxin or thioredoxin gene is essential for viability in the yeast Saccharomyces cerevisiae. *Mol Microbiol,* 36**,** 1167-74.

DURIGON, R., WANG, Q., CEH PAVIA, E., GRANT, C. M. & LU, H. 2012. Cytosolic thioredoxin system facilitates the import of mitochondrial small Tim proteins. *EMBO reports,* 13**,** 916-22.

ENDRES, M., NEUPERT, W. & BRUNNER, M. 1999. Transport of the ADP/ATP carrier of mitochondria from the TOM complex to the TIM22.54 complex. *EMBO J,* 18**,** 3214-21.

ERDOGAN, A. J., ALI, M., HABICH, M., SALSCHEIDER, S. L., SCHU, L., PETRUNGARO, C., THOMAS, L. W., ASHCROFT, M., LEICHERT, L. I., ROMA, L. P. & RIEMER, J. 2018. The mitochondrial oxidoreductase CHCHD4 is present in a semi-oxidized state in vivo. *Redox Biology,* 17**,** 200-6.

ERNSTER, L. & SCHATZ, G. 1981. Mitochondria: a historical review. *J Cell Biol,* 91**,** 227s-255s.

FERNANDES, A. P. & HOLMGREN, A. 2004. Glutaredoxins: glutathione-dependent redox enzymes with functions far beyond a simple thioredoxin backup system. *Antioxid Redox Signal,* 6**,** 63-74.

FERREIRA, C., VAN VOORST, F., MARTINS, A., NEVES, L., OLIVEIRA, R., KIELLAND-BRANDT, M. C., LUCAS, C. & BRANDT, A. 2005. A member of the sugar transporter family, Stl1p is the glycerol/H+ symporter in Saccharomyces cerevisiae. *Mol Biol Cell,* 16**,** 2068-76.

FISCHER, M., HORN, S., BELKACEMI, A., KOJER, K., PETRUNGARO, C., HABICH, M., ALI, M., KUTTNER, V., BIEN, M., KAUFF, F., DENGJEL, J., HERRMANN, J. M. & RIEMER, J. 2013. Protein import and oxidative folding in the mitochondrial intermembrane space of intact mammalian cells. *Mol Biol Cell,* 24**,** 2160-70.

FLEURY, C., MIGNOTTE, B. & VAYSSIERE, J. L. 2002. Mitochondrial reactive oxygen species in cell death signaling. *Biochimie,* 84**,** 131-41.

FOUNTOULAKIS, M. 1995. Resistance of recombinant proteins to proteolysis during folding and in the folded state. *Journal of Chemical Technology & Biotechnology,* 62**,** 81-90.

FRIEDMAN, J. R., MOURIER, A., YAMADA, J., MCCAFFERY, J. M. & NUNNARI, J. 2015. MICOS coordinates with respiratory complexes and lipids to establish mitochondrial inner membrane architecture. *Elife,* 4**,** 1-25.

FU, S., GEBICKI, S., JESSUP, W., GEBICKI, J. M. & DEAN, R. T. 1995. Biological fate of amino acid, peptide and protein hydroperoxides. *Biochem J,* 311 (Pt 3)**,** 821-7.

GABRIEL, K., MILENKOVIC, D., CHACINSKA, A., MULLER, J., GUIARD, B., PFANNER, N. & MEISINGER, C. 2007. Novel mitochondrial intermembrane space proteins as substrates of the MIA import pathway. *J Mol Biol,* 365**,** 612-20.

GARRIDO, E. O. & GRANT, C. M. 2002. Role of thioredoxins in the response of Saccharomyces cerevisiae to oxidative stress induced by hydroperoxides. *Mol Microbiol,* 43**,** 993-1003.

GARTNER, F., VOOS, W., QUEROL, A., MILLER, B. R., CRAIG, E. A., CUMSKY, M. G. & PFANNER, N. 1995. Mitochondrial import of subunit Va of cytochrome c oxidase characterized with yeast mutants. *J Biol Chem,* 270**,** 3788-95.

GEBERT, N., CHACINSKA, A., WAGNER, K., GUIARD, B., KOEHLER, C. M., REHLING, P., PFANNER, N. & WIEDEMANN, N. 2008. Assembly of the three small Tim proteins precedes docking to the mitochondrial carrier translocase. *EMBO Rep,* 9**,** 548-54.

GEBICKI, S., GILL, K. H., DEAN, R. T. & GEBICKI, J. M. 2002. Action of peroxidases on protein hydroperoxides. *Redox Rep,* 7**,** 235-42.

GEISSLER, A., KRIMMER, T., BOMER, U., GUIARD, B., RASSOW, J. & PFANNER, N. 2000. Membrane potential-driven protein import into mitochondria. The sorting sequence of cytochrome b(2) modulates the deltapsi-dependence of translocation of the matrix-targeting sequence. *Mol Biol Cell,* 11**,** 3977-91.

GHEZZI, P. 2005. Regulation of protein function by glutathionylation. *Free Radic Res,* 39**,** 573-80.

GHEZZI, P. 2013. Protein glutathionylation in health and disease. *Biochimica et Biophysica Acta (BBA) - General Subjects,* 1830**,** 3165-72.
GILBERT, H. F. 1984. Redox control of enzyme activities by thiol/disulfide exchange. *Methods in Enzymology*. Academic Press.
GLICK, B. S. 1991. Protein import into isolated yeast mitochondria. *Methods Cell Biol,* 34**,** 389-99.
GLICK, B. S., WACHTER, C., REID, G. A. & SCHATZ, G. 1993. Import of cytochrome b2 to the mitochondrial intermembrane space: the tightly folded heme-binding domain makes import dependent upon matrix ATP. *Protein Sci,* 2**,** 1901-17.
GRABOWSKA, D. & CHELSTOWSKA, A. 2003. The ALD6 gene product is indispensable for providing NADPH in yeast cells lacking glucose-6-phosphate dehydrogenase activity. *J Biol Chem,* 278**,** 13984-8.
GRANT, C. M. 2001. Role of the glutathione/glutaredoxin and thioredoxin systems in yeast growth and response to stress conditions. *Mol Microbiol,* 39**,** 533-41.
GRANT, C. M., LUIKENHUIS, S., BECKHOUSE, A., SODERBERGH, M. & DAWES, I. W. 2000. Differential regulation of glutaredoxin gene expression in response to stress conditions in the yeast Saccharomyces cerevisiae. *Biochim Biophys Acta,* 1490**,** 33-42.
GRANT, C. M., MACIVER, F. H. & DAWES, I. W. 1996. Glutathione is an essential metabolite required for resistance to oxidative stress in the yeast Saccharomyces cerevisiae. *Curr Genet,* 29**,** 511-5.
GRANT, C. M., MACIVER, F. H. & DAWES, I. W. 1997. Glutathione synthetase is dispensable for growth under both normal and oxidative stress conditions in the yeast Saccharomyces cerevisiae due to an accumulation of the dipeptide gamma-glutamylcysteine. *Mol Biol Cell,* 8**,** 1699-707.
GRAUSCHOPF, U., WINTHER, J. R., KORBER, P., ZANDER, T., DALLINGER, P. & BARDWELL, J. C. 1995. Why is DsbA such an oxidizing disulfide catalyst? *Cell,* 83**,** 947-55.
GRUBER, C. W., CEMAZAR, M., HERAS, B., MARTIN, J. L. & CRAIK, D. J. 2006. Protein disulfide isomerase: the structure of oxidative folding. *Trends Biochem Sci,* 31**,** 455-64.
GUIARD, B. 1985. Structure, expression and regulation of a nuclear gene encoding a mitochondrial protein: the yeast L(+)-lactate cytochrome c oxidoreductase (cytochrome b2). *EMBO J,* 4**,** 3265-72.
GUSE, A. H. & LEE, H. C. 2008. NAADP: a universal Ca2+ trigger. *Sci Signal,* 1**,** 1-7.
HARTIG, A. & RUIS, H. 1986. Nucleotide sequence of the Saccharomyces cerevisiae CTT1 gene and deduced amino-acid sequence of yeast catalase T. *Eur J Biochem,* 160**,** 487-90.
HAWLITSCHEK, G., SCHNEIDER, H., SCHMIDT, B., TROPSCHUG, M., HARTL, F. U. & NEUPERT, W. 1988. Mitochondrial protein import: identification of processing peptidase and of PEP, a processing enhancing protein. *Cell,* 53**,** 795-806.
HERRMANN, J. M. & HELL, K. 2005. Chopped, trapped or tacked – protein translocation into the IMS of mitochondria. *Trends in Biochemical Sciences,* 30**,** 205-12.
HERRMANN, J. M. & RIEMER, J. 2014. Three approaches to one problem: protein folding in the periplasm, the endoplasmic reticulum, and the intermembrane space. *Antioxid Redox Signal,* 21**,** 438-56.

HIBBS, J. B., JR., TAINTOR, R. R. & VAVRIN, Z. 1987. Macrophage cytotoxicity: role for L-arginine deiminase and imino nitrogen oxidation to nitrite. *Science,* 235**,** 473-6.

HILL, K., MODEL, K., RYAN, M. T., DIETMEIER, K., MARTIN, F., WAGNER, R. & PFANNER, N. 1998. Tom40 forms the hydrophilic channel of the mitochondrial import pore for preproteins *Nature,* 395**,** 516-21.

HO, H. Y., CHENG, M. L. & CHIU, D. T. 2007. Glucose-6-phosphate dehydrogenase--from oxidative stress to cellular functions and degenerative diseases. *Redox Rep,* 12**,** 109-18.

HÖHR, A. I. C., LINDAU, C., WIRTH, C., QIU, J., STROUD, D. A., KUTIK, S., GUIARD, B., HUNTE, C., BECKER, T., PFANNER, N. & WIEDEMANN, N. 2018. Membrane protein insertion through a mitochondrial ß-barrel gate. *Science,* 359**,** 1-12.

HOLMGREN, A. 1995. Thioredoxin structure and mechanism: conformational changes on oxidation of the active-site sulfhydryls to a disulfide. *Structure,* 3**,** 239-43.

HOLMGREN, A., SODERBERG, B. O., EKLUND, H. & BRANDEN, C. I. 1975. Three-dimensional structure of Escherichia coli thioredoxin-S2 to 2.8 A resolution. *Proc Natl Acad Sci U S A,* 72**,** 2305-9.

HONG, S. P., LEIPER, F. C., WOODS, A., CARLING, D. & CARLSON, M. 2003. Activation of yeast Snf1 and mammalian AMP-activated protein kinase by upstream kinases. *Proc Natl Acad Sci U S A,* 100**,** 8839-43.

HOUTKOOPER, R. H. & VAZ, F. M. 2008. Cardiolipin, the heart of mitochondrial metabolism. *Cell Mol Life Sci,* 65**,** 2493-506.

HU, J., DONG, L. & OUTTEN, C. E. 2008. The redox environment in the mitochondrial intermembrane space is maintained separately from the cytosol and matrix. *J Biol Chem,* 283**,** 29126-34.

IZAWA, S., INOUE, Y. & KIMURA, A. 1996. Importance of catalase in the adaptive response to hydrogen peroxide: analysis of acatalasaemic Saccharomyces cerevisiae. *Biochem J,* 320 (Pt 1)**,** 61-7.

IZAWA, S., MAEDA, K., MIKI, T., MANO, J., INOUE, Y. & KIMURA, A. 1998. Importance of glucose-6-phosphate dehydrogenase in the adaptive response to hydrogen peroxide in Saccharomyces cerevisiae. *Biochemical Journal,* 330**,** 811-17.

IZAWA, S., MAEDA, K., SUGIYAMA, K., MANO, J., INOUE, Y. & KIMURA, A. 1999. Thioredoxin deficiency causes the constitutive activation of Yap1, an AP-1-like transcription factor in Saccharomyces cerevisiae. *J Biol Chem,* 274**,** 28459-65.

JESSOP, C. E. & BULLEID, N. J. 2004. Glutathione directly reduces an oxidoreductase in the endoplasmic reticulum of mammalian cells. *J Biol Chem,* 279**,** 55341-7.

JIANG, R. & CARLSON, M. 1996. Glucose regulates protein interactions within the yeast SNF1 protein kinase complex. *Genes Dev,* 10**,** 3105-15.

JORES, T., KLINGER, A., GROSS, L. E., KAWANO, S., FLINNER, N., DUCHARDT-FERNER, E., WOHNERT, J., KALBACHER, H., ENDO, T., SCHLEIFF, E. & RAPAPORT, D. 2016. Characterization of the targeting signal in mitochondrial beta-barrel proteins. *Nat Commun,* 7**,** 1-16.

KACHROO, A. H., LAURENT, J. M., YELLMAN, C. M., MEYER, A. G., WILKE, C. O. & MARCOTTE, E. M. 2015. Evolution. Systematic humanization of yeast genes reveals conserved functions and genetic modularity. *Science,* 348**,** 921-5.

KARNIELY, S. & PINES, O. 2005. Single translation--dual destination: mechanisms of dual protein targeting in eukaryotes. *EMBO Rep,* 6**,** 420-5.

KAYIKCI, Ö. & NIELSEN, J. 2015. Glucose repression in Saccharomyces cerevisiae. *FEMS Yeast Research,* 15**,** 1-8.

KEMMINK, J., DARBY, N. J., DIJKSTRA, K., NILGES, M. & CREIGHTON, T. E. 1997. The folding catalyst protein disulfide isomerase is constructed of active and inactive thioredoxin modules. *Curr Biol,* 7**,** 239-45.

KERSCHER, O., HOLDER, J., SRINIVASAN, M., LEUNG, R. S. & JENSEN, R. E. 1997. The Tim54p-Tim22p complex mediates insertion of proteins into the mitochondrial inner membrane. *J Cell Biol,* 139**,** 1663-75.

KISPAL, G., STEINER, H., COURT, D. A., ROLINSKI, B. & LILL, R. 1996. Mitochondrial and cytosolic branched-chain amino acid transaminases from yeast, homologs of the myc oncogene-regulated Eca39 protein. *J Biol Chem,* 271**,** 24458-64.

KLOPPEL, C., SUZUKI, Y., KOJER, K., PETRUNGARO, C., LONGEN, S., FIEDLER, S., KELLER, S. & RIEMER, J. 2011. Mia40-dependent oxidation of cysteines in domain I of Ccs1 controls its distribution between mitochondria and the cytosol. *Mol Biol Cell,* 22**,** 3749-57.

KOEHLER, C. M. 2004. The small Tim proteins and the twin Cx3C motif. *Trends Biochem Sci,* 29**,** 1-4.

KOEHLER, C. M., LEUENBERGER, D., MERCHANT, S., RENOLD, A., JUNNE, T. & SCHATZ, G. 1999. Human deafness dystonia syndrome is a mitochondrial disease. *Proc Natl Acad Sci U S A,* 96**,** 2141-6.

KOJER, K., BIEN, M., GANGEL, H., MORGAN, B., DICK, T. P. & RIEMER, J. 2012. Glutathione redox potential in the mitochondrial intermembrane space is linked to the cytosol and impacts the Mia40 redox state. *EMBO J,* 31**,** 3169-82.

KOJER, K., PELEH, V., CALABRESE, G., HERRMANN, J. M. & RIEMER, J. 2015. Kinetic control by limiting glutaredoxin amounts enables thiol oxidation in the reducing mitochondrial intermembrane space. *Mol Biol Cell,* 26**,** 195-204.

KOJER, K. & RIEMER, J. 2014. Balancing oxidative protein folding: the influences of reducing pathways on disulfide bond formation. *Biochim Biophys Acta,* 1844**,** 1383-90.

KOTYK, A. & ALONSO, A. 1985. Transport of ethanol in baker's yeast. *Folia Microbiol (Praha),* 30**,** 90-1.

KOVERMANN, P., TRUSCOTT, K. N., GUIARD, B., REHLING, P., SEPURI, N. B., MULLER, H., JENSEN, R. E., WAGNER, R. & PFANNER, N. 2002. Tim22, the essential core of the mitochondrial protein insertion complex, forms a voltage-activated and signal-gated channel. *Mol Cell,* 9**,** 363-73.

KRAMER, R. & KLINGENBERG, M. 1977. Reconstitution of adenine nucleotide transport with purified ADP, ATP-carrier protein. *FEBS Lett,* 82**,** 363-7.

KRAUSE, G., LUNDSTROM, J., BAREA, J. L., PUEYO DE LA CUESTA, C. & HOLMGREN, A. 1991. Mimicking the active site of protein disulfide-isomerase by substitution of proline 34 in Escherichia coli thioredoxin. *J Biol Chem,* 266**,** 9494-500.

KRITSILIGKOU, P., CHATZI, A., CHARALAMPOUS, G., MIRONOV, A., JR., GRANT, C. M. & TOKATLIDIS, K. 2017. Unconventional Targeting of a Thiol Peroxidase to the Mitochondrial Intermembrane Space Facilitates Oxidative Protein Folding. *Cell Rep,* 18**,** 2729-41.

KRUGER, N. J. & VON SCHAEWEN, A. 2003. The oxidative pentose phosphate pathway: structure and organisation. *Curr Opin Plant Biol,* 6**,** 236-46.

KUMAR, C., IGBARIA, A., D'AUTREAUX, B., PLANSON, A. G., JUNOT, C., GODAT, E., BACHHAWAT, A. K., DELAUNAY-MOISAN, A. & TOLEDANO, M. B. 2011. Glutathione revisited: a vital function in iron metabolism and ancillary role in thiol-redox control. *Embo j,* 30**,** 2044-56.

KUTIK, S., STOJANOVSKI, D., BECKER, L., BECKER, T., MEINECKE, M., KRUGER, V., PRINZ, C., MEISINGER, C., GUIARD, B., WAGNER, R., PFANNER, N. & WIEDEMANN, N. 2008. Dissecting membrane insertion of mitochondrial beta-barrel proteins. *Cell,* 132**,** 1011-24.

LANE, N. & MARTIN, W. 2010. The energetics of genome complexity. *Nature,* 467**,** 929-34.

LEE, A. C., XU, X., BLACHLY-DYSON, E., FORTE, M. & COLOMBINI, M. 1998. The Role of Yeast VDAC Genes on the Permeability of the Mitochondrial Outer Membrane. *The Journal of Membrane Biology,* 161**,** 173-81.

LEE, J. C., STRAFFON, M. J., JANG, T. Y., HIGGINS, V. J., GRANT, C. M. & DAWES, I. W. 2001. The essential and ancillary role of glutathione in Saccharomyces cerevisiae analysed using a grande gsh1 disruptant strain. *FEMS Yeast Res,* 1**,** 57-65.

LEE, S., KIM, S. M. & LEE, R. T. 2013. Thioredoxin and thioredoxin target proteins: from molecular mechanisms to functional significance. *Antioxid Redox Signal,* 18**,** 1165-207.

LIONAKI, E., AIVALIOTIS, M., POZIDIS, C. & TOKATLIDIS, K. 2010. The N-terminal Shuttle Domain of Erv1 Determines the Affinity for Mia40 and Mediates Electron Transfer to the Catalytic Erv1 Core in Yeast Mitochondria. *Antioxidants & Redox Signaling,* 13**,** 1327-39.

LIOU, G. G., TANNY, J. C., KRUGER, R. G., WALZ, T. & MOAZED, D. 2005. Assembly of the SIR complex and its regulation by O-acetyl-ADP-ribose, a product of NAD-dependent histone deacetylation. *Cell,* 121**,** 515-27.

LIU, W., LI, L., YE, H., CHEN, H., SHEN, W., ZHONG, Y., TIAN, T. & HE, H. 2017. From Saccharomyces cerevisiae to human: The important gene co-expression modules. *Biomed Rep,* 7**,** 153-8.

LODI, T. & FERRERO, I. 1993. Isolation of the DLD gene of Saccharomyces cerevisiae encoding the mitochondrial enzyme D-lactate ferricytochrome c oxidoreductase. *Molecular and General Genetics MGG,* 238**,** 315-24.

LOFTUS, T. M., HALL, L. V., ANDERSON, S. L. & MCALISTER-HENN, L. 1994. Isolation, characterization, and disruption of the yeast gene encoding cytosolic NADP-specific isocitrate dehydrogenase. *Biochemistry,* 33**,** 9661-7.

LU, H., ALLEN, S., WARDLEWORTH, L., SAVORY, P. & TOKATLIDIS, K. 2004a. Functional TIM10 chaperone assembly is redox-regulated in vivo. *J Biol Chem,* 279**,** 18952-8.

LU, H., GOLOVANOV, A. P., ALCOCK, F., GROSSMANN, J. G., ALLEN, S., LIAN, L. Y. & TOKATLIDIS, K. 2004b. The structural basis of the TIM10 chaperone assembly. *J Biol Chem,* 279**,** 18959-66.

LU, J. & HOLMGREN, A. 2014. The thioredoxin antioxidant system. *Free Radic Biol Med,* 66**,** 75-87.

LUIKENHUIS, S., PERRONE, G., DAWES, I. W. & GRANT, C. M. 1998. The yeast Saccharomyces cerevisiae contains two glutaredoxin genes that are required for protection against reactive oxygen species. *Mol Biol Cell,* 9**,** 1081-91.

LUTZ, T., NEUPERT, W. & HERRMANN, J. M. 2003. Import of small Tim proteins into the mitochondrial intermembrane space. *Embo j,* 22**,** 4400-8.

LYONS, T. J., NERSISSIAN, A., HUANG, H., YEOM, H., NISHIDA, C. R., GRADEN, J. A., GRALLA, E. B. & VALENTINE, J. S. 2000. The metal binding properties of the zinc site of yeast copper-zinc superoxide dismutase: implications for amyotrophic lateral sclerosis. *J Biol Inorg Chem,* 5**,** 189-203.

MANGANAS, P. 2017. *Oxidative Regulation Mechanisms in the Mitochondrial Intermembrane Space*. Doctor of Philosophy, University of Glasgow.

MARTIN, J., MAHLKE, K. & PFANNER, N. 1991. Role of an energized inner membrane in mitochondrial protein import. Delta psi drives the movement of presequences. *J Biol Chem,* 266**,** 18051-7.

MARTIN, J. L., BARDWELL, J. C. & KURIYAN, J. 1993. Crystal structure of the DsbA protein required for disulphide bond formation in vivo. *Nature,* 365**,** 464-8.

MARTÍNEZ, M. C. & ANDRIANTSITOHAINA, R. 2009. Reactive Nitrogen Species: Molecular Mechanisms and Potential Significance in Health and Disease. *Antioxidants & Redox Signaling,* 11**,** 669-702.

MCCARTNEY, R. R. & SCHMIDT, M. C. 2001. Regulation of Snf1 kinase. Activation requires phosphorylation of threonine 210 by an upstream kinase as well as a distinct step mediated by the Snf4 subunit. *J Biol Chem,* 276**,** 36460-6.

MEINECKE, M., WAGNER, R., KOVERMANN, P., GUIARD, B., MICK, D. U., HUTU, D. P., VOOS, W., TRUSCOTT, K. N., CHACINSKA, A., PFANNER, N. & REHLING, P. 2006. Tim50 maintains the permeability barrier of the mitochondrial inner membrane. *Science,* 312**,** 1523-6.

MEISTER, A. 1988. On the discovery of glutathione. *Trends Biochem Sci,* 13**,** 185-8.

MEISTER, A. & ANDERSON, M. E. 1983. Glutathione. *Annu Rev Biochem,* 52**,** 711-60.

MESECKE, N., BIHLMAIER, K., GRUMBT, B., LONGEN, S., TERZIYSKA, N., HELL, K. & HERRMANN, J. M. 2008. The zinc-binding protein Hot13 promotes oxidation of the mitochondrial import receptor Mia40. *EMBO Rep,* 9**,** 1107-13.

MESECKE, N., TERZIYSKA, N., KOZANY, C., BAUMANN, F., NEUPERT, W., HELL, K. & HERRMANN, J. M. 2005. A disulfide relay system in the intermembrane space of mitochondria that mediates protein import. *Cell,* 121**,** 1059-69.

MEZGHRANI, A., FASSIO, A., BENHAM, A., SIMMEN, T., BRAAKMAN, I. & SITIA, R. 2001. Manipulation of oxidative protein folding and PDI redox state in mammalian cells. *EMBO J,* 20**,** 6288-96.

MILENKOVIC, D., RAMMING, T., MULLER, J. M., WENZ, L. S., GEBERT, N., SCHULZE-SPECKING, A., STOJANOVSKI, D., ROSPERT, S. & CHACINSKA, A. 2009. Identification of the signal directing Tim9 and Tim10 into the intermembrane space of mitochondria. *Mol Biol Cell,* 20**,** 2530-9.

MINARD, K. I., JENNINGS, G. T., LOFTUS, T. M., XUAN, D. & MCALISTER-HENN, L. 1998. Sources of NADPH and expression of mammalian NADP+-specific isocitrate dehydrogenases in Saccharomyces cerevisiae. *J Biol Chem,* 273**,** 31486-93.

MINARD, K. I. & MCALISTER-HENN, L. 2001. Antioxidant function of cytosolic sources of NADPH in yeast. *Free Radic Biol Med,* 31**,** 832-43.

MINARD, K. I. & MCALISTER-HENN, L. 2005. Sources of NADPH in yeast vary with carbon source. *J Biol Chem,* 280**,** 39890-6.

MINUCCI, A., MORADKHANI, K., HWANG, M. J., ZUPPI, C., GIARDINA, B. & CAPOLUONGO, E. 2012. Glucose-6-phosphate dehydrogenase (G6PD)

mutations database: review of the "old" and update of the new mutations. *Blood Cells Mol Dis,* 48**,** 154-65.

MISSIAKAS, D., SCHWAGER, F. & RAINA, S. 1995. Identification and characterization of a new disulfide isomerase-like protein (DsbD) in Escherichia coli. *EMBO J,* 14**,** 3415-24.

MOKRANJAC, D. & NEUPERT, W. 2015. Architecture of a protein entry gate. *Nature,* 528**,** 201-2.

MOSSMANN, D., MEISINGER, C. & VOGTLE, F. N. 2012. Processing of mitochondrial presequences. *Biochim Biophys Acta,* 1819**,** 1098-106.

MULLER, E. G. 1991. Thioredoxin deficiency in yeast prolongs S phase and shortens the G1 interval of the cell cycle. *J Biol Chem,* 266**,** 9194-202.

MULLER, E. G. 1994. Deoxyribonucleotides are maintained at normal levels in a yeast thioredoxin mutant defective in DNA synthesis. *J Biol Chem,* 269**,** 24466-71.

NELSON, N. & SCHATZ, G. 1979. Energy-dependent processing of cytoplasmically made precursors to mitochondrial proteins. *Proc Natl Acad Sci U S A,* 76**,** 4365-9.

NISHIDA, M., HARADA, S., NOGUCHI, S., SATOW, Y., INOUE, H. & TAKAHASHI, K. 1998. Three-dimensional structure of Escherichia coli glutathione S-transferase complexed with glutathione sulfonate: catalytic roles of Cys10 and His106. *J Mol Biol,* 281**,** 135-47.

NOGAE, I. & JOHNSTON, M. 1990. Isolation and characterization of the ZWF1 gene of Saccharomyces cerevisiae, encoding glucose-6-phosphate dehydrogenase. *Gene,* 96**,** 161-9.

OKADA, N., OGAWA, J. & SHIMA, J. 2014. Comprehensive analysis of genes involved in the oxidative stress tolerance using yeast heterozygous deletion collection. *FEMS Yeast Res,* 14**,** 425-34.

OLIVEIRA, R., LAGES, F., SILVA-GRACA, M. & LUCAS, C. 2003. Fps1p channel is the mediator of the major part of glycerol passive diffusion in Saccharomyces cerevisiae: artefacts and re-definitions. *Biochim Biophys Acta,* 1613**,** 57-71.

OOI, B. G., MCMULLEN, G. L., LINNANE, A. W., NAGLEY, P. & NOVITSKI, C. E. 1985. Biogenesis of mitochondria: DNA sequence analysis of mit- mutations in the mitochondrial oli1 gene coding for mitochondrial ATPase subunit 9 in Saccharomyces cerevisiae. *Nucleic Acids Res,* 13**,** 1327-39.

OUTTEN, C. E. & CULOTTA, V. C. 2003. A novel NADH kinase is the mitochondrial source of NADPH in Saccharomyces cerevisiae. *EMBO J,* 22**,** 2015-24.

PACHER, P., BECKMAN, J. S. & LIAUDET, L. 2007. Nitric oxide and peroxynitrite in health and disease. *Physiol Rev,* 87**,** 315-424.

PAGLIARINI, D. J., CALVO, S. E., CHANG, B., SHETH, S. A., VAFAI, S. B., ONG, S. E., WALFORD, G. A., SUGIANA, C., BONEH, A., CHEN, W. K., HILL, D. E., VIDAL, M., EVANS, J. G., THORBURN, D. R., CARR, S. A. & MOOTHA, V. K. 2008. A mitochondrial protein compendium elucidates complex I disease biology. *Cell,* 134**,** 112-23.

PAIVA, S., DEVAUX, F., BARBOSA, S., JACQ, C. & CASAL, M. 2004. Ady2p is essential for the acetate permease activity in the yeast Saccharomyces cerevisiae. *Yeast,* 21**,** 201-10.

PAPIĆ, D., KRUMPE, K., DUKANOVIC, J., DIMMER, K. S. & RAPAPORT, D. 2011. Multispan mitochondrial outer membrane protein Ugo1 follows a unique Mim1-dependent import pathway. *The Journal of Cell Biology,* 194**,** 397-405.

PARADIES, G., PARADIES, V., DE BENEDICTIS, V., RUGGIERO, F. M. & PETROSILLO, G. 2014. Functional role of cardiolipin in mitochondrial bioenergetics. *Biochimica et Biophysica Acta (BBA) - Bioenergetics,* 1837**,** 408-17.

PARK, J. S., DAVIS, R. L. & SUE, C. M. 2018. Mitochondrial Dysfunction in Parkinson's Disease: New Mechanistic Insights and Therapeutic Perspectives. *Curr Neurol Neurosci Rep,* 18**,** 1-11.

PEDRAJAS, J. R., KOSMIDOU, E., MIRANDA-VIZUETE, A., GUSTAFSSON, J. A., WRIGHT, A. P. & SPYROU, G. 1999. Identification and functional characterization of a novel mitochondrial thioredoxin system in Saccharomyces cerevisiae. *J Biol Chem,* 274**,** 6366-73.

PETROVA, V. Y., DRESCHER, D., KUJUMDZIEVA, A. V. & SCHMITT, M. J. 2004. Dual targeting of yeast catalase A to peroxisomes and mitochondria. *Biochem J,* 380**,** 393-400.

PFANNER, N., MULLER, H. K., HARMEY, M. A. & NEUPERT, W. 1987. Mitochondrial protein import: involvement of the mature part of a cleavable precursor protein in the binding to receptor sites. *EMBO J,* 6**,** 3449-54.

PFANNER, N. & NEUPERT, W. 1985. Transport of proteins into mitochondria: a potassium diffusion potential is able to drive the import of ADP/ATP carrier. *EMBO J,* 4**,** 2819-25.

PFANNER, N. & NEUPERT, W. 1987. Distinct steps in the import of ADP/ATP carrier into mitochondria. *J Biol Chem,* 262**,** 7528-36.

PHULL, A. R., NASIR, B., HAQ, I. U. & KIM, S. J. 2018. Oxidative stress, consequences and ROS mediated cellular signaling in rheumatoid arthritis. *Chem Biol Interact,* 281**,** 121-36.

POLJAK, A., DAWES, I. W., INGELSE, B. A., DUNCAN, M. W., SMYTHE, G. A. & GRANT, C. M. 2003. Oxidative damage to proteins in yeast cells exposed to adaptive levels of H(2)O(2). *Redox Rep,* 8**,** 371-7.

POPOV-CELEKETIC, J., WAIZENEGGER, T. & RAPAPORT, D. 2008. Mim1 functions in an oligomeric form to facilitate the integration of Tom20 into the mitochondrial outer membrane. *J Mol Biol,* 376**,** 671-80.

RADI, R., RODRIGUEZ, M., CASTRO, L. & TELLERI, R. 1994. Inhibition of mitochondrial electron transport by peroxynitrite. *Arch Biochem Biophys,* 308**,** 89-95.

REN, G., STEPHAN, D., XU, Z., ZHENG, Y., TANG, D., HARRISON, R. S., KURZ, M., JARROTT, R., SHOULDICE, S. R., HINIKER, A., MARTIN, J. L., HERAS, B. & BARDWELL, J. C. 2009. Properties of the thioredoxin fold superfamily are modulated by a single amino acid residue. *J Biol Chem,* 284**,** 10150-9.

RIETSCH, A., BELIN, D., MARTIN, N. & BECKWITH, J. 1996. An in vivo pathway for disulfide bond isomerization in Escherichia coli. *Proc Natl Acad Sci U S A,* 93**,** 13048-53.

RIGANTI, C., GAZZANO, E., POLIMENI, M., ALDIERI, E. & GHIGO, D. 2012. The pentose phosphate pathway: an antioxidant defense and a crossroad in tumor cell fate. *Free Radic Biol Med,* 53**,** 421-36.

ROBINSON, B. H., MACMILLAN, H., PETROVA-BENEDICT, R. & SHERWOOD, W. G. 1987. Variable clinical presentation in patients with defective E1 component of pyruvate dehydrogenase complex. *J Pediatr,* 111**,** 525-33.

ROBINSON, B. H., TAYLOR, J. & SHERWOOD, W. G. 1980. The genetic heterogeneity of lactic acidosis: occurrence of recognizable inborn errors of metabolism in pediatric population with lactic acidosis. *Pediatr Res,* 14**,** 956-62.

ROBINSON, J. B., JR. & SRERE, P. A. 1985. Organization of Krebs tricarboxylic acid cycle enzymes. *Biochem Med,* 33**,** 149-57.

ROESCH, K., CURRAN, S. P., TRANEBJAERG, L. & KOEHLER, C. M. 2002. Human deafness dystonia syndrome is caused by a defect in assembly of the DDP1/TIMM8a-TIMM13 complex. *Hum Mol Genet,* 11**,** 477-86.

ROLLAND, F., WINDERICKX, J. & THEVELEIN, J. M. 2002. Glucose-sensing and -signalling mechanisms in yeast. *FEMS Yeast Res,* 2**,** 183-201.

ROZHKOVA, A., STIRNIMANN, C. U., FREI, P., GRAUSCHOPF, U., BRUNISHOLZ, R., GRÜTTER, M. G., CAPITANI, G. & GLOCKSHUBER, R. 2004. Structural basis and kinetics of inter- and intramolecular disulfide exchange in the redox catalyst DsbD. *EMBO J,* 23**,** 1709-19.

RUTTER, J., REICK, M., WU, L. C. & MCKNIGHT, S. L. 2001. Regulation of clock and NPAS2 DNA binding by the redox state of NAD cofactors. *Science,* 293**,** 510-4.

SABINE HOFMANN, U. R., NICOLE MÜHLENBEIN, WALTER NEUPERT, KLAUS-DIETER GERBITZ, MICHAEL BRUNNER AND MATTHIAS F. BAUER 2002. The C66W Mutation in the Deafness Dystonia Peptide 1 (DDP1) Affects the Formation of Functional DDP1·TIM13 Complexes in the Mitochondrial Intermembrane Space. *Journal of Biological Chemistry,* 227**,** 23287-93.

SANZ, P., ALMS, G. R., HAYSTEAD, T. A. & CARLSON, M. 2000. Regulatory interactions between the Reg1-Glc7 protein phosphatase and the Snf1 protein kinase. *Mol Cell Biol,* 20**,** 1321-8.

SCHAFER, F. Q. & BUETTNER, G. R. 2001. Redox environment of the cell as viewed through the redox state of the glutathione disulfide/glutathione couple. *Free Radical Biology and Medicine,* 30**,** 1191-212.

SCHATZ, G. 2013. Getting mitochondria to center stage. *Biochem Biophys Res Commun,* 434**,** 407-10.

SCHEFFLER, I. E. 2002. Metabolic Pathways Inside Mitochondria. *In:* JOHN WILEY & SONS, I. (ed.) *Mitochondria.*

SCHMIDT, M. C. & MCCARTNEY, R. R. 2000. beta-subunits of Snf1 kinase are required for kinase function and substrate definition. *EMBO J,* 19**,** 4936-43.

SEVIER, C. S., QU, H., HELDMAN, N., GROSS, E., FASS, D. & KAISER, C. A. 2007. Modulation of cellular disulfide-bond formation and the ER redox environment by feedback regulation of Ero1. *Cell,* 129**,** 333-44.

SHADEL, GERALD S. & HORVATH, TAMAS L. 2015. Mitochondrial ROS Signaling in Organismal Homeostasis. *Cell,* 163**,** 560-9.

SHERMAN, F. 1964. MUTANTS OF YEAST DEFICIENT IN CYTOCHROME C. *Genetics,* 49**,** 39-48.

SIDERIS, D. P., PETRAKIS, N., KATRAKILI, N., MIKROPOULOU, D., GALLO, A., CIOFI-BAFFONI, S., BANCI, L., BERTINI, I. & TOKATLIDIS, K. 2009. A novel intermembrane space-targeting signal docks cysteines onto Mia40 during mitochondrial oxidative folding. *J Cell Biol,* 187**,** 1007-22.

SIDERIS, D. P. & TOKATLIDIS, K. 2007. Oxidative folding of small Tims is mediated by site-specific docking onto Mia40 in the mitochondrial intermembrane space. *Mol Microbiol,* 65**,** 1360-73.

SIDERIS, D. P. & TOKATLIDIS, K. 2010. Oxidative protein folding in the mitochondrial intermembrane space. *Antioxid Redox Signal,* 13**,** 1189-204.

SLEKAR, K. H., KOSMAN, D. J. & CULOTTA, V. C. 1996. The yeast copper/zinc superoxide dismutase and the pentose phosphate pathway play overlapping roles in oxidative stress protection. *J Biol Chem,* 271**,** 28831-6.

SOLLNER, T., PFALLER, R., GRIFFITHS, G., PFANNER, N. & NEUPERT, W. 1990. A mitochondrial import receptor for the ADP/ATP carrier. *Cell,* 62**,** 107-15.

STILLER, S. B., HOPKER, J., OELJEKLAUS, S., SCHUTZE, C., SCHREMPP, S. G., VENT-SCHMIDT, J., HORVATH, S. E., FRAZIER, A. E., GEBERT, N., VAN DER LAAN, M., BOHNERT, M., WARSCHEID, B., PFANNER, N. & WIEDEMANN, N. 2016. Mitochondrial OXA Translocase Plays a Major Role in Biogenesis of Inner-Membrane Proteins. *Cell Metab,* 23**,** 901-8.

STOJANOVSKI, D., BRAGOSZEWSKI, P. & CHACINSKA, A. 2012. The MIA pathway: a tight bond between protein transport and oxidative folding in mitochondria. *Biochim Biophys Acta,* 1823**,** 1142-50.

STURTZ, L. A., DIEKERT, K., JENSEN, L. T., LILL, R. & CULOTTA, V. C. 2001. A fraction of yeast Cu,Zn-superoxide dismutase and its metallochaperone, CCS, localize to the intermembrane space of mitochondria. A physiological role for SOD1 in guarding against mitochondrial oxidative damage. *J Biol Chem,* 276**,** 38084-9.

SUBRAMANIAN, S. 2018. *Safeguarding Mitochondria In Stress By Targeting Cytosolic Antioxidant Machinery*. MRes Biomedical Sciences, University of Glasgow.

SUN, N., YOULE, R. J. & FINKEL, T. 2016. The Mitochondrial Basis of Aging. *Mol Cell,* 61**,** 654-66.

SUTHERLAND, C. M., HAWLEY, S. A., MCCARTNEY, R. R., LEECH, A., STARK, M. J., SCHMIDT, M. C. & HARDIE, D. G. 2003. Elm1p is one of three upstream kinases for the Saccharomyces cerevisiae SNF1 complex. *Curr Biol,* 13**,** 1299-305.

TAIT, S. W. G. & GREEN, D. R. 2012. Mitochondria and cell signalling. *Journal of Cell Science,* 125**,** 807-15.

TAKAHASHI, Y. H., INABA, K. & ITO, K. 2004. Characterization of the menaquinone-dependent disulfide bond formation pathway of Escherichia coli. *J Biol Chem,* 279**,** 47057-65.

TAKAKUBO, F., CARTWRIGHT, P., HOOGENRAAD, N., THORBURN, D. R., COLLINS, F., LITHGOW, T. & DAHL, H. H. 1995. An amino acid substitution in the pyruvate dehydrogenase E1 alpha gene, affecting mitochondrial import of the precursor protein. *Am J Hum Genet,* 57**,** 772-80.

TAMURA, Y., HARADA, Y., SHIOTA, T., YAMANO, K., WATANABE, K., YOKOTA, M., YAMAMOTO, H., SESAKI, H. & ENDO, T. 2009a. Tim23-Tim50 pair coordinates functions of translocators and motor proteins in mitochondrial protein import. *J Cell Biol,* 184**,** 129-41.

TAMURA, Y., HARADA, Y., SHIOTA, T., YAMANO, K., WATANABE, K., YOKOTA, M., YAMAMOTO, H., SESAKI, H. & ENDO, T. 2009b. Tim23–Tim50 pair coordinates functions of translocators and motor proteins in mitochondrial protein import. *The Journal of Cell Biology,* 184**,** 129-41.

TAYLOR, S. W., FAHY, E., ZHANG, B., GLENN, G. M., WARNOCK, D. E., WILEY, S., MURPHY, A. N., GAUCHER, S. P., CAPALDI, R. A., GIBSON, B. W. & GHOSH, S. S. 2003. Characterization of the human heart mitochondrial proteome. *Nat Biotechnol,* 21**,** 281-6.

THOMAS, D., CHEREST, H. & SURDIN-KERJAN, Y. 1991. Identification of the structural gene for glucose-6-phosphate dehydrogenase in yeast. Inactivation leads to a nutritional requirement for organic sulfur. *EMBO J,* 10**,** 547-53.

TOKATLIDIS, K., JUNNE, T., MOES, S., SCHATZ, G., GLICK, B. S. & KRONIDOU, N. 1996. Translocation arrest of an intramitochondrial sorting signal next to Tim11 at the inner-membrane import site. *Nature,* 384**,** 585-8.

TRACHOOTHAM, D., LU, W., OGASAWARA, M. A., NILSA, R. D. & HUANG, P. 2008. Redox regulation of cell survival. *Antioxid Redox Signal,* 10**,** 1343-74.

TREITEL, M. A. & CARLSON, M. 1995. Repression by SSN6-TUP1 is directed by MIG1, a repressor/activator protein. *Proc Natl Acad Sci U S A,* 92**,** 3132-6.

TREITEL, M. A., KUCHIN, S. & CARLSON, M. 1998. Snf1 protein kinase regulates phosphorylation of the Mig1 repressor in Saccharomyces cerevisiae. *Mol Cell Biol,* 18**,** 6273-80.

TROTTER, E. W. & GRANT, C. M. 2002. Thioredoxins are required for protection against a reductive stress in the yeast Saccharomyces cerevisiae. *Mol Microbiol,* 46**,** 869-78.

TROTTER, E. W. & GRANT, C. M. 2003. Non-reciprocal regulation of the redox state of the glutathione-glutaredoxin and thioredoxin systems. *EMBO Rep,* 4**,** 184-8.

TROTTER, E. W. & GRANT, C. M. 2005. Overlapping roles of the cytoplasmic and mitochondrial redox regulatory systems in the yeast Saccharomyces cerevisiae. *Eukaryot Cell,* 4**,** 392-400.

TRUSCOTT, K. N., KOVERMANN, P., GEISSLER, A., MERLIN, A., MEIJER, M., DRIESSEN, A. J., RASSOW, J., PFANNER, N. & WAGNER, R. 2001. A presequence- and voltage-sensitive channel of the mitochondrial preprotein translocase formed by Tim23. *Nat Struct Biol,* 8**,** 1074-82.

TURCOTTE, B., LIANG, X. B., ROBERT, F. & SOONTORNGUN, N. 2010. Transcriptional regulation of nonfermentable carbon utilization in budding yeast. *FEMS Yeast Res,* 10**,** 2-13.

VAN DEN BERG, M. A., DE JONG-GUBBELS, P., KORTLAND, C. J., VAN DIJKEN, J. P., PRONK, J. T. & STEENSMA, H. Y. 1996. The two acetyl-coenzyme A synthetases of Saccharomyces cerevisiae differ with respect to kinetic properties and transcriptional regulation. *J Biol Chem,* 271**,** 28953-9.

VAN WILPE, S., RYAN, M. T., HILL, K., MAARSE, A. C., MEISINGER, C., BRIX, J., DEKKER, P. J., MOCZKO, M., WAGNER, R., MEIJER, M., GUIARD, B., HONLINGER, A. & PFANNER, N. 1999. Tom22 is a multifunctional organizer of the mitochondrial preprotein translocase. *Nature,* 401**,** 485-9.

VANDER HEIDEN, M. G., CHANDEL, N. S., LI, X. X., SCHUMACKER, P. T., COLOMBINI, M. & THOMPSON, C. B. 2000. Outer mitochondrial membrane permeability can regulate coupled respiration and cell survival. *Proc Natl Acad Sci U S A,* 97**,** 4666-71.

VIAL, S., LU, H., ALLEN, S., SAVORY, P., THORNTON, D., SHEEHAN, J. & TOKATLIDIS, K. 2002. Assembly of Tim9 and Tim10 into a functional chaperone. *J Biol Chem,* 277**,** 36100-8.

VINCENT, O., TOWNLEY, R., KUCHIN, S. & CARLSON, M. 2001. Subcellular localization of the Snf1 kinase is regulated by specific beta subunits and a novel glucose signaling mechanism. *Genes Dev,* 15**,** 1104-14.

VÖGTLE, F. N., BURKHART, J. M., GONCZAROWSKA-JORGE, H., KÜCÜKKÖSE, C., TASKIN, A. A., KOPCZYNSKI, D., AHRENDS, R., MOSSMANN, D., SICKMANN, A., ZAHEDI, R. P. & MEISINGER, C. 2017. Landscape of submitochondrial protein distribution. *Nature Communications,* 8**,** 1-10.

VÖGTLE, F. N., BURKHART, J. M., RAO, S., GERBETH, C., HINRICHS, J., MARTINOU, J. C., CHACINSKA, A., SICKMANN, A., ZAHEDI, R. P. & MEISINGER, C. 2012. Intermembrane space proteome of yeast mitochondria. *Mol Cell Proteomics,* 11**,** 1840-52.

VOOS, W. & ROTTGERS, K. 2002. Molecular chaperones as essential mediators of mitochondrial biogenesis. *Biochim Biophys Acta,* 1592**,** 51-62.

WALTHER, D. M. & RAPAPORT, D. 2009. Biogenesis of mitochondrial outer membrane proteins. *Biochimica et Biophysica Acta (BBA) - Molecular Cell Research,* 1793**,** 42-51.

WATSON, W. H., POHL, J., MONTFORT, W. R., STUCHLIK, O., REED, M. S., POWIS, G. & JONES, D. P. 2003. Redox potential of human thioredoxin 1 and identification of a second dithiol/disulfide motif. *J Biol Chem,* 278**,** 33408-15.

WEINBERG, F., HAMANAKA, R., WHEATON, W. W., WEINBERG, S., JOSEPH, J., LOPEZ, M., KALYANARAMAN, B., MUTLU, G. M., BUDINGER, G. R. S. & CHANDEL, N. S. 2010. Mitochondrial metabolism and ROS generation are essential for Kras-mediated tumorigenicity. *Proceedings of the National Academy of Sciences,* 107**,** 8788-93.

WENZ, L. S., OPALINSKI, L., SCHULER, M. H., ELLENRIEDER, L., IEVA, R., BOTTINGER, L., QIU, J., VAN DER LAAN, M., WIEDEMANN, N., GUIARD, B., PFANNER, N. & BECKER, T. 2014. The presequence pathway is involved in protein sorting to the mitochondrial outer membrane. *EMBO Rep,* 15**,** 678-85.

WIEDEMANN, N., KOZJAK, V., CHACINSKA, A., SCHONFISCH, B., ROSPERT, S., RYAN, M. T., PFANNER, N. & MEISINGER, C. 2003. Machinery for protein sorting and assembly in the mitochondrial outer membrane. *Nature,* 424**,** 565-71.

WIEDEMANN, N. & PFANNER, N. 2017. Mitochondrial Machineries for Protein Import and Assembly. *Annu Rev Biochem,* 86**,** 685-714.

WINK, D. A., KASPRZAK, K. S., MARAGOS, C. M., ELESPURU, R. K., MISRA, M., DUNAMS, T. M., CEBULA, T. A., KOCH, W. H., ANDREWS, A. W., ALLEN, J. S. & ET AL. 1991. DNA deaminating ability and genotoxicity of nitric oxide and its progenitors. *Science,* 254**,** 1001-3.

WOHLRAB, H. 2009. Transport proteins (carriers) of mitochondria. *IUBMB Life,* 61**,** 40-6.

WU, Y. & SHA, B. 2006. Crystal structure of yeast mitochondrial outer membrane translocon member Tom70p. *Nat Struct Mol Biol,* 13**,** 589-93.

YAMANO, K., YATSUKAWA, Y., ESAKI, M., HOBBS, A. E., JENSEN, R. E. & ENDO, T. 2008. Tom20 and Tom22 share the common signal recognition pathway in mitochondrial protein import. *J Biol Chem,* 283**,** 3799-807.

YANG, X., JIANG, R. & CARLSON, M. 1994. A family of proteins containing a conserved domain that mediates interaction with the yeast SNF1 protein kinase complex. *EMBO J,* 13**,** 5878-86.

YING, W. 2008. NAD+/NADH and NADP+/NADPH in cellular functions and cell death: regulation and biological consequences. *Antioxid Redox Signal,* 10**,** 179-206.

YOUNG, J. C., HOOGENRAAD, N. J. & HARTL, F. U. 2003. Molecular chaperones Hsp90 and Hsp70 deliver preproteins to the mitochondrial import receptor Tom70. *Cell,* 112**,** 41-50.

ZHANG, J., WANG, X., VIKASH, V., YE, Q., WU, D., LIU, Y. & DONG, W. 2016. ROS and ROS-Mediated Cellular Signaling. *Oxid Med Cell Longev,* 2016**,** 4350965.

ZHUANG, J., WANG, P. Y., HUANG, X., CHEN, X., KANG, J. G. & HWANG, P. M. 2013. Mitochondrial disulfide relay mediates translocation of p53 and partitions its subcellular activity. *Proc Natl Acad Sci U S A,* 110**,** 17356-61.